9-3-2013

Effects of Osmolytes on Amyloid-beta Protein Surface Activity and Membrane Interactions

Juan Anaya

Juan Anaya
Candidate

Biomedical Engineering
Department

This thesis is approved, and it is acceptable in quality and form for publication:

Approved by the Thesis Committee:

Dr. Eva Chi, Chairperson

Dr. Andrew Shreve

Dr. Heather Canavan

EFFECTS OF OSMOLYTES ON AMYLOID-BETA PROTEIN SURFACE ACTIVITY AND MEMBRANE INTERACTION

by

JUAN ANAYA

Biology, Bachelors of Science
2006

THESIS

Submitted in Partial Fulfillment of the
Requirements for the Degree of

MASTERS OF SCIENCE
BIOMEDICAL ENGINEERING

The University of New Mexico
Albuquerque, New Mexico

JULY, 2013

Acknowledgements

I would like to thank my academic advisor, Prof. Eva Chi, Assistant Professor in Chemical and Nuclear Engineering, for her support and help with experimental design and revisions of my manuscript. I would like to thank the University of Chicago for supplying crude Aβ40 for use in Langmuir trough experiments. I would also like to thank the University of New Mexico Mass Spectrometry Facility, and Kenneth Sherrell in particular, for help with lyophilization and molecular weight analysis of purified Aβ40. I would like to thank Greg Soliz, Melissa Hernandez, Emmalee Jones and all of the other students in the Chi lab group for help with experimentation and constructive help analyzing data. I would like to also thank Lauren Fleddermann for assistance with adsorption isotherm experiments. I would also like to thank the Alzheimer's Association (NIRG-09-132478), Margaret Bell with The Endowment Gift Agreement and Planned Estate Funding, Prof. Chi's NSF CAREER grant (CBET-1150855), the University of New Mexico Research Allocation Committee, and The Oak Ridge Associated Universities Ralph E. Powe Junior Faculty Enhancement Award for support and funding. I would like to thank Danielle Lussier for all her support during writing of this thesis.

Effects of Osmolytes Amyloid-beta Protein Surface Activity and Membrane Interaction

By

Juan Anaya

B.S., Biology, New Mexico Tech, 2006

M.S., Biomedical Engineering, University of New Mexico, 2013

ABSTRACT

The misfolding and aggregation of proteins into fibrillar aggregates in the brain are linked to the pathogenesis of over 20 neurodegenerative diseases. Specifically, the toxicity and neurodegenerative symptoms of Alzheimer's disease are directly related to the aggregation of the amyloid-β (Aβ) protein into β-sheet rich insoluble fibrils. However, the mechanism and driving forces of Aβ fibril formation *in vivo* are still unknown. It has been shown previously that Aβ's surface activity and favorable interaction with lipid membranes can induce the formation of fibrils, suggesting a possible membrane-based mechanism of Aβ aggregation in Alzheimer's disease. Unlike dilute solutions used for *in vitro* experiments, the cellular environment is highly crowded, with macromolecules and osmolytes occupying up to 40% of the cellular volume. The resulting molecular crowding and preferential exclusion modulate the thermodynamics of protein reactions to favor those that reduce total system volume and minimize solvent

exposed surface area, respectively. To assess the effects of molecular crowding and preferential exclusion on interface-induced Aβ fibril formation, we investigate the effects of the osmolyte sucrose on Aβ surface activity and membrane interaction. We hypothesize that due to preferential exclusion, sucrose will favor the interface-partitioned states, i.e., air/water interface adsorbed and membrane associated, of Aβ. As such, sucrose is expected to enhance the surface activity and membrane interaction of Aβ. Adsorption isotherms of Aβ40 to the air/subphase interface confirm our hypothesis. With increasing sucrose concentration in the subphase, Aβ40 adsorbed to the air/subphase interface more readily, increasing the final adsorption surface pressure, decreasing the lag time before adsorption begins and increasing the rate of adsorption. Similarly, Aβ40 inserted into anionic DMPG and zwitterionic DPPC monolayers more readily in the presence of increasing sucrose concentrations. The amount of insertion increased, the lag time decreased, and the rate of insertion increased with increasing sucrose concentration. This increased interfacial activity in the presence of sucrose is important because association of Aβ in membranes has been associated with nucleation of fibril formation that leads to the neurodegenerative pathology of Alzheimer's disease. The effects of preferential exclusion and molecular crowding associated with sucrose on the interfacial dynamics of Aβ thus play an important role in formation of fibrils. The cellular environment is even more crowded and osmotically active than the dilute solutions investigated here. This suggests that the interactions of Aβ with membrane interfaces may be even more significant in the cellular environment and may serve as a nucleation site for the aggregation of Aβ *in vivo*.

Table of Contents

Abstract iv

Table of Contents vi

List of Figures ix

List of Tables xiii

Nomenclature xiv

1. Background 1

1.1 Alzheimer's Disease 1

1.2 Amyloid Beta (Aβ) 2

1.3 Molecular Crowding and Osmolytes 4

2. Experimental Theory 7

2.1 Surface Tension 7

2.2 Langmuir Trough 8

2.3 Langmuir Films 10

2.3.1. Analysis of Adsorption Isotherms 10

2.3.2 Analysis of Lipid Compression Isotherms and Insertion Isotherms 11

2.3.3 Fluorescence Imaging Analysis 14

3. Materials and Methods 16

3.1 Materials 16

3.2 Aβ40 Purification 17

3.3 Aβ40 Adsorption Isotherms 20

3.4 Lipid Monolayer Compression Isotherms 21

3.5 Aβ40 Insertion into Lipid Monolayers 22

3.6 Fluorescence Imaging **23**

4. Results **24**

4.1 Mass Spectrometry **24**

4.2 Langmuir Trough Adsorption Data **26**

4.2.1 Adsorption Isotherm 26

4.2.2 Final Surface Pressure of Aβ40 Adsorption Isotherms 27

4.2.3. Lag Time of Aβ40 Adsorption Isotherms 29

4.2.4 – Rate of Aβ40 Adsorption in Adsorption Isotherms 30

4.3 Langmuir Model Membrane Compression Isotherms **31**

4.3.1. DMPG Compression Isotherm 32

4.3.2. DMPG Isotherm Onset of Domain Formation 33

4.3.4. DMPG Isotherm Area per Molecule of Liftoff 34

4.3.5. DMPG Isotherm Fluorescence Imaging 36

4.4 Aβ40 Insertion into Lipid Monolayers **42**

4.4.1. Aβ40 Insertion into DMPG Monolayer with Varying Sucrose Concentration 42

4.4.2. Aβ40 Insertion into DMPG at 30 mN/m 44

4.4.3. Lag Time of Aβ40 Insertion into DMPG Isotherms 47

4.4.4 – Rate of Aβ40 Insertion in DMPG Isotherms 48

4.4.4. Aβ40 Insertion into DMPG Fluorescence Imaging 50

4.5 Aβ40 Insertion into DPPC Lipid Monolayers **54**

4.5.1. Aβ40 Insertion into DPPC Monolayer with Varying Sucrose Concentration 56

4.5.2. Final Equilibrium Insertion of Aβ40 into DPPC Monolayers 57

4.5.3. Lag Time of Aβ40 Insertion into DPPC Isotherms 58

4.5.4. Rate of Aβ40 Insertion into DPPC Isotherms 59

4.6 Ionic Strength and pH of Sucrose Solutions **61**

5. Discussion 62

5.1 Proposed Mechanism for Aβ40 Adsorption and the Effect of Sucrose 64

5.2 Sucrose Enhances the Adsorption of Aβ40 to the Air/Subphase Interface..... 65

5.3 Sucrose Increases the Rigidity of Lipid Membranes 68

5.4 Sucrose Greatly Enhances the Insertion of Aβ40 into Anionic and Zwitterionic Membranes..... 70

5.5 Sucrose Increases the Disruption of Membranes by Aβ40 72

6. Conclusion 73

7. References 74

List of Figures

Figure 1: Aggregates in neurodegenerative diseases 1

Figure 2: Formation of Aβ from APP by β and γ secretases 2

Figure 3: Schematic of reaction coordinate diagram of a protein aggregation free energy diagram 3

Figure 4: Schematic of the effect of preferential exclusion on protein conformation 5

Figure 5: Forces at air/liquid interface 7

Figure 6: Chi lab Langmuir Trough 8

Figure 7: Schematic of Wilhelmy plate at the air/subphase interface 9

Figure 8: Example of Aβ40 adsorption isotherm 11

Figure 9: Example of lipid isotherm and Aβ40 insertion experiments 13

Figure 10: Example of Aβ40 percent insertion plot 14

Figure 11: Schematic of fluorescence imaging of a lipid compression isotherm experiment 15

Figure 12: Example of ImageJ software analysis for determining the percent area light vs. dark 16

Figure 13: Time of Flight mass spectrometry with Electrospray ionization analysis of purified Aβ40 25

Figure 14: Adsorption isotherms surface pressure vs. time after injection of Aβ40 in varying sucrose subphases 27

Figure 15: Final adsorption pressure vs. sucrose concentration of Aβ40 adsorption isotherms 28

Figure 16: Lag time vs. sucrose concentration of Aβ40 adsorption isotherms 30

Figure 17: Adsorption rate vs. sucrose concentration of Aβ40 adsorption isotherms 31

Figure 18: DMPG compression isotherms surface pressure vs. area per molecule in varying sucrose subphases 33

Figure 19: The surface pressure of the onset of domain formation vs. sucrose concentration of DMPG compression isotherms 34

Figure 20: The area per molecule of liftoff vs. sucrose concentration of DMPG compression isotherms. 35

Figure 21: DMPG compression isotherm on water at 30±0.5 °C 37

Figure 22: DMPG compression isotherm on 0.1 M sucrose at 30±0.5 °C 37

Figure 23: DMPG compression isotherm on 0.25 M sucrose at 30±0.5 °C 38

Figure 24: DMPG compression isotherm on 0.5 M sucrose at 30±0.5 °C 38

Figure 25: DMPG compression isotherm on 0.75 M sucrose at 30±0.5 °C 39

Figure 26: DMPG compressibility at various surface pressures and sucrose 40

Figure 27: Fluorescent images of DMPG compression isotherms on varying sucrose concentrations at (A) 25 mN/m and (B) 30 mN/m and 30°C 41

Figure 28: Aβ40 insertion example into DMPG monolayers in constant surface pressure assay at 25mN/m at 30°C 43

Figure 29: Aβ40 insertion into DMPG isotherms percent insertion vs. time after injection of Aβ40 into varying sucrose subphases 44

Figure 30: Aβ40 insertion into DMPG isotherms percent insertion vs. time after injection of Aβ40 into sucrose subphases at a constant surface pressure of 30 mN/m 45

Figure 31: Final percent insertion vs. sucrose concentration of Aβ40 insertion into DMPG isotherms 47

Figure 32: Lag time vs. sucrose concentration of Aβ40 insertion in DMPG isotherms ... 48

Figure 33: Aβ40 insertion rate vs. sucrose concentration of Aβ40 insertion into DMPG isotherms ... 49

Figure 34: Aβ40 insertion into DMPG isotherm on water at 30±0.5 °C ... 51

Figure 35: Aβ40 insertion into DMPG isotherm on 0.1 M sucrose at 30±0.5 °C ... 51

Figure 36: Aβ40 insertion into DMPG isotherm on 0.25 M sucrose at 30±0.5 °C ... 52

Figure 37: Aβ40 insertion into DMPG isotherm on 0.5 M sucrose at 30±0.5 °C ... 52

Figure 38: Aβ40 insertion into DMPG isotherm on 0.75 M sucrose at 30±0.5 °C ... 53

Figure 39: Aβ40 insertion into DMPG isotherm on 1.0 M sucrose at 30±0.5 °C ... 53

Figure 40: Maximum Aβ40 insertion pressure in DPPC on water ... 55

Figure 41: Surface pressure vs. sucrose concentration for maximum surface pressure for insertion of Aβ40 into DPPC compared with adsorption final surface pressure on a clean subphase ... 56

Figure 42: Aβ40 insertion into DPPC isotherms percent insertion vs. time after injection of Aβ40 into varying sucrose subphases at 25 mN/m ... 57

Figure 43: Final percent insertion vs. sucrose concentration of Aβ40 insertion into DPPC isotherms ... 58

Figure 44: Lag time vs. sucrose concentration of Aβ40 insertion into DPPC ... 59

Figure 45: Aβ40 insertion rate vs. sucrose concentration of Aβ40 insertion into DPPC isotherms ... 62

Figure 46: Schematic illustration of the adsorption of a natively folded protein to an air/liquid interface ... 63

Figure 47: Schematic of proposed mechanism of Aβ40 interaction and adsorption to an interface 64

Figure 48: Effects of sucrose on the conformation of Aβ40 adsorbed to the air/subphase interface 66

List of Tables

Table 1: Aβ40 purification gradient program on HPLC software 17

Table 2: HPLC column cleaning program 18

Table 3: Conductivity and pH of varying sucrose solutions 62

Nomenclature

Aβ	Amyloid-beta peptide
APP	Amyloid precursor protein
IDP	Intrinsically disordered protein
N	Native conformation of protein
TS^*	Partially folded transition state conformation of protein
A_n	Aggregation competent protein conformation intermediate
A_m	Protein aggregate
A_{m+1}	Protein aggregate
$\Delta G^{\ddagger}$	Energy of activation
ΔG	Change in Gibb's free energy
G	Gibb's free energy
F	Force
ρ_p	Density of Wilhelmy plate
l_p	Length of Wilhelmy plate
w_p	Width of Wilhelmy plate
t_p	Thickness of Wilhelmy plate
g	Gravitational force (9.8 m/s^2)
γ	Surface tension of liquid
θ	Contact angle of the liquid on the plane
ρ_l	Density of liquid
h_l	Height of proportion of Wilhelmy plate immersed in liquid
w_l	Width of proportion of Wilhelmy plate immersed in liquid
t_l	Thickness of proportion of Wilhelmy plate immersed in liquid
π	Surface pressure (mN/m)
γ_0	Surface tension of a clean air/subphase interface
pI_t	Isoelectric point
MMA	Mean molecular area, or area per molecule ($Å^2$/molecule)
Å	Angstrom (10^{-10} meter)
ΔA	Change in trough area in insertion isotherms
A_0	Trough area at the time of injection
Aβ40	40 amino acid long Aβ40 peptide used in Langmuir trough experiments
HPLC	High performance liquid chromatography
TFA	Trifluoroacetic acid
DMSO	Dimethyl sulfoxide
DMPG	1,2-dimyristoyl-*sn*-glycero-3-phospho-(1'-rac-glycerol)
DPPC	1,2-dipalmitoyl-*sn*-glycero-3-phosphocholine
TR-DHPE	Texas Red® 1,2-Dihexadecanoyl-*sn*-Glycero-3-Phosphoethanolamine
ToF	Time of flight mass spectrometry
EI	Electrospray Ionization

1. Background

1.1 Alzheimer's Disease

Many neurodegenerative diseases share the same common pathology of the accumulation of deposits of misfolded and aggregated proteins.[1,10] There are over 20 diseases that are associated with protein aggregation and fibril formation. While the pathology of each of these diseases is described by a different protein, they all share the pathology of protein aggregation and fibril formation (**Figure 1**).[10]

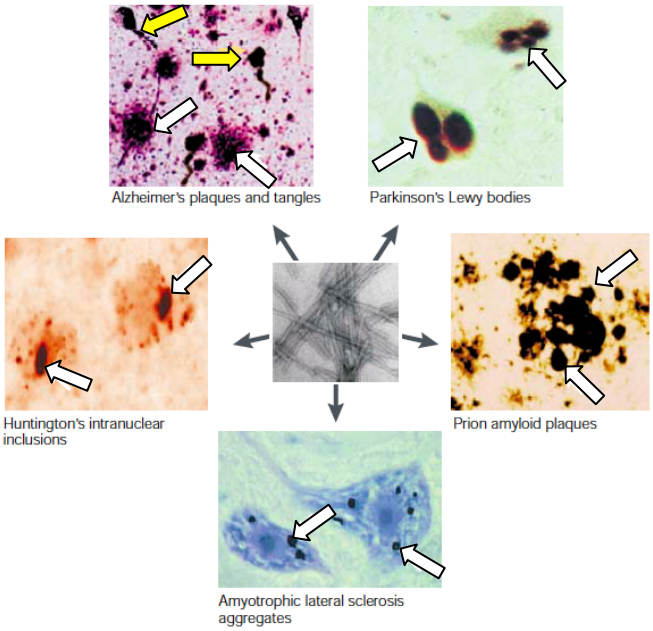

Figure 1: Aggregates in neurodegenerative diseases. The misfolding and aggregation of proteins can lead to several neurodegenerative diseases. Amyloid plaques (white arrows) and intra-cytoplasmic neurofibrillary tangles (yellow arrows) are the pathological markers of disease.[10]

Alzheimer's disease is the most common age-related neurodegenerative disease and results in the loss of short- and long-term memory, loss of bodily functions and, eventually, death.[2] According to the Alzheimer's Association, in the United States, symptoms typically appear after the age of 65, 5.4 million people have Alzheimer's disease, and it costs $183 billion annually for medical care and hospice care.[3] The mechanism of pathology is still poorly understood. What is known, however, is that there

are two proteins, amyloid-β (Aβ) and tau protein, which aggregate to form low molecular weight oligomers that are then converted to insoluble, β-sheet rich amyloid fibrils.[1,10] The toxicity and neurodegenerative symptoms of Alzheimer's disease are directly related to Aβ aggregation and fibril formation. The pathology of Alzheimer's disease is characterized by the formation of extracellular amyloid plaques (**Figure 1** white arrows) that are derived from Aβ and intra-cytoplasmic neurofibrillary tangles (**Figure 1** yellow arrows), which are derived from tau protein.[10,11] The amyloid plaques develop in the hippocampus, a structure deep in the brain that helps to encode memories, and in other areas of the cerebral cortex that are used in thinking and making decisions, which explains the loss of short and long term memory associated with the disease.[11] Understanding the structure and nature of Aβ is important to discern the mechanism of misfolding and aggregation.

1.2 Amyloid Beta (Aβ)

Aβ is a protein that is produced from the integral membrane protein amyloid precursor protein (APP) (**Figure 2**).[11] APP is known to function in neural plasticity,[12] iron export,[13] and synapse formation .[14] Aβ is cleaved from APP by the β- and γ-secretases and becomes an extracellular protein.[11] Normal functions of Aβ are not well understood but they are thought to include activation of kinase enzymes[15] and antimicrobial activities.[16]

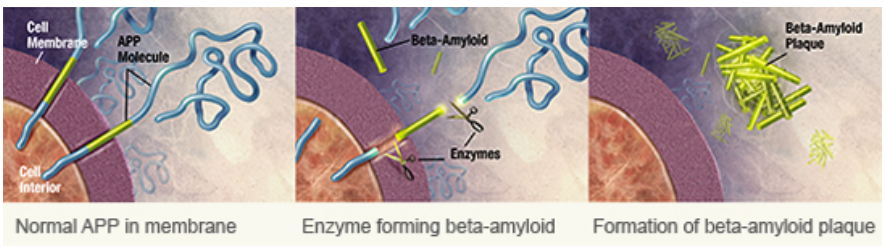

Figure 2: Formation of Aβ from APP by β and γ secretases. An integral membrane protein (APP), is cleaved by β and γ secretases in the extracellular matrix to form Aβ (green).[11]

Aβ is a soluble 39 to 43 amino acid amphiphilic peptide, containing a hydrophobic C-terminus that spans the transmembrane portion of APP that is cleaved by γ-secretase and a hydrophilic N-terminus that is cleaved by β-secretase. In physiological conditions, Aβ takes on a conformation that is a random coil.[18] In a membrane-like environment, Aβ takes on a largely α-helical conformation[19], and, in fibrils, Aβ takes on the characteristic β-sheet structure.[20]

Aβ belongs to a class of proteins known as intrinsically disordered proteins (IDPs). This means that Aβ lacks a well-defined tertiary structure, which is normally seen in most natively folded proteins.[17] Because Aβ is structurally disordered, before it can become aggregation competent, it undergoes conformational changes to a more compact, ordered conformation (i.e. a β-sheet conformation). The proposed mechanism of misfolding and aggregation of either IDPs or normally folded proteins can be seen in **Figure 3**.

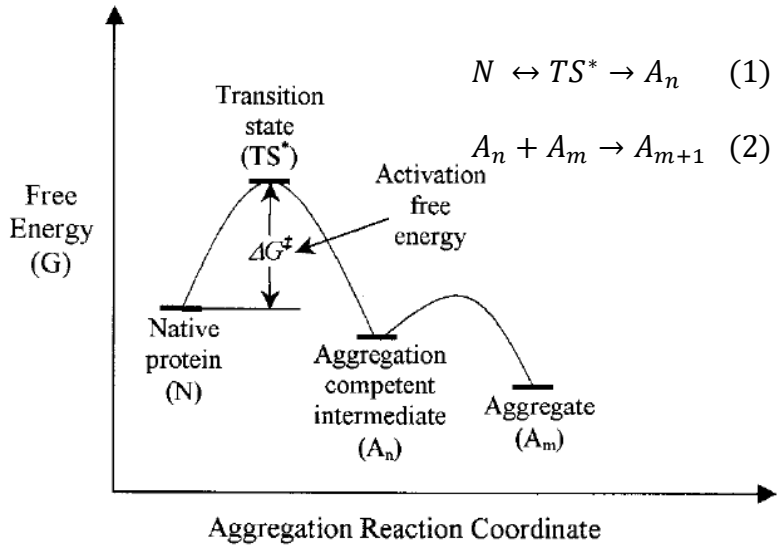

Figure 3: Schematic of reaction coordinate diagram of a protein aggregation free energy diagram. There is a reduction in the activation free energy to reach the transition state (TS) required for aggregation by interactions with interfaces such as a membrane.[9,21] (Inset) The Lumry-Eyring framework for protein aggregation.

While the mechanism itself is the same for both classes of proteins, there are important differences. In normally folded proteins, the native protein structure (N) is the folded, active state. In IDPs, the native protein structure (N) is in an unfolded state. The Lumry-Eyring mechanism for aggregation (**Figure 3 inset**) suggests that there is a transition from N to a reversible transition state (TS^*) that involves an energy of activation ($\Delta G^{\ddagger}$). In natively folded proteins TS^* is unfolded compared to N, and in IDPs, TS^* is a more folded state. From here, TS^* can either go back to its native state or proceed irreversibly to an aggregation competent intermediate (A_n). In Aβ in particular, TS^* represents the partially folded state and A_n represents the conformation that contains a highly ordered β-sheet. From here, there is a irreversible assembly into higher order aggregates (A_m and A_{m+1}).[9,21] Environments that favor more compact conformations of the native structure of Aβ, for example interactions with interfaces such as membranes,[7] a highly crowded environment, or the presence of certain osmolytes, for example, will lower the energy of activation ($\Delta G^{\ddagger}$) required for the transition from natively unfolded (N) to the transition state (TS^*). This means that osmolytes, interactions with membranes, and molecular crowding can lead to an increased propensity of Aβ to misfold and aggregate into fibrils.

1.3 Molecular Crowding and Osmolytes

The cellular environment is highly crowded with up to 35% of the intracellular and interstitial volume being occupied by solutes and macromolecules.[17,22,23] This crowded environment has been shown to favor processes that reduce total system volume.[22] This effect has been shown increase the folding of partially folded IDPs, suggesting that once an IDP reaches the partially folded transition state (TS^*) previously

discussed, the volume exclusion effect pushes the equilibrium towards the folded, aggregation competent intermediate (A_n).[22] The transition to a partially folded state, TS^* also enhances the ability of Aβ to interact with interfaces.[20,25]

Another factor that could influence protein folding and interaction with membranes and interfaces are small co-solutes that influence and counterbalance the osmotic pressure of the cell and the cellular environment, known as osmolytes.[24] The main naturally-occurring osmolytes include polyols (glucose and sucrose), urea and methylamines.[30] Osmolytes also exert non-specific interfacial effects on proteins by being preferentially excluded over water from the protein surface, which increases the surface tension of the protein/solvent interface, or they are preferentially bound to the protein surface, decreasing the surface tension of the protein/solvent interface.[23] In this way, preferentially excluded osmolytes, like sucrose, stabilize protein structure, shifting the equilibrium of the protein conformation towards a more folded state (**Figure 4).**

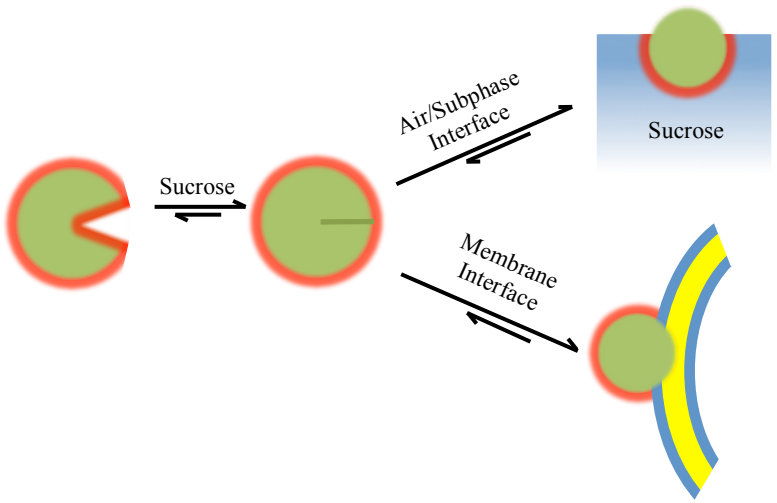

Figure 4: Schematic of the effect of preferential exclusion on protein conformation. Sucrose shifts the protein conformation equilibrium towards a minimal exposed surface area (red). In the presence of interfaces, the protein will adsorb (air/subphase interface) or insert into a leaflet of a lipid (membrane interface) to further minimize solvent exposed surface area.

Thermodynamically, this suggests a reduction of the energy of activation ($\Delta G^{\ddagger}$) required for the transition from natively unfolded (N) to the slightly more folded transition state (TS^{*}). This reduction in activation energy increases the relative amount of partially folded protein, leading to interaction with interfaces. Insertion into lipid membranes nucleates aggregation, which leads to an increase in fibril formation.[9]

While the effects of molecular crowding and osmolytes on protein behaviors in solution have been extensively studied,[9] their effects on protein dynamics at interfaces have not been explored. Because it has been shown that interactions with cellular membranes nucleate the misfolding and aggregation of Aβ into oligomers and fibrils, it is important to understand how osmolytes affect the ability of Aβ to interact with interfaces. This is the first study that will bridge the gap in research on the effects of membranes and osmolytes on the aggregation of Aβ.

Without this understanding, it will be impossible to understand the cascade of events that follow that leads to toxicity and pathogenesis of Alzheimer's disease. It is our hypothesis that the osmolyte sucrose will increase the ability of Aβ to interact with membranes, which can easily seed aggregation. This thesis will use the idealized air/subphase and membrane/subphase interfaces to investigate the effect of sucrose on the ability of Aβ to interact with a hydrophobic/hydrophilic interface in order to further examine the mechanism of misfolding. These two interfaces, along with the presence of the osmolyte sucrose, which represents an ideal stabilizing co-solute, will show how preferential exclusion and molecular crowding affect the dynamics of Aβ at interfaces.[21]

2. Experimental Theory

The Langmuir trough is a tool used to measure the properties of a film made up of amphiphilic molecules; molecules consisting of hydrophobic and hydrophilic regions at an interface. The trough measures surface pressure (π) at the air/water interfaces. The surface pressure is a measure of how the surface tension (γ) of the clean liquid is reduced by surface-active molecules.[26] Here, the theory of surface tension, measurements of surface pressure, Langmuir isotherms, and the instrumentation of the Langmuir trough will be explained.

2.1 Surface Tension

Surface tension is the measurement, in units of force per unit length, of the energy present at an interface. This energy is the total cohesive, or attractive, forces on the liquid molecules. In the bulk, the cohesive forces on any particular molecule are "balanced" by equal cohesive forces on all sides, which result in a net force of zero. Molecules at the surface do not have molecules on all sides, which leave a non-zero net force (**Figure 5**).

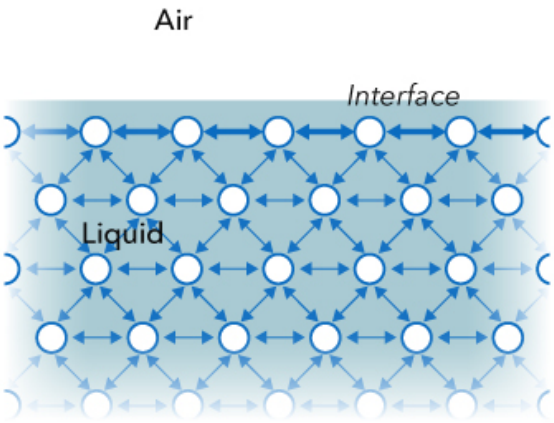

Figure 5: Forces at air/liquid interface[27]

The liquid at the air/water interface is pulled towards the bulk and will minimize its surface area. The overall effect is that there is an excess of free energy. This free

energy is responsible for the surface tension of the liquid.[27] Any disturbance in the strength of the forces at the surface will decrease the surface tension of the liquid.

2.2 Langmuir Trough

The Langmuir trough utilized in this project was custom built by KSV NIMA (Espoo, Finland) (**Figure 6)**. It consists of a hydrophobic Teflon trough, two hydrophilic Delrin barriers to prevent leakage of the film beneath the barriers, a motor to control the position of the barriers, a platinum Wilhelmy plate attached to a force reader, and a circulating water bath beneath the trough to control the temperature of the subphase in the trough. This is set on top of an inverted, Olympus IX51, fluorescence microscope (Center Valley, PA) for imaging.

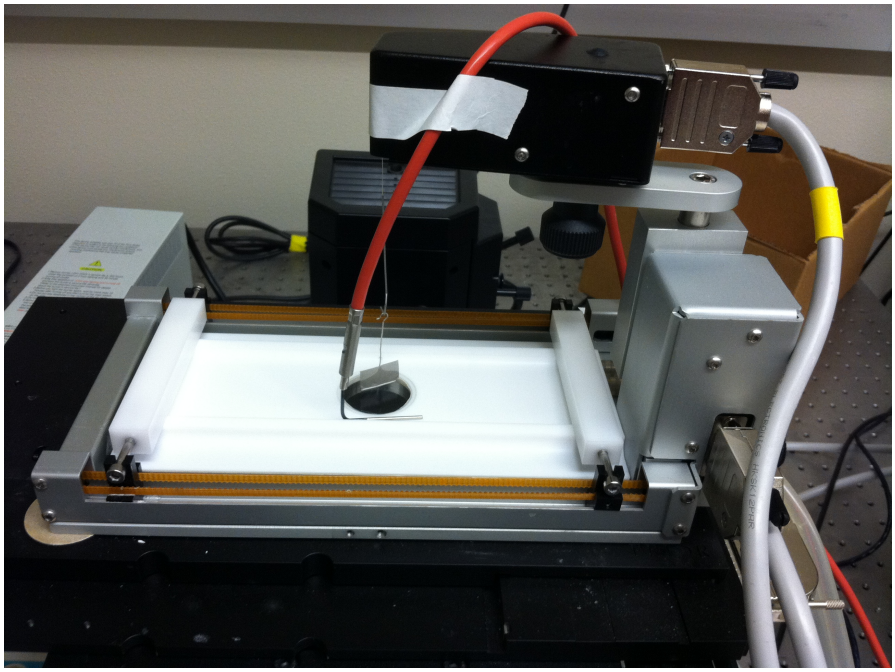

Figure 6: Chi lab Langmuir Trough. Wilhelmy plate in center, attached to force reader, white Delrin barriers mounted on stages attached to motor, red temperature probe inserted in subphase.

The Langmuir trough measures surface pressure of a film by measuring the surface tension with the use of the Wilhelmy plate method. The plate is partially suspended in the subphase and the force due to surface tension of the subphase is

measured. This force is then converted to surface tension (in units of mN/m) with the dimensions of the plate (**Figure 7**).[27]

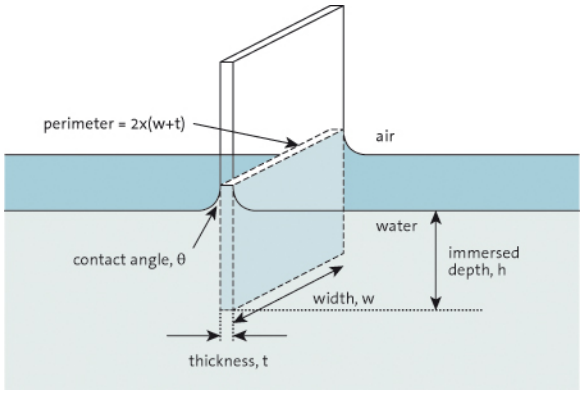

Figure 7: Schematic of Wilhelmy plate at the air/subphase interface[27]

The forces acting on this plate consist of the forces of gravity and surface tension downward and buoyancy due to the displaced water upward. The downward force acting on the plate is given by:

$$F = (Weight\ of\ Plate) + (Surface\ Tension\ Force) - (Buoyant\ Force) \quad (1)$$

$$F = g\rho_p l_p w_p t_p + 2\gamma(w_p + t_p)(cos\theta) - g\rho_l h_l w_l t_l \quad (2)$$

Where the values are given by:

$\rho_p l_p w_p t_p =$ Density, length, width and thickness of the plate, respectively
$g =$ Gravitational force (9.8 m/s^2)
$\gamma =$ Surface tension of the liquid
$\theta =$ Contact angle of the liquid on the plate
$\rho_l =$ Density of the liquid
$h_l w_l t_l =$ Height, width, and thickness of proportion of plate immersed in liquid

Surface pressure is defined as the difference in surface tension measured between a clean subphase and a subphase with a film (Equation 3).[27] As discussed previously, any interference with the strength of the forces of the molecules at the surface, such as Aβ surface activity, will reduce surface tension, and increase surface pressure.

$$\pi = \gamma_0 - \gamma \quad (3)$$

Where the values are given by:

π = Surface pressure
γ_0 = Surface tension of clean air/subphase interface
γ = Surface tension in the presence of film

This surface pressure is measured by measuring the change in force between a clean surface and the same surface containing a film. If the plate is completely wetted, the contact angle becomes 0°, and solving for the change in surface tension gives:

$$\pi = -\Delta\gamma = -\left[\Delta F/2\left(t_p + w_p\right)\right] \quad (4)$$

If $w_p \gg t_p$

$$\pi = -\Delta\gamma = -\Delta F/2w_p \quad (5)$$

In the Langmuir trough, the force is measured by the difference in weight of the Wilhelmy plate that is attached to a sensitive force reader.[26,27] The Langmuir trough in the Chi lab group was used in all experiments investigating the surface activity of Aβ40.

2.3 Langmuir Films

2.3.1. Analysis of Adsorption Isotherms

Figure 8 shows an example of a typical adsorption isotherm experiment from the start of compression, to injection, to final surface pressure. In these experiments, first, a clean subphase is compressed to a known surface area and held constant. Then, a known concentration of the 40 amino acid long Aβ peptide used in the Langmuir trough experiments (Aβ40) is injected into the subphase. Finally, the surface pressure is recorded over time while Aβ40 adsorbs to the air/subphase interface.

The Aβ40 adsorption isotherms are analyzed for specific properties. The lag time is the time after injection before the resulting increase in surface pressure. The lag time was calculated by increasing the magnification around the area where surface pressure

begins to increase. The final adsorption pressure is calculated by taking the average of the last few minutes of the experiment after the rise in surface pressure plateaus. Finally, the rate of adsorption is calculated by taking the slope of the line of the linear rise phase.

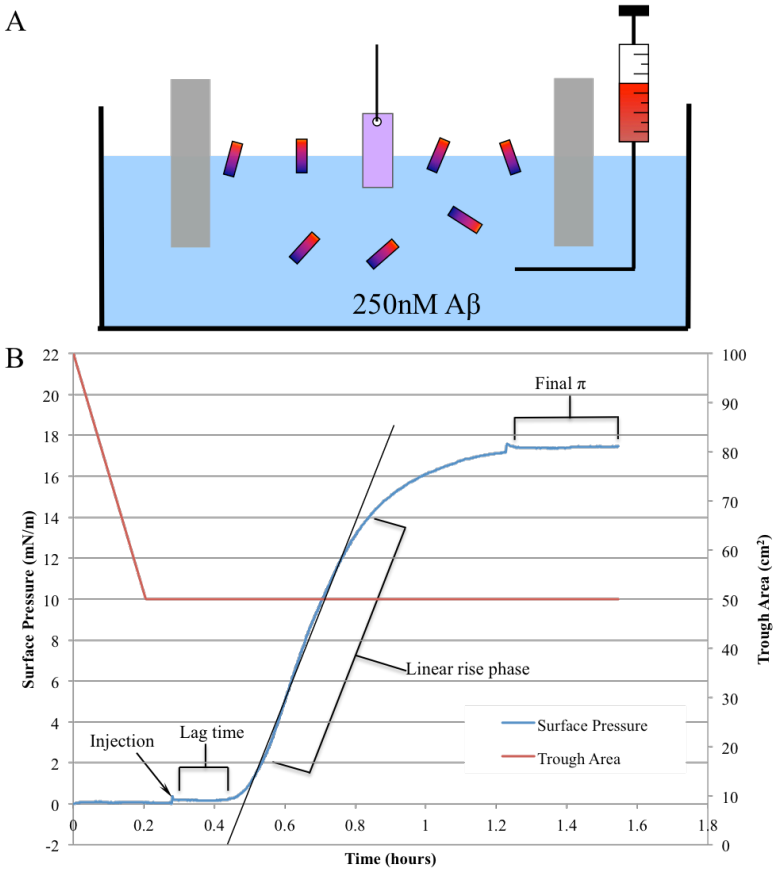

Figure 8: Example of Aβ40 adsorption isotherm. (A) Schematic of Langmuir trough adsorption experiment. In this experiment, there are two barriers on either side of a Wilhelmy plate. In the schematic the Wilhelmy plate is purple. In these experiments the surface area is compressed to a constant area. Then Aβ40 is injected into the subphase and surface pressure is read over time. If the Aβ40 adsorbs to the air water interface the surface pressure rises, indicating surface activity. (B) An example of an adsorption isotherm. The blue plot is the surface pressure over time and the red plot is the trough area over time. The lag time is the time after injection before surface pressure begins increasing. The slope of the linear rise phase corresponds to the rate of adsorption. The final surface pressure is the average of the last few minutes after the surface pressure plateaus.

2.3.2 Analysis of Lipid Compression Isotherms and Insertion Isotherms

Figure 9 shows an example of two types of lipid monolayer experiments. First, the lipid compression isotherm (red plot) is described. A lipid is spread on a clean

subphase. In this fully expanded state, the lipids are in what is described as the gas phase. This is where the lipid molecules are spread out and do not feel influences from other lipid molecules. Next, the trough barriers are compressed to a point known as liftoff where the lipid molecules begin to interact leading to increase in surface pressure. This phase transition leads to a more fluid-like phase called the liquid expanded phase where the lipid is highly compressible (i.e. the change in surface pressure per change in area per molecule is small). In the liquid expanded phase, the hydrocarbon tails are randomly arrayed. Under further compression there is a 1st order phase transition that can be seen by the appearance of a plateau. This is the point where an ideal lipid monolayer would begin to form condensed domains (onset of domain formation). This is where highly ordered tail structures begin to stick out of the subphase. The liquid condensed phase comes after the transition. Here molecules are aligned at the interface with the hydrocarbon tails extended out towards the air. The liquid condensed phase is characterized by longer-ranged molecular order, known as condensed domains, and lower compressibility than the liquid expanded phase. Next, there is a transition to a crystalline-like solid phase where the molecules are closely packed and aligned on a lattice. Upon further compression, the monolayer collapses. Determining the point of liftoff is completed in the same manner as the lag time in the adsorption isotherms, the plot is zoomed in around the area of liftoff to determine the exact point of an increase in surface pressure. The onset of domain formation is determined using fluorescence microscopy to determine the point where domains begin to form (small black dots on a bright expanded phase).

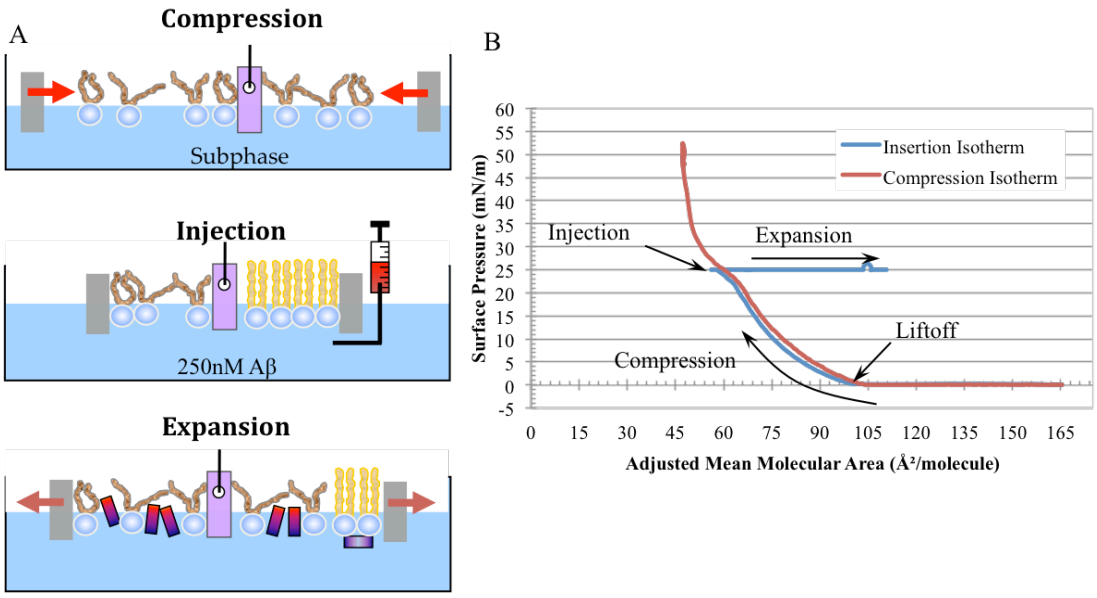

Figure 9: Example of lipid isotherm and Aβ40 insertion experiments. (A) Schematic of lipid compression, injection and expansion. In the compression phase, lipid begins in the gas phase, with the hydrophobic tail groups organized randomly. The grey trough barriers are compressed. Once compressed to a predetermined surface pressure, the pressure is held constant and Aβ40 is injected into the subphase. If Aβ40 interacts with the lipid monolayer, the barriers must expand in order to maintain the surface pressure. (B) Example of a compression isotherm (red) and an insertion isotherm (blue). Before compression starts, the lipid is in the gas phase, as compression continues, liftoff occurs. This is where the lipid molecules begin to interact, which leads to an increase in surface pressure. This phase transition leads to a more fluid-like phase called the highly compressible liquid expanded phase. Under further compression there is a 1st order phase transition that can be seen by the appearance of a plateau. This is the point where an ideal lipid monolayer would begin to form condensed domains (onset of domain formation). The liquid condensed phase comes after the transition. Here molecules are aligned at the interface with the hydrocarbon tails extended out towards the air. Further compression (red plot) leads to a solid phase and eventual collapse of the monolayer. If the surface pressure is held at a constant pressure, Aβ40 can be injected into the subphase (blue). As Aβ40 inserts, the area must expand in order to maintain the surface pressure.

In the Aβ40 insertion isotherm (blue plot), compression was completed in the same fashion as the compression isotherm. Instead of continuing to compress, the surface pressure was held at a constant surface pressure and Aβ40 was injected into the subphase. If Aβ40 interacts with the lipid monolayer, in order to maintain the surface pressure, the trough area must be expanded. The surface area continues to expand until equilibrium is reached where Aβ40 cannot insert further into the monolayer. Analysis of the insertion isotherms (**Figure 10**) involves calculation of the percent insertion, which is calculated as the change in area after injection divided by the area at injection ($\Delta A/A_0$, see inset **Figure**

10), the lag time before insertion begins, the rate of insertion, and the final percent insertion. These are calculated in the same manner as the adsorption isotherms. The lag time was calculated by zooming in around the area where insertion begins to determine the exact point of an increase in percent insertion. The slope of the linear rise phase was used to determine the rate of insertion. Finally, the final percent insertion was calculated by taking the average of the last few minutes of the experiment after the percent insertion plateaus.

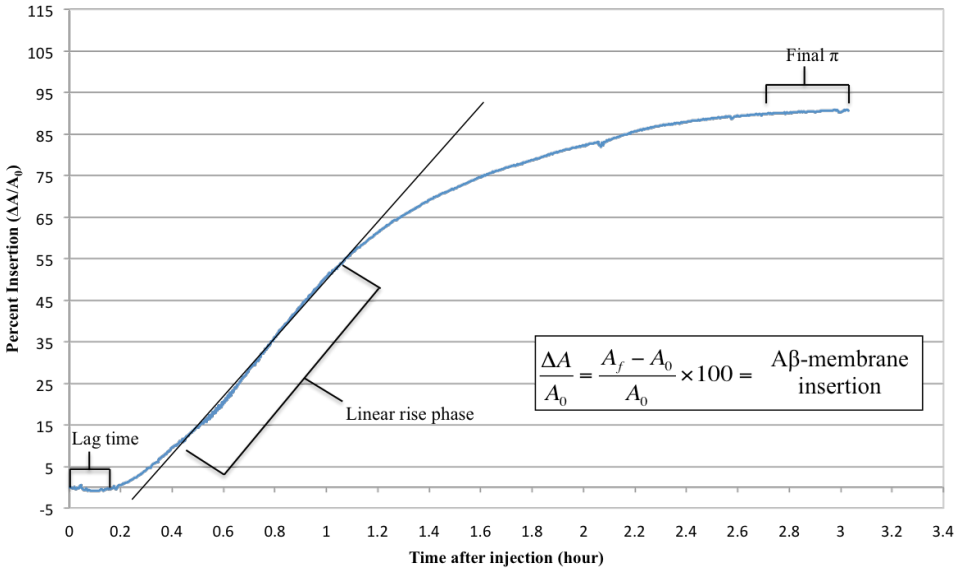

Figure 10: Example of Aβ40 percent insertion plot. The plot is the percent insertion over time after injection of Aβ40. The lag time is the time after injection before percent insertion begins increasing. The slope of the linear rise phase corresponds to the rate of insertion. The final percent insertion is the average of the last few minutes after insertion plateaus. (Inset) The percent insertion is calculated by taking the change in trough area divided by the trough area at injection.

2.3.3 Fluorescence Imaging Analysis

In a typical lipid compression isotherm, as the barriers are compressed, there are phase changes of the lipid monolayer (Section 2.3.2). With fluorescence imaging, these phases can be visualized. **Figure 11** shows a schematic of a typical compression isotherm with imaging. Again, the purple plate is the Wilhelmy plate that is attached to a force reader, which measures surface tension and displays it as surface pressure. The grey

barriers are closed together to compress the lipids and can be seen to form black condensed domains in fluorescence imaging with Texas Red-DHPE dye. The large Texas Red-DHPE molecules are excluded from the condensed domains due to the size of the head group, which is excluded from condensed domain due to steric effects of the large head group preventing tight packing of the alkyl chains on the tails. Because of this, the dye molecules partition to the fluid phase and comprise the light areas.

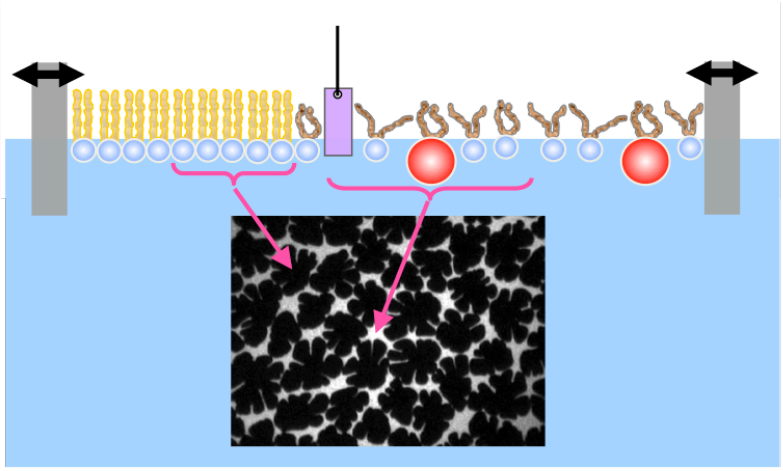

Figure 11: Schematic of fluorescence imaging of a lipid compression isotherm experiment. The purple plate is the Wilhelmy plate that is attached to a force reader, which measures surface tension and displays it as surface pressure. The grey barriers are closed together to compress the lipids and can be seen to form black condensed domains in fluorescence imaging with Texas Red dye. The large Texas Red-DHPE molecules are excluded from the condensed domains due to the size of the head group, which disallows condensed domain formation due to steric effects of the large head group preventing tight packing of the alkyl chains on the tails. Because of this, the dye molecules partition to the fluid phase and comprise the light areas.[28]

Using the photo editing software, ImageJ, fluorescence images of lipid monolayer were analyzed to determine the amount of light phase (liquid expanded phase) and dark phase (condensed phase) present. The image contrast was increased to better distinguish between the dark, condensed domains and the light, liquid phase. The software was then used to select all of the dark areas above a certain threshold and then the image was converted to black and white rather than grey and the percent black was determined using

the analysis software in ImageJ to determine the percentage of the image that was dark. An example is shown in **Figure 12**.

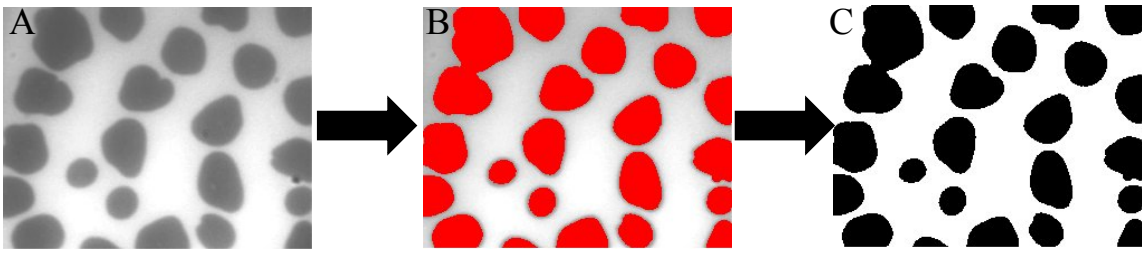

Figure 12: Example of ImageJ software analysis for determining the percent area light vs. dark. (A) the original image, with enhanced contrast. (B) The threshold selection for dark area is represented by the red coloring of the image. (C) Image J converts all areas that are not red into white, and the red areas into black to determine percent dark. This image shows a percent dark area, i.e. percent condensed domains, of 41.12%.

This imaging analysis was used solely in the compression isotherm experiments because the lipid domain edges were well resolved. In the Aβ40 insertion experiments, quantitative analysis of the images were not possible because the insertion of Aβ40 into the lipid domains made the images fuzzy since there was no longer a clear boundary to focus on.

3. Materials and Methods

3.1 Materials

The Aβ used for all experiments was the 40 amino acid long version (Aβ40) and was synthesized using 9-fluorenylmethoxycarbonyl chemistry on an Applied Biosystems 433A Peptide Synthesizer (Foster City, CA) at the University of Chicago. The crude Aβ40 received from the University of Chicago was purified with reverse-phase high performance liquid chromatography (HPLC) on a preparative Zorbax C18 column at 60°C. HPLC grade acetonitrile was purchased from OMNISOLV (Salisbury, NC). Triflouroacetic acid (TFA) was purchased from Thermo Fisher Scientific (Pittsburgh, PA). Other solvents used were: ACS grade acetone from VWR® (West Chester, PA),

HPLC grade chloroform from Sigma-Aldrich® (St. Louis, MO), ACS grade anhydrous ethyl alcohol (200 proof) from Pharmco-Aaper (Brookfield, CT), ACS grade methanol from Honeywell Burdick and Jackson® (Muskegon, MI). High purity, low endotoxin sucrose was purchased from Ferro-Pfanstiehl (Waukegan, IL). All water used was filtered through a Milli-Q Ultrapure water purification system (Millipore, Bedford, MA). 1,2-dimyristoyl-*sn*-glycero-3-phospho-(1'-rac-glycerol) (DMPG) and 1,2-dipalmitoyl-*sn*-glycero-3-phosphocholine (DPPC) lipids were purchased from Avanti Polar Lipids, Inc. (Alabaster, AL). Texas Red® 1,2-Dihexadecanoyl-*sn*-Glycero-3-Phosphoethanolamine (TR-DHPE) was purchased from Life Technologies (Grand Island, NY).

3.2 Aβ40 Purification

Purification of Aβ40 was conducted through HPLC. The mobile phase consisted of two solutions: a 0.1% TFA in water solution (Solution A) and a 0.1% TFA in acetonitrile solution (Solution B). The HPLC used a gradient program (**Table 1**) to mix the solutions and purified Aβ40 typically has a retention time of 22-24 minutes.

Table 1: Aβ40 purification gradient program on HPLC software

Mobile Phase	Time (minutes after start)
70% A / 30% B	0
70% A / 30% B	5
40% A / 60% B	50
0% A / 100% B	55
0% A / 100% B	65
70% A / 30% B	70

The Aβ40 samples were prepared for injection onto the HPLC column by measuring 15 mg of crude Aβ into an acid cleaned glass vial. 5 mL of a 7:3 Solution A:B

mixture was added to solubilize the crude peptide. The solution was heated at 60°C on a hot plate with stirring for 15 minutes to completely solubilize the crude peptide. The peptide was then divided into 5 1 mL aliquots and centrifuged at 13,000 rpm for 10 minutes. The supernatant was transferred to clean Eppendorf tubes and were then ready for injection. The HPLC column was cleaned before the first sample was injected according to the protocol in **Table 2**.

Table 2: HPLC column cleaning program

Mobile Phase	Time (minutes)
0% A / 100% B	5 minutes
50% A / 50% B	10 minutes
70% A / 30% B	10 minutes

4 mL of 7:3 A:B solution was added to the 1 mL crude peptide aliquot immediately prior to injection and solution was injected into the HPLC column through the manual injection port. The purification program from **Table 1** was started. Purified Aβ40 was collected in a clean glass vial from the peaks determined by the UV-Vis absorption spectra.

After collection of all of all purified samples, the samples were pooled into a large round-bottom flask. The acetonitrile was evaporated using a Rotovap at 25°C for 15 minutes or until half of the volume in the flask is evaporated. The remaining sample taken to the UNM Mass Spectrometry Facility in Clark Hall and was freeze-dried in a lyophilizer. The Labconco FreeZone Benchtop Freeze Dry System (Kansas City, Missouri) was manually turned on, and the refrigeration system was started half an hour before use. The temperature must get below -40°C before the vacuum can be turned on

(i.e. when the temperature light turns solid green). When the temperature reaches -40°C, the vacuum button was pressed to start the vacuum process. The vacuum must reach 0.120 mBar before the instrument is ready for use (i.e. when the vacuum light turns solid green). The sample was prepared for lyophilization by inserting the round-bottom flask into an ethanol and dry ice bath and continually rotating the flask in order to freeze the sample on the walls of the flask to increase the surface area. When completely frozen, the sample was attached to the port of the FreeZone lyophilizer using a glass stopcock connector and the knob on the sample port was turned towards the sample to start the freeze-drying process. The sample was then watched until the vacuum again drops below 0.120 mBar. After 24-48 hours, the dried, purified peptide was transferred to an acid cleaned 20 mL glass vial, weighed, sealed with Teflon tape, and stored at -80°C for further experiments. Typical yields of purified Aβ40 range between 25-35%. A small sample, either dried or solubilized in dimethyl sulfoxide (DMSO), was given to the UNM Mass Spectrometry Facility for protein molecular weight analysis with an LCT Premier Time of Flight Mass Spectrometer with Electrospray ionization source (Waters Corporation, Milford Massachusetts).

Prior to the Aβ40 adsorption and insertion experiments that follow, dried Aβ40 was removed from the freezer, weighed, and dissolved in DMSO to a concentration of 2 mg/mL and placed in a sonicating bath for 20-30 seconds. Aliquots for Langmuir trough experiments were prepared by transferring 24.52 μL of the solution to individual Eppendorf tubes. These were stored in the -20°C freezer until just prior to the experiment and the remaining dried peptide was stored again in the -80°C freezer.

3.3 Aβ40 Adsorption Isotherms

To ensure proper calibration of the Wilhelmy plate, calibration diagnostics were performed monthly. The Wilhelmy plate was placed on the force reader then the calibration diagnostic utility in the software was accessed and the first set-point weight was marked. A calibration weight that was provided by KSV was then placed on the force reader with the Wilhelmy plate and the second set-point weight was marked. In addition, prior to the start of every Langmuir trough experiment, calibration was checked again after cleaning. A pure water subphase was first added to the trough, ensuring complete whetting of the Wilhelmy plate and the pressure was set to zero. The water was then removed by aspiration. The new surface pressure was checked to ensure that it was within ±1 mN/m of the surface tension of water (72 mN/m). Ideally, water added back into the trough should read 0 mN/m without zeroing. If this measurement was not within the expected values, the calibration using the weight set points was repeated.

The Aβ40 adsorption experiments were all performed in a 45 mL subphase at a monitored with a temperature probe at 30 °C, unless otherwise stated. A circulating water bath underneath the trough was set to a temperature ranging from 33-36 °C in order to maintain 30°C in the trough. The final concentration of Aβ40 in all experiments was 250 nM. Each set of sucrose concentrations used as a subphase was prepared just prior to each experiment. The Langmuir trough, hydrophilic Delrin barriers, and Wilhelmy plate were cleaned thoroughly prior to each experiment. First, a lint-free cloth was whetted with chloroform and then used to wipe the trough. This was repeated three times. Next, a lint-free cloth was whetted with acetone and the trough was wiped three times. Then, the trough was filled with clean MilliQ water and aspirated several times. Next, the Delrin

barriers and temperature probe were sprayed with acetone, ethanol, and finally MilliQ water. The Wilhelmy plate was removed from ethanol storage and sprayed with ethanol, acetone, and then water.[27]

The Langmuir trough was filled with 45 mL of subphase, ranging from 0-1.0 M sucrose, and the surface was tested for cleanliness compressing the barriers over the clean subphase while measuring the surface pressure. A surface pressure below ±0.6 mN/m indicated a clean surface. Once the surface was determined to be satisfactorily clean, the trough barriers were compressed to, and held constant at, a trough area of 50 cm^2 using the associated software. The surface pressure and temperature were given time to equilibrate. During this time, an individual 2 mg/ml Aβ40 aliquot in DMSO was removed from the freezer and allowed to thaw. It was then placed in a sonicating bath for 30 seconds and diluted with the subphase to a total volume of 300 µL and allowed to equilibrate for 30 minutes. This solution was then injected slowly into the trough subphase through an injection port over a period of 20 seconds, giving a final trough concentration of Aβ40 of 250 nM. The surface pressure (π) was continuously measured against time throughout the experiment. The experiment was concluded when the surface pressure plateaued at a final π.

3.4 Lipid Monolayer Compression Isotherms

The DMPG and DPPC lipid compression isotherm experiments were all performed in a 45 mL subphase at a monitored 30°C, unless otherwise stated. Each set of sucrose concentrations used as a subphase was prepared just prior to each experiment. The Langmuir trough (KSV), hydrophilic Delrin barriers, and Wilhelmy plate were

cleaned thoroughly prior to each experiment. Cleanliness testing and calibration were all performed as previously discussed.

The lipids used for the experiments (DMPG and DPPC) were prepared as follows. ~10 mg of powder lipid was weighed out into an acid cleaned glass vial. 3 mL of a 7:3 chloroform:methanol solution was added to dissolve the lipid to a final concentration of at least 3 mg/mL and then placed in a sonicating bath for 3 minutes. This stock was stored at -20°C. The spreading solution was prepared from the stock solution by diluting a portion of the stock solution and 0.5 mg/mL Texas Red-DHPE (TR-DHPE) in chloroform, with 7:3 chloroform:methanol to a final concentration of 0.2 mg/mL lipid with 0.5 mol% TR-DHPE. Proper care was taken to ensure the fluorescent TR-DHPE was not exposed to light. The spreading solution was stored at -20 °C until just prior to use.

The Langmuir trough was filled with 45 mL of subphase, ranging from 0-1.0 M sucrose and the surface was tested for cleanliness. The lipid spreading solution was removed from the freezer and placed in a sonicating bath for 30 seconds. 25-35 μL of the spreading solution was spread on the surface of the subphase with a syringe. This setup was allowed to equilibrate for 10-15 minutes. Once equilibrated, the barriers were slowly compressed at a rate of 2 mm/minute until a surface pressure of 60 mN/m was obtained. The time, surface pressure, area/molecule, trough area, and temperature were continuously measured against the area/molecule of the lipid monolayer.

3.5 Aβ40 Insertion into Lipid Monolayers

The Aβ40 insertion into DMPG and DPPC monolayer experiments were all performed in a 45 mL subphase at a monitored 30 °C, unless otherwise stated. The final

concentration of Aβ40 in all experiments was 250 nM. Each set of sucrose concentrations used as a subphase was prepared just prior to each experiment. The lipid stock solutions and spreading solutions were all prepared as described in *Section 2*.3. The Langmuir trough, hydrophilic Delrin barriers, and Wilhelmy plate were cleaned thoroughly prior to each experiment. Cleanliness testing and was performed as previously discussed.

The Langmuir trough was filled with 45 mL of subphase, ranging from 0-1.0 M sucrose, and the surface was tested for cleanliness. The lipid spreading solution was removed from the freezer and placed in a sonicating bath for 30 seconds. 25-35 μL of the spreading solution was spread on the surface of the subphase with a syringe. This setup was allowed to equilibrate for 10-15 minutes. Once equilibrated, the barriers were slowly compressed at a rate of 2 mm/minute until a surface pressure of 25 mN/m, unless otherwise stated, was obtained. This surface pressure was held constant by the software and allowed to equilibrate at 25 mN/m for 10-15 minutes. During the compression, an aliquot of Aβ40 was removed from the freezer, allowed to thaw, and placed in a sonicating bath for 30 seconds. The aliquot was then diluted with subphase to a volume of 300 μL and allowed to equilibrate for 30 minutes. The solution was then injected slowly into the subphase through the injection port. The change in surface area over time was measured continuously until the surface area reached a plateau. Fluorescence imaging was taken at regular intervals prior to and after injection of Aβ40.

3.6 Fluorescence Imaging

During the compression isotherm and Aβ40 insertion experiments, fluorescence images of the lipid monolayer were taken at regular intervals. A 50X long objective was mounted on an Olympus IX51 (Center Valley, Pennsylvania) inverted fluorescence light

microscope. The Langmuir trough was mounted on a motorized xyz translational stage. The z-axis was used for focusing and the xy axes are for translating the trough to find different regions of the monolayer. A 100 W mercury apo (Olympus U-LH100HGAPO) lamp is used for fluorescence excitement. A Texas Red filter cube was used to filter the emitted fluorescence at a wavelength of 615 nm. Fluorescence is collected on an Olympus camera (U-TV0-63XC) camera that collects a series of 25 images each time images are collected in the QCapture Pro 6.0 software. Data analysis was performed using ImageJ.

4. Results

4.1 Mass Spectrometry

Time of flight (ToF) mass spectrometry analysis with electrospray ionization (EI) was performed by the UNM Mass Spectrometry Facility on purified Aβ40 to ensure the molecular weight of the purified Aβ40 sample obtained from HPLC and lyophilization of crude Aβ40. The expected molecular weight of the purified Aβ40 was 4329.86 Daltons, and the molecular weight obtained for our sample was 4329.3 Daltons, with very minimal peaks of other molecular weights (See **Figure 13**). The bottom spectrum is the raw data of the EI response of the protein. Several peaks on the mass-to-charge ratio (m/z) axis were observed because the protein can carry several charges when ionized in an EI source, giving a peak for the molecular weight divided by successive numbers of charges. As the spectra move to the right, each successive peak has additional charge. The top graph is the transformed spectra, giving calculated molecular weight for Aβ40 based on the peaks with multiple charges that were detected in the raw data. The other, smaller peaks on the molecular mass profile graph indicate the presence of isotopes of

different molecular weights. These other peaks are in relatively small and indicate that our purification process worked well. All other batches of purified Aβ40 showed a similar level of purification (data not shown).

Other analysis of Aβ40 through ToF mass spectrometry included analysis of a purified sample in different solutions, including dried Aβ40, Aβ40 in DMSO, Aβ40 in water, Aβ40 in 0.25 M sucrose, and finally Aβ40 in 0.5M sucrose (data not shown). These samples were incubated for 1-2 hours before they were analyzed. The molecular weight in each solution was within ±1 Dalton of the expected molecular weight (4329.86 Daltons), indicating that the solutions had not exposed Aβ40 to conditions that would allow for reactions that would change the composition of our purified sample.

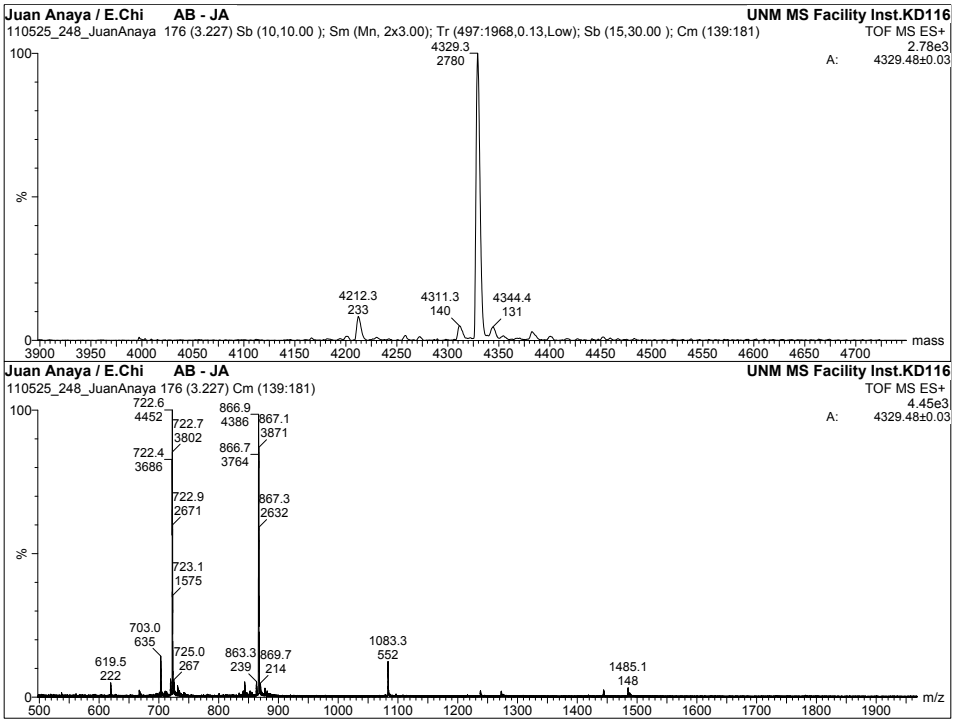

Figure 13: Time of Flight mass spectrometry with Electrospray ionization analysis of purified Aβ40. Dried Aβ40 was given to the UNM Mass Spectrometry Facility for protein molecular weight analysis. (Bottom) Represents the raw spectra of the mass-to-charge ratio of the EI response of the protein. Several peaks are observed because Aβ40 can carry several charges when ionized, giving a peak for m/z increasing by one additional charge per successive peak group. (Top) Transformation of the raw data into a calculated molecular weight of the protein based on all the peaks with multiple charges.

4.2 Langmuir Trough Adsorption Data

The surface activity of Aβ40 was assessed by measuring the final surface pressure reached by the adsorption of Aβ40 from the bulk aqueous phase to the air/subphase interface. Adsorption isotherms of Aβ40 to the clean air/subphase interface were collected using a Langmuir trough to determine how changes in concentration of the osmolyte sucrose in the subphase affect the adsorption kinetics and equilibrium of Aβ40. This will help assess the surface activity of Aβ40 by measuring the changes in the surface pressure (π) over a given time. The adsorption of Aβ40 for subphases with varying sucrose concentration was measured to determine the effect of the preferential exclusion and volume exclusion theories on the surface activity of Aβ40 at the idealized air/subphase interface.

4.2.1 Adsorption Isotherm

All adsorption isotherm experiments were conducted according to the protocol in *Section 3*.3. **Figure 14** shows the adsorption isotherms on the following concentrations of sucrose: 0, 0.1, 0.25, 0.5, 0.75 and 1.0 M. The volume of subphase used was 45 mL and the final concentration of Aβ40 in the trough was 250 nM. All experiments were conducted at 30±0.5° C and conducted at a trough area of 50 cm^2.

After Aβ40 was injected into the subphase, the peptide adsorbed to the air/subphase interface, which resulted in an increase in the surface pressure. The adsorption isotherm of water in every set of experiments showed characteristic adsorption isotherm behavior, such as a lag time of close to 20 minutes before surface pressure increases, followed by a fast rise in surface pressure, and, finally, a plateau in surface pressure.[20,28] **Figure 14** is an example of a complete set of Langmuir trough adsorption

isotherms after injection of Aβ40. The trends that can be determined from this figure are that in water (green line) the adsorption of Aβ40 exhibited the longest lag time before adsorption begins and the lag time is reduced as sucrose concentration increases. The final equilibrium adsorption pressure also increases as sucrose concentration increases and the rate of adsorption (the slope of the linear portion of the surface pressure increase) also appears to increase with sucrose concentration.

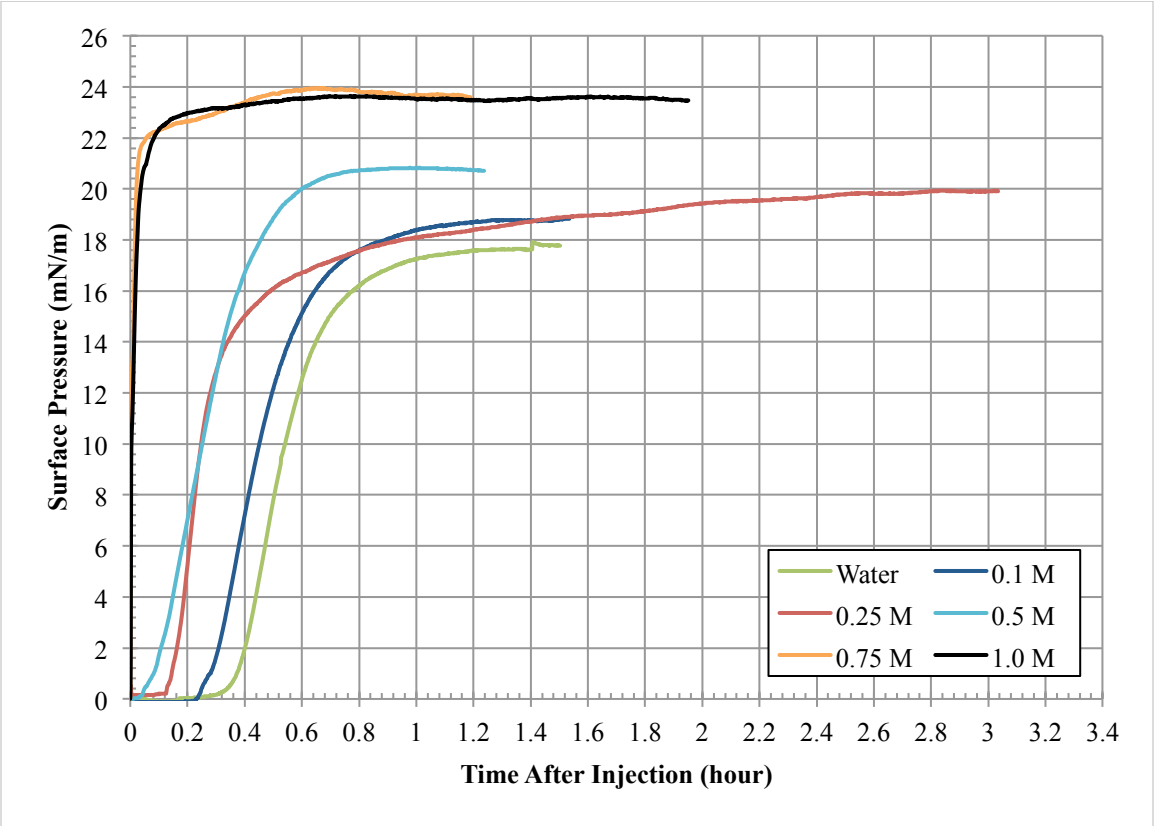

Figure 14: Adsorption isotherms surface pressure vs. time after injection of Aβ40 in varying sucrose subphases. Final Aβ in trough is 250 nM, volume of subphase is 45 mL, all experiments conducted at a trough area of 50 cm^2 and a trough temperature of 30±0.5 °C. Increasing sucrose concentration increases adsorption rate, final Aβ40 adsorption pressure, and decreases lag time before adsorption occurs.

4.2.2 Final Surface Pressure of Aβ40 Adsorption Isotherms

The data was analyzed as described in *Section 2.3.1* to determine the average final equilibrium surface pressure, lag time, and rate of adsorption (See **Figures 15, 16,** and

17, respectively). Adsorption isotherms for each concentration of sucrose were repeated in triplicate, unless otherwise noted.

The data from **Figure 14** was analyzed to represent final equilibrium pressure for three sets of adsorption isotherms (**Figure 15**). The error bars show one standard deviation. The final adsorption pressure was calculated, as previously described, by taking the average of the last few minutes of the surface pressure in the adsorption isotherms (**Figure 14**), well after the system equilibrated. There was a steady increase of final adsorption pressure Aβ40 from 0 M sucrose (17.65±0.21 mN/m) to 1 M sucrose (23.09±0.59 mN/m), indicating that the presence of sucrose increased the final equilibrium surface pressure.

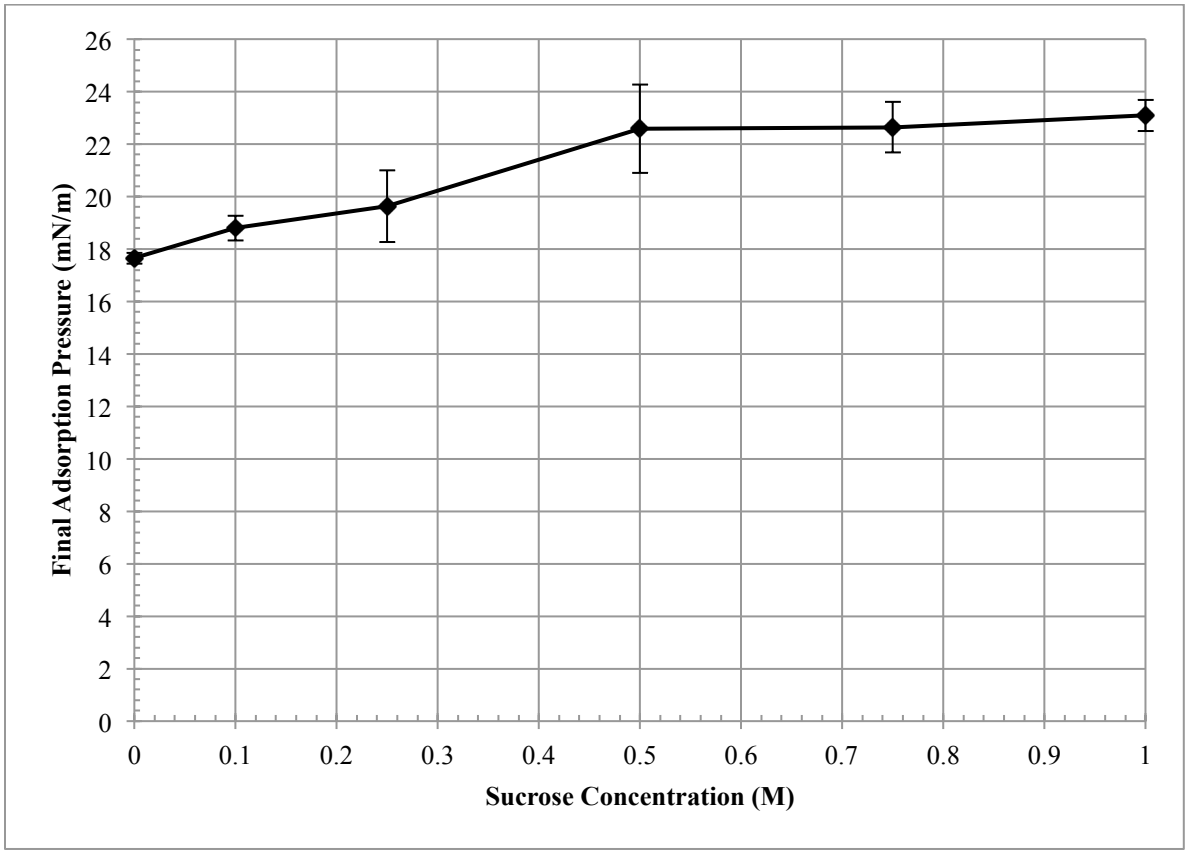

Figure 15: Final adsorption pressure vs. sucrose concentration of Aβ40 adsorption isotherms. Final pressure increases as sucrose concentration increases for Aβ40 adsorption to the air/subphase interface at 30±0.5 °C. Error bars indicated one standard deviation of triplicate repeats.

4.2.3. Lag Time of Aβ40 Adsorption Isotherms

Another characteristic of the adsorption isotherm that was analyzed was the lag time between the injection of Aβ40 and the observed increase in surface pressure (**Figure 16).** The lag time was calculated as previously described in *Section 2.3.1* by increasing the magnification of the plot in the adsorption isotherm around the area where surface pressure there was a step change in the surface pressure, i.e., the point where a slight drift upwards changes to a fast increase in surface pressure. This lag time indicates the time required for Aβ40 to reach the surface of the subphase and begin reducing the surface tension of clean air/subphase interface(σ_0), thus increasing the surface pressure, π ($\pi = \sigma_0 - \sigma$). In a pure water subphase, the lag time should be 15-20 minutes,[20,28] but our lag time in water was consistently less (12.89±0.78 minutes). At low concentrations of sucrose (0.1 M), the change in lag time was minimal (12.87±0.28 minutes). As sucrose concentration increased, the lag time was significantly reduced, where at high sucrose concentrations, surface pressure increased before the injection was even completed. The average lag time in 1.0 M sucrose was 0.083±0.0005 minutes (4.98±0.03 seconds), which was at the limit of detection for the recording software. The injection was carried out over 20-30 seconds so, at higher concentrations, Aβ40 reached the surface before the injection was completed.

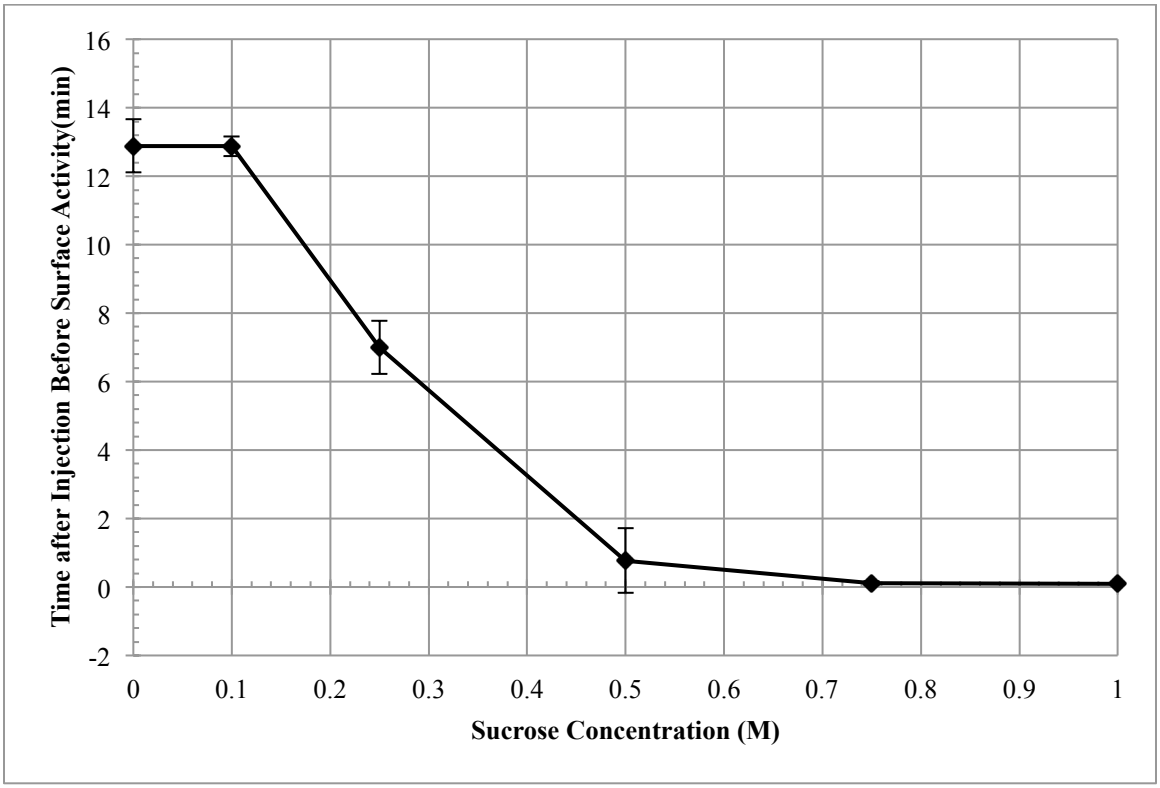

Figure 16: Lag time vs. sucrose concentration of Aβ40 adsorption isotherms. Lag time decreases as sucrose concentration increases for Aβ40 adsorption to the air/subphase interface at 30±0.5 °C. Error bars indicated one standard deviation of triplicate repeats.

4.2.4 – Rate of Aβ40 Adsorption in Adsorption Isotherms

Figure 17 shows the adsorption rate as a function of sucrose concentration. The rate of adsorption was calculated as previously described in *Section 2.3.1* by taking the slope of the line of the linear portion of each adsorption isotherm. This indicates how quickly Aβ40 adsorbs to the air/subphase interface once adsorption begins. In water, the rate of adsorption of Aβ40 in the linear portion of the isotherm was an average rate of 0.79±0.17 (mN/m)/min, while at 1.0 M sucrose, the average rate of adsorption was 96.4±7.68 (mN/m)/min. This was estimated from the observation that the surface pressure was already in the 14-18 mN/m range within 30 seconds of injection. At low concentrations, Aβ40 adsorbs at much slower rates than at higher sucrose concentrations, which was expected. The rate increases consistently increased as the sucrose

concentration increases, but there is a substantial increase between 0.75 and 1.0 M sucrose.

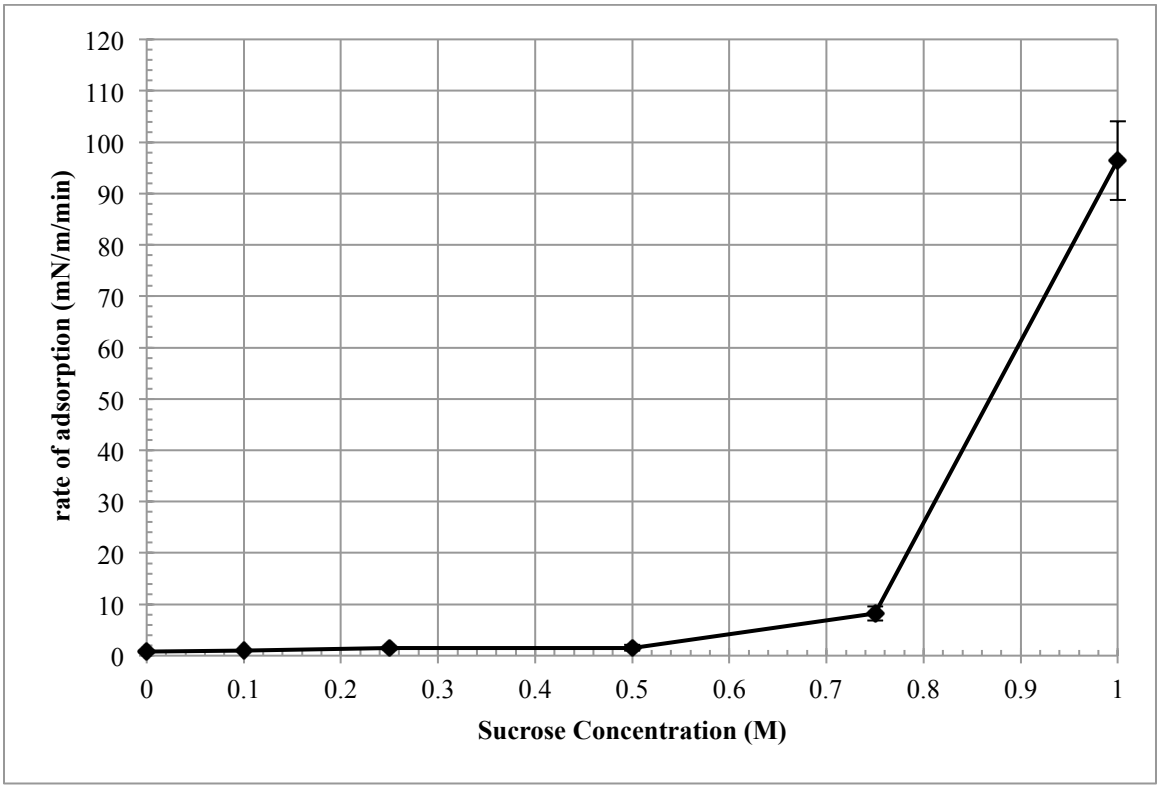

Figure 17: Adsorption rate vs. sucrose concentration of Aβ40 adsorption isotherms. Rate of adsorption increases as sucrose concentration increases for Aβ adsorption to air/subphase interface at 30±0.5 °C. Error bars indicated one standard deviation of triplicate repeats.

4.3 Langmuir Model Membrane Compression Isotherms

While this idealized air/subphase interface is indicative of increased Aβ40 surface activity, to understand how Aβ40 interacts with lipid membranes in a cellular environment, it is important to investigate Aβ40 interactions with membranes. To explore the effects of sucrose on the ability of Aβ40 to insert into lipids, the Langmuir trough was used to determine the extent of Aβ40 insertion into a model membrane, lipid monolayers at the air/subphase interface. Before that was completed, however, it was important to understand how different concentrations of sucrose affected the lipid monolayer.

4.3.1. DMPG Compression Isotherm

A series of lipid monolayer compression isotherms with varying sucrose subphase concentrations was completed for the monolayer used, the anionic 1,2-dimyristoyl-sn-glycero-3-phosphoglycerol (DMPG). The experiments were set up as previously described in *Section 3.4*. In short, 0.2 mg/ml DMPG with 0.5 mol% Texas Red-DHPE fluorescent dye was spread on top of a 45 ml subphase of varying sucrose concentrations in the Langmuir trough at 30°C. The trough barriers were then compressed until the surface pressure reached 50 mN/m. The resulting isotherm and fluorescence images were analyzed. **Figure 18** shows the compression isotherms of DMPG monolayers as sucrose concentration increases.

The important features in this set of experiments is the increase in the area per molecule ($Å^2$/molecule) where the gas phase lipid molecules begin to interact with each other, increasing the surface pressure (liftoff), as well as the surface pressure where condensed domain formation occurs (onset of domain formation). This liftoff area corresponds to the minimal surface density at which lipids begin to interact[37] and it increases significantly as sucrose concentration increases. The onset of domain formation was determined visually with fluorescence imaging. Also of note is the disappearance of the plateau that is associated with the liquid expanded to liquid condensed phase transition.

The data in **Figure 18** was analyzed as described in *Section 2.3.2* to determine the onset of domain formation and the point of liftoff (See **Figures 19** and **20**, respectively). Compression isotherms for DMPG on each concentration of sucrose were repeated in triplicate, unless otherwise noted. Error bars represent one standard deviation.

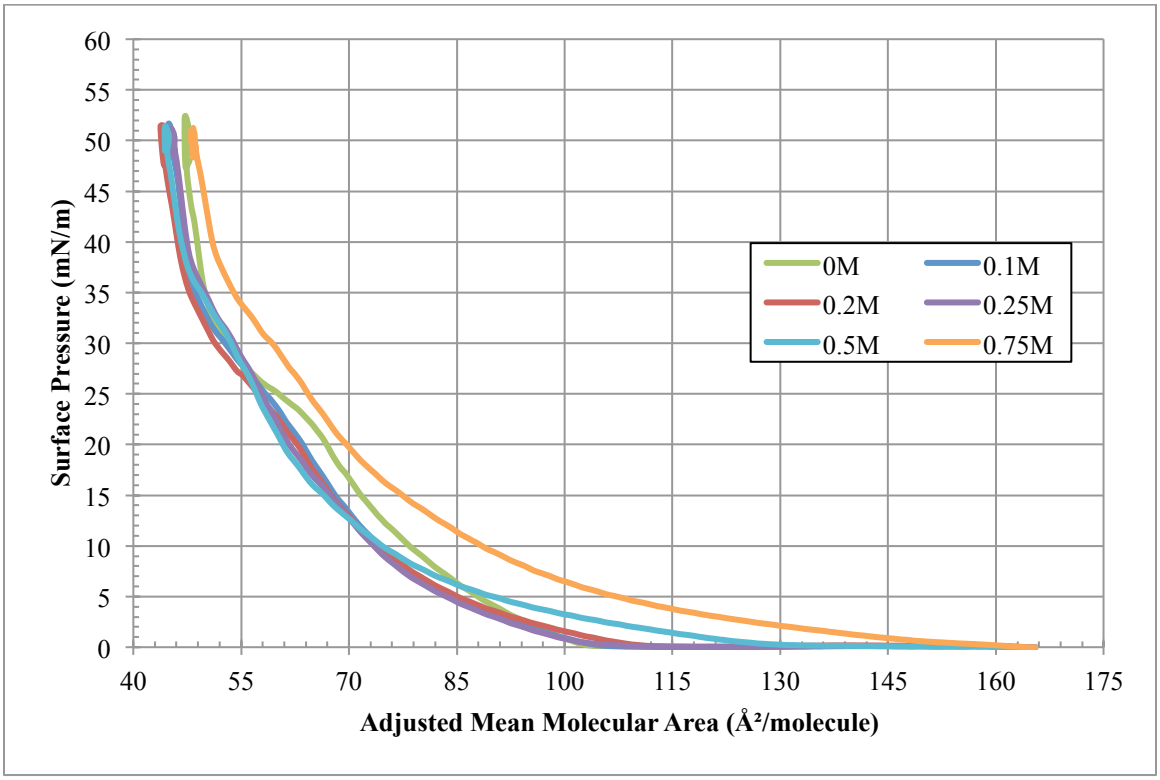

Figure 18: DMPG compression isotherms surface pressure vs. area per molecule in varying sucrose subphases. DMPG spreading concentration is 0.2 mg/mL with 0.5 mol% Texas Red-DHPE, volume of subphase is 45 mL, conducted at a trough temperature of 30±0.5 °C. Increasing sucrose concentration increases the area per molecule where liftoff occurs. There is also a disappearance of the 1st order phase transition with the addition of sucrose.

4.3.2. DMPG Isotherm Onset of Domain Formation

The data in **Figure 18** was analyzed to represent the onset of domain formation for five sets of DMPG compression isotherms (**Figure 19**). The error bars represent one standard deviation. The onset of domain formation was determined using fluorescence microscopy with the camera attached to the fluorescence microscope to determine the point where condensed domain formation begins during the DMPG compression isotherm experiments (**Figure 18**). The surface pressure where domain formation first occurred was noted for each concentration of sucrose.

There was a significant decrease of the surface pressure where domain formation began from 0 M sucrose (21.83±1.44 mN/m) to 1 M sucrose (11.68±1.48 mN/m). This

significant decrease in the pressure where condensed domains begin to form indicates that the lipid monolayer undergoes a phase transition from the liquid expanded phase to a liquid condensed phase at a much lower surface pressure in the presence of sucrose. This suggests that sucrose affects the ordering of the lipid molecule tail groups, allowing for the hydrophobic interactions that are present in condensed domains to become more significant at lower pressures.[37]

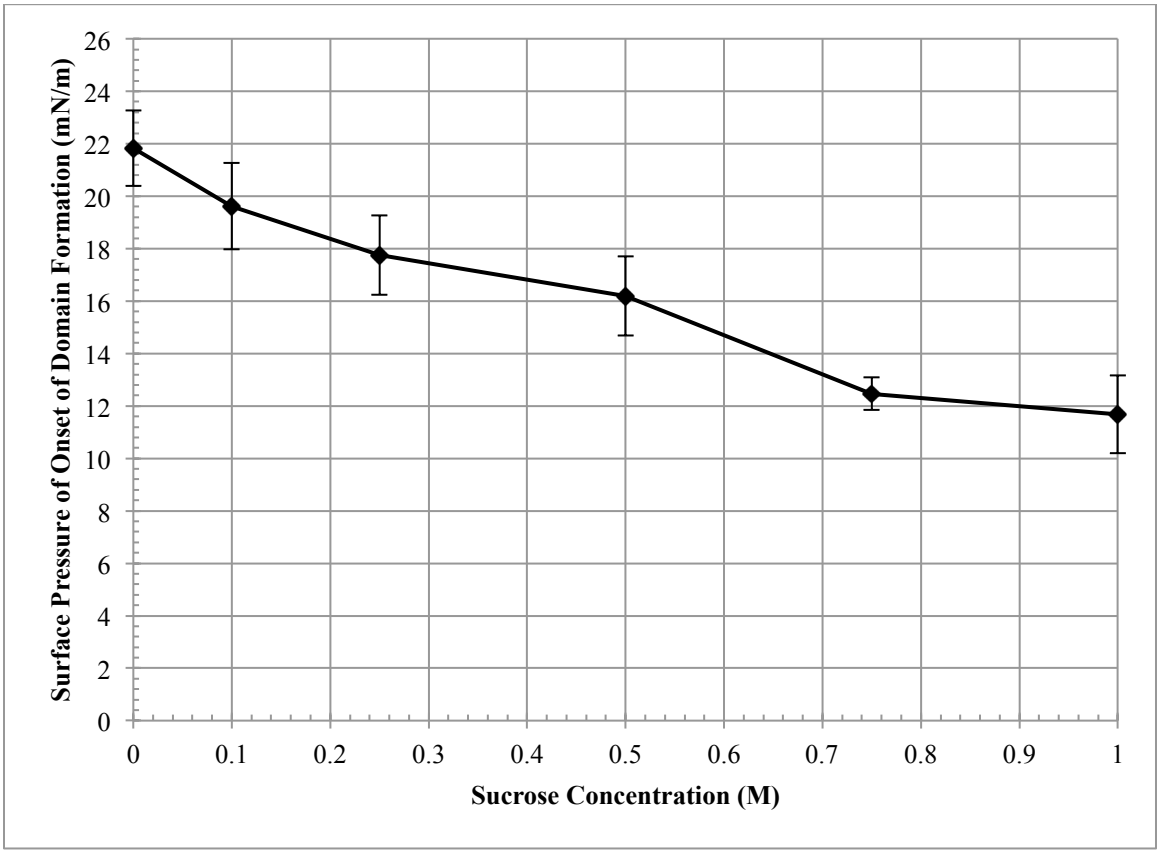

Figure 19: The surface pressure of the onset of domain formation vs. sucrose concentration of DMPG compression isotherms. The onset of domain formation occurs at a lower surface pressure in DMPG monolayers as sucrose concentration increases at 30±0.5 °C. Error bars indicated one standard deviation of triplicate repeats.

4.3.4. DMPG Isotherm Area per Molecule of Liftoff

Another characteristic of the DMPG compression isotherms that was analyzed was the area per molecule ($Å^2$/molecule) where the gas phase lipid molecules begin to

interact with each other, increasing the surface pressure (liftoff) (**Figure 20**). The area/molecule of liftoff was determined as previously described in *Section 2.3.2.*

The liftoff was calculated from eight different DMPG compression isotherm experiments. There was an increase in the area per molecule of liftoff from 0 M sucrose (106.14±5.97 $Å^2$/molecule) to 1.0 M sucrose (152.35±22.31 $Å^2$/molecule). The increase in liftoff area occurred early on and then stabilized as sucrose concentration increased. There was a very large error in determining the liftoff area because several isotherms would reach liftoff very early even on a clean surface. The trend, however, was towards liftoff occurring at a larger area/molecule, which suggests that sucrose affects the long-range lipid-lipid interactions.

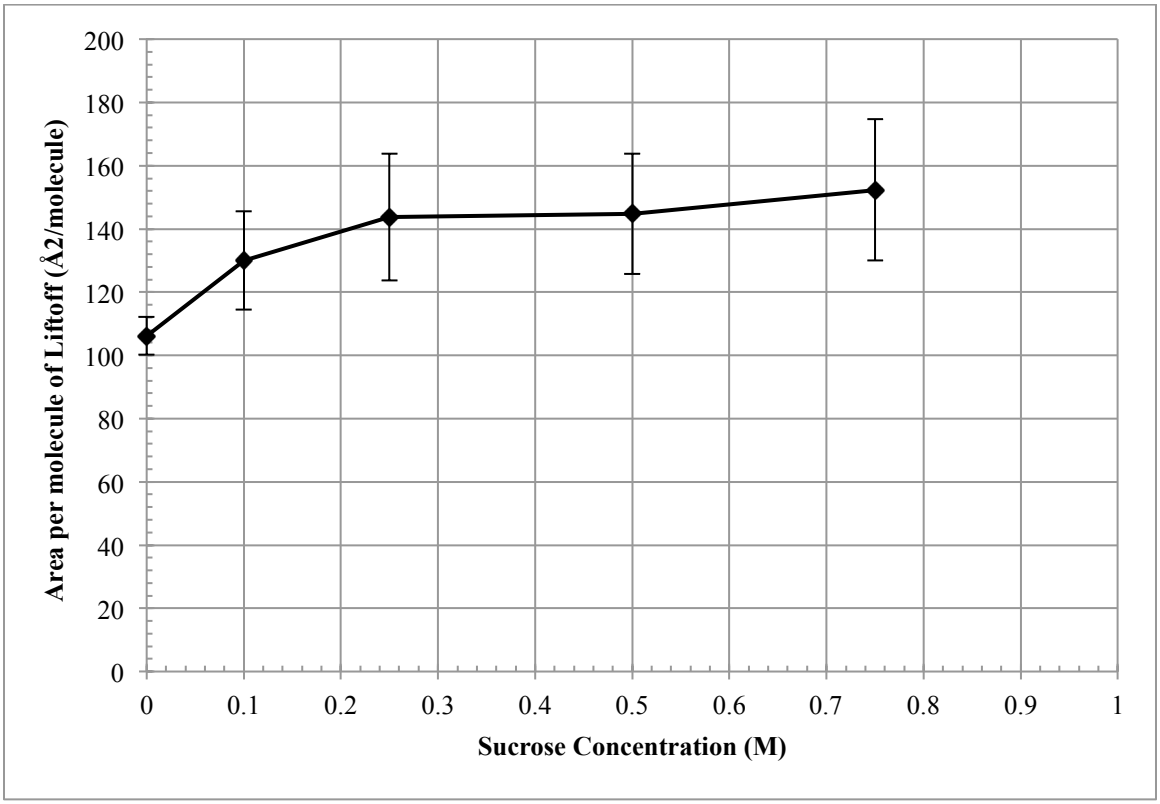

Figure 20: The area per molecule of liftoff vs. sucrose concentration of DMPG compression isotherms. Liftoff occurs at a higher area/molecule in DMPG isotherms as sucrose concentration increases at 30±0.5°C. Error bars indicated one standard deviation of triplicate repeats.

4.3.5. DMPG Isotherm Fluorescence Imaging

The graphs of the individual isotherms (**Figures 21-25**) were prepared to show the fluorescence imaging of the monolayer with compression (a decrease in area/molecule). The isotherm undergoes phase transitions as described in Section 2.3.2. In short, the fluorophor Texas Red-DHPE, which fluoresces at 615 nm, is incorporated in the DMPG spreading solution, which is spread on the clean subphase. After spreading, images were taken before compression began. At a large area/molecule, lipids were in the gas phase (bright area of image) and the areas that are dark were areas without lipids. As the surface is compressed, the lipid film became completely bright at liftoff, indicating that the entire film was composed of lipid in the liquid expanded phase. As the lipid was compressed further, areas of compact lipid domains began to form (onset of domain formation) because the large head group of the Texas Red-DHPE (TR-DHPE) was excluded from the condensed domain due to steric hindrance because the DMPG molecules pack very tightly due to hydrophobic interactions of the long chain hydrocarbons. As can be seen in the figures, the onset of domain formation occurs at lower surface pressure as sucrose concentration increases. The condensed domains appear to fill a larger percentage of the viewing area as sucrose concentration increases and there are many domains that are not uniform in size, which is unexpected.

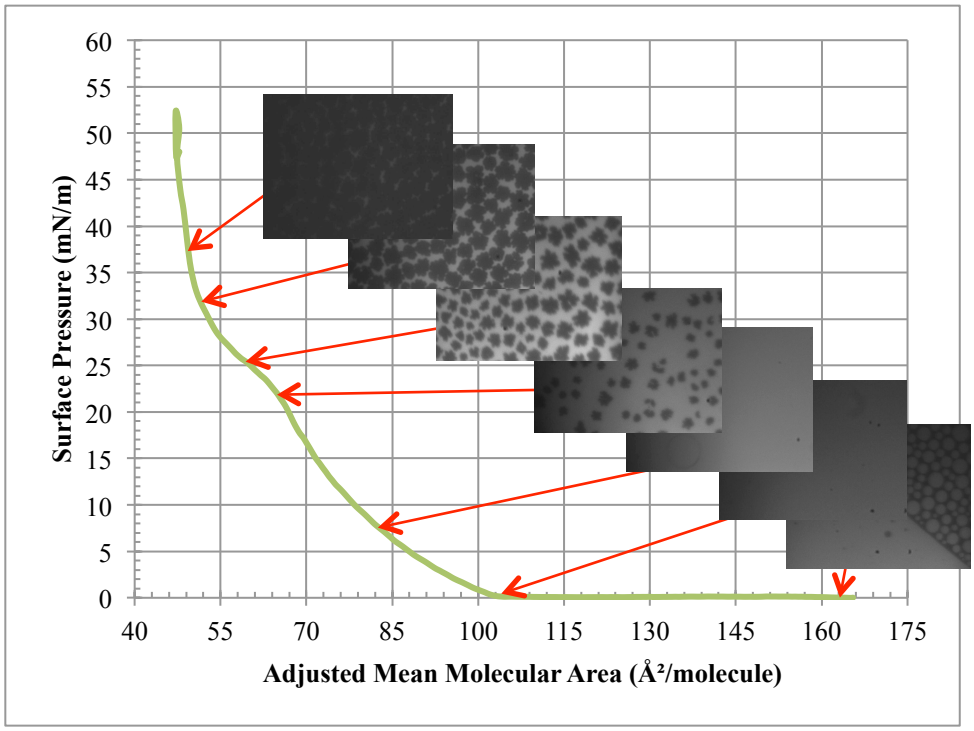

Figure 21: DMPG compression isotherm on water at 30±0.5 °C. 0.2 mg/mL DMPG with 0.5 mol% TR-DHPE was spread on the clean subphase. Onset of domain formation occurs at 22.6 mN/m and liftoff occurs at 105.6 Å²/molecule. Fluorescence images were taken at several time points to show the progression of domain formation.

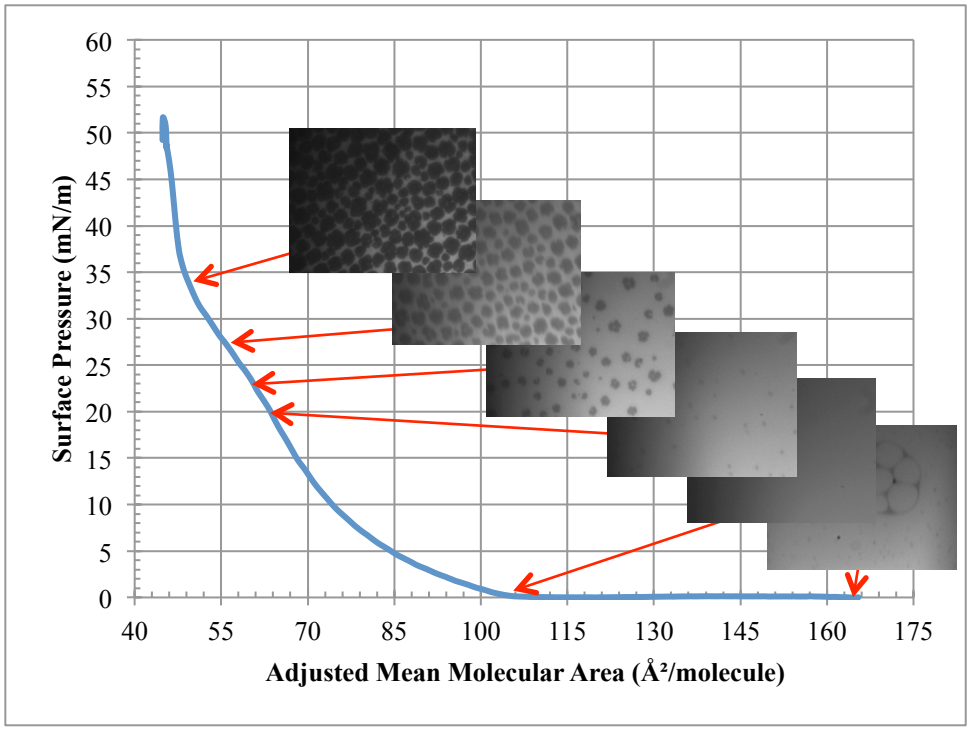

Figure 22: DMPG compression isotherm on 0.1 M sucrose at 30±0.5 °C. 0.2 mg/mL DMPG with 0.5 mol% TR-DHPE was spread on the clean subphase. Onset of domain formation occurs at 20.4 mN/m and liftoff occurs at 107.35 Å²/molecule. Fluorescence images were taken at several time points to show the progression of domain formation.

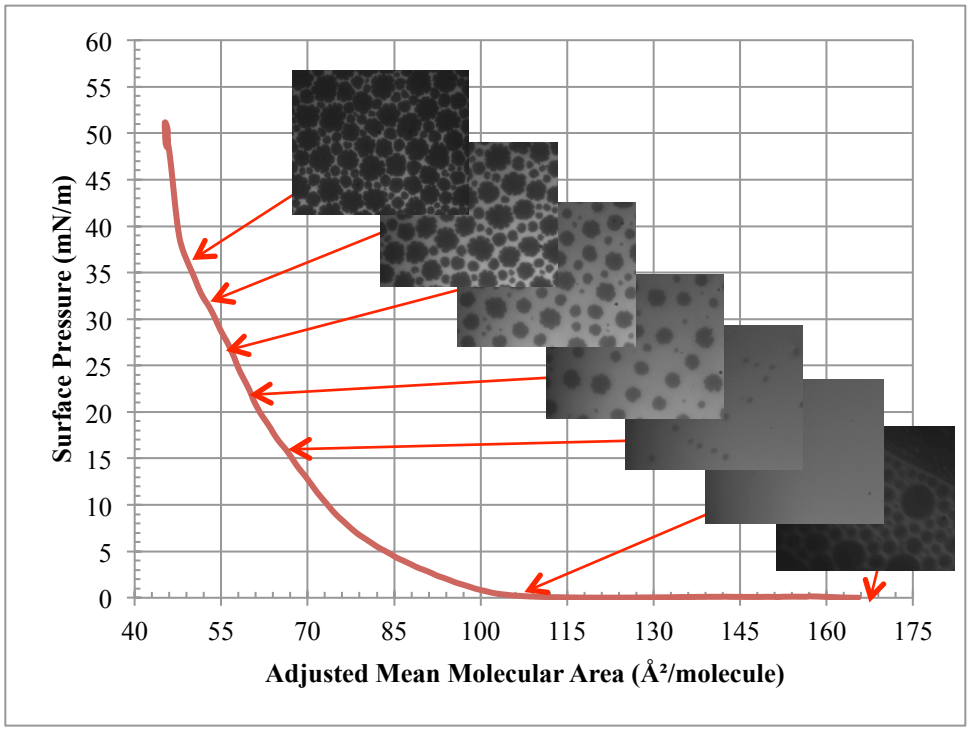

Figure 23: DMPG compression isotherm on 0.25 M sucrose at 30±0.5 °C. 0.2 mg/mL DMPG with 0.5 mol% TR-DHPE was spread on the clean subphase. Onset of domain formation occurs at 16.8 mN/m and liftoff occurs at 109 Å²/molecule. Fluorescence images were taken at several time points to show the progression of domain formation.

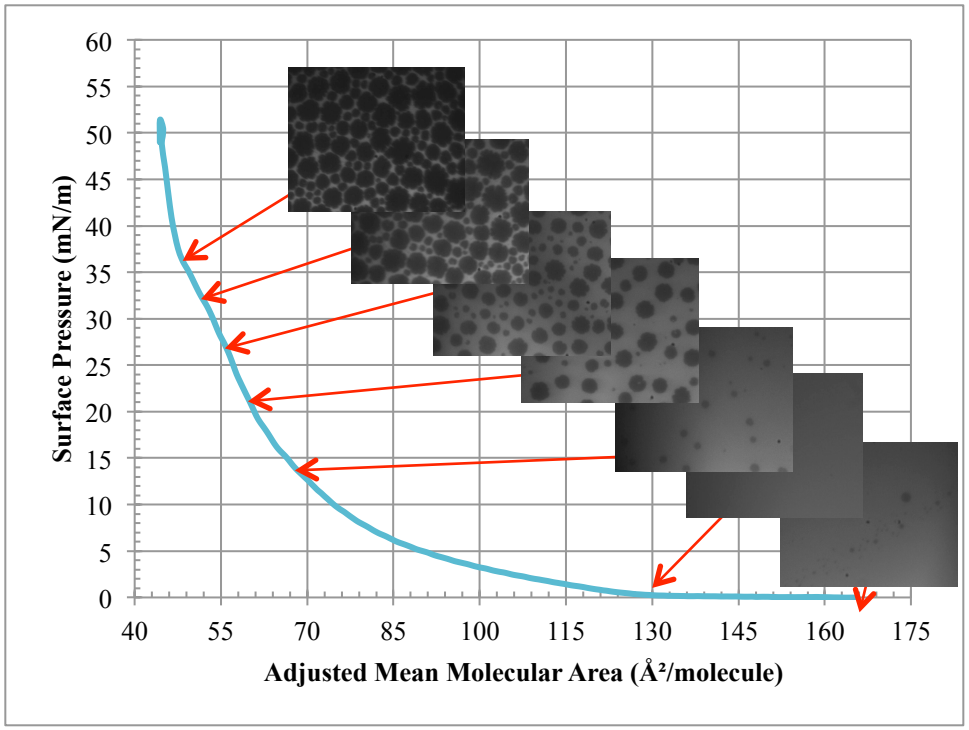

Figure 24: DMPG compression isotherm on 0.5 M sucrose at 30±0.5 °C. 0.2 mg/mL DMPG with 0.5 mol% TR-DHPE was spread on the clean subphase. Onset of domain formation occurs at 14.2 mN/m and liftoff occurs at 129.6 Å²/molecule. Fluorescence images were taken at several time points to show the progression of domain formation.

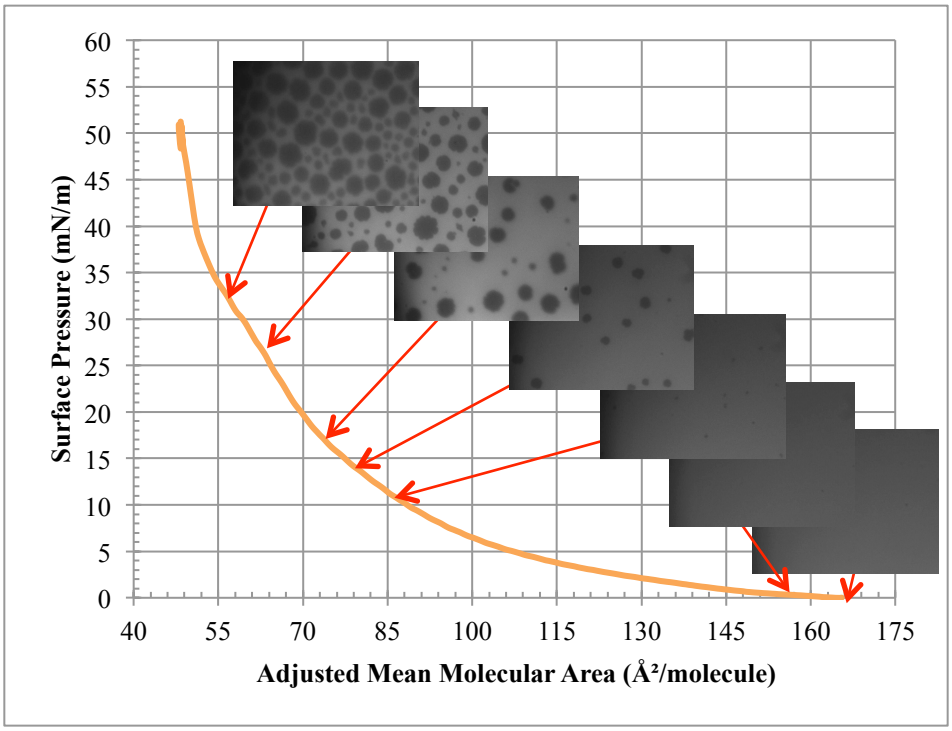

Figure 25: DMPG compression isotherm on 0.75 M sucrose at 30±0.5 °C. 0.2 mg/mL DMPG with 0.5 mol% TR-DHPE was spread on the clean subphase. Onset of domain formation occurs at 12.21 mN/m and liftoff occurs at 158.3 Å²/molecule. Fluorescence images were taken at several time points to show the progression of domain formation.

Figure 26 is a plot of the compressibility of the DMPG monolayers at the surface pressures 5, 25 and 30 mN/m. Compressibility was calculated by taking the change in the area at the specified surface pressure and multiplying by one over the area at that surface pressure. At a low surface pressure of 5 mN/m, the DMPG monolayer is more compressible as sucrose concentrations increase, at a compressibility of 0.0243±0.000145 m/mN in water to a compressibility of 0.0549±0.000649 m/mN in 1.0 M sucrose. At high surface pressures that are relevant to the pressures used for insertion experiments (25 and 30 mN/m), the compressibility decreases with increasing sucrose concentrations (from 0.0222±0.000527 m/mN in water to 0.0115±0.000237 m/mN in 0.5 M sucrose at 25 mN/m).

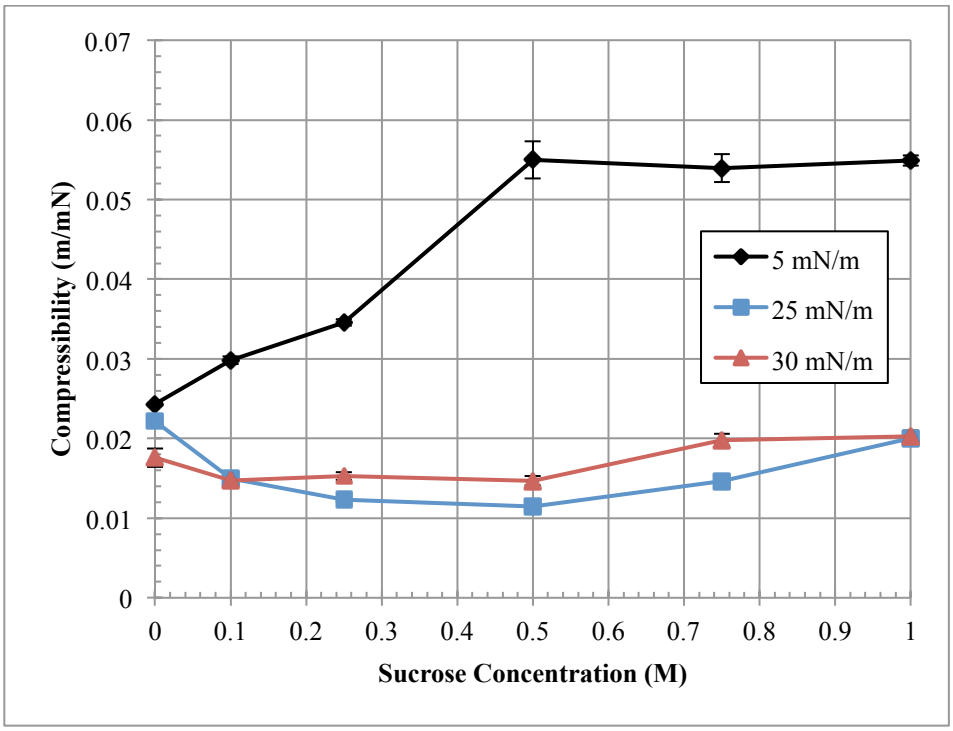

Figure 26: DMPG compressibility at various surface pressures and sucrose concentrations. The compressibility was calculated as the change in surface area with respect to surface pressure multiplied by the one over the area (C_s=1/A*(dA/dπ). DMPG is highly compressible at low surface pressure in sucrose and less compressible at high surface pressure than water.

Figure 27 is a set of fluorescent images of DMPG compression isotherms taken at 25 mN/m and 30 mN/m for varying sucrose concentrations. The images at 25 mN/m show a progression of increasing density of condensed domains. Another interesting note is that domains were not uniform in size in solutions containing sucrose. ImageJ photo editing software was used as described in *Section 2.3*.3 to determine the percentage of condensed domains as a function of sucrose concentration at both surface pressures. At 25 mN/m, the relative amount of condensed domains tends to increase with sucrose concentration. At 30 mN/m, the change in condensed domain percentage is minimal.

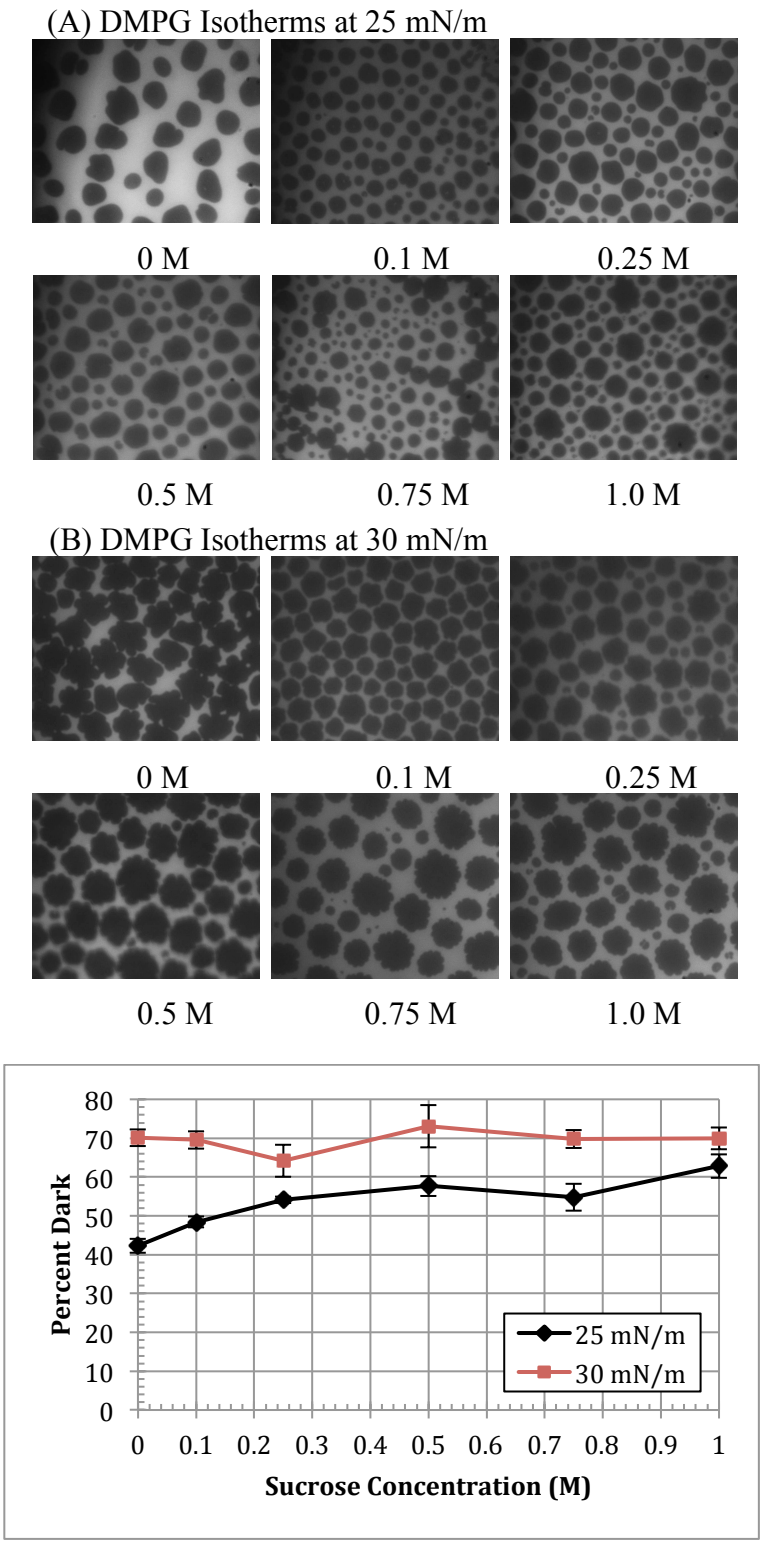

Figure 27: Fluorescent images of DMPG compression isotherms on varying sucrose concentrations at (A) 25 mN/m and (B) 30 mN/m and 30°C. (C) ImageJ analysis of the percent dark vs. light in fluorescence images of DMPG with increasing sucrose concentration in the subphase. At 25 mN/m, there is an increase in the percent dark domains with increasing sucrose. At 30 mN/m, however, the difference in dark domains is not apparent.

4.4 Aβ40 Insertion into Lipid Monolayers

To explore the interactions of Aβ40 in a more physiologically relevant environment, the interfacial activity of Aβ40 at the membrane/subphase interface was assessed by measuring the change in surface area ($\Delta A/A_0$) of the Langmuir trough containing an anionic DMPG or zwitterionic DPPC monolayer that was held at a constant surface pressure after injection of Aβ40 into the subphase. DMPG and DPPC were selected because the head groups carry charges that are found under physiological conditions. DMPG is a lipid containing a negatively charged head group. The change in area after injection was recorded and was used to calculate a percent insertion of Aβ40 into the lipid monolayer.

4.4.1. Aβ40 Insertion into DMPG Monolayer with Varying Sucrose Concentration

All experiments were conducted according to the protocol in *Section 3.5* unless otherwise noted. Initially, the insertion experiments were conducted at a constant surface pressure of 25 mN/m. However, Aβ40 inserted into the monolayer so readily at high sucrose concentrations that the barriers completely expanded and the surface pressure began to raise, making the experiments less meaningful and more complex to analyze. The results can be seen in **Figure 28**. The end result of these experiments was the choice to increase the surface pressure to 30 mN/m for DMPG insertion experiments in order to obtain a more manageable change in trough area that would stay within the bounds of the instrument.

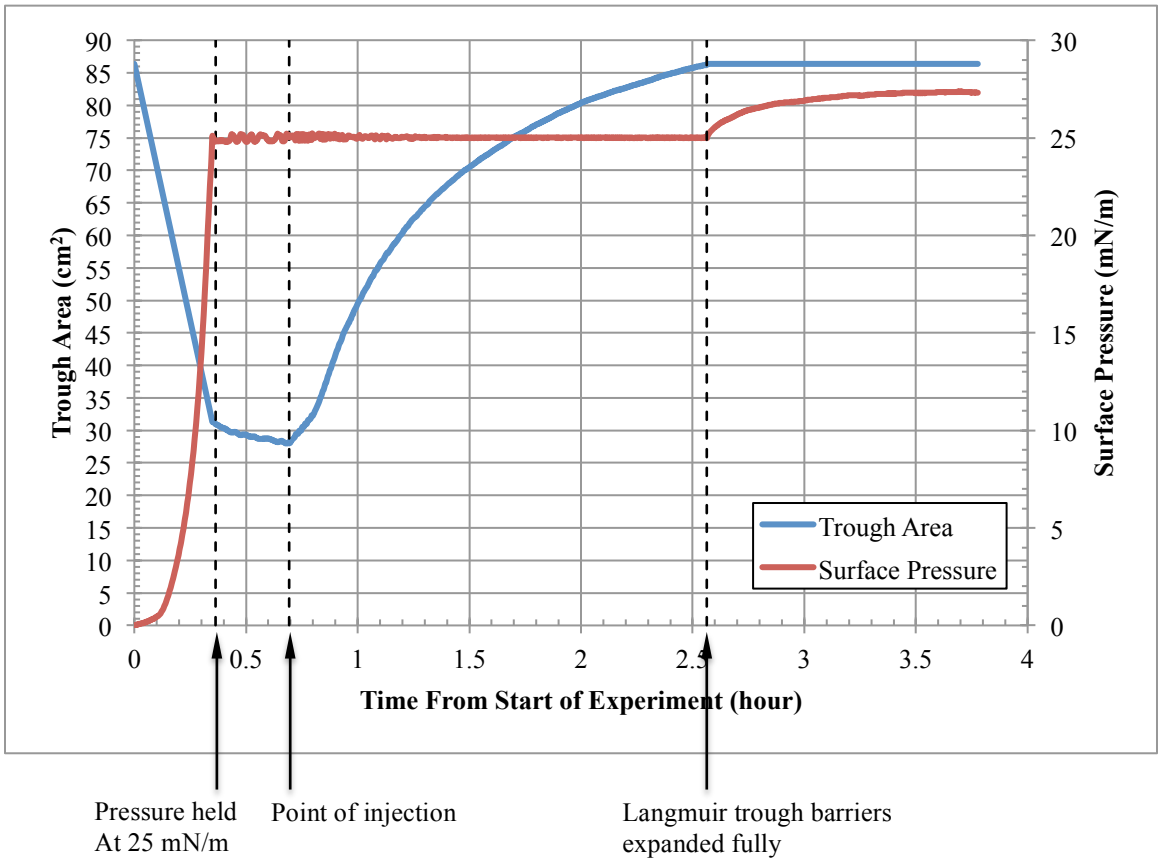

Figure 28: Aβ40 insertion example into DMPG monolayers in constant surface pressure assay at 25mN/m at 30°C. This example is on 0.75M sucrose and shows that the barriers of the Langmuir trough fully extended during insertion and the trough software was not able to maintain a constant surface pressure and the surface pressure began to increase.

Figure 28 illustrates an entire insertion experiment from the beginning of monolayer compression, the injection of peptide, and through peptide insertion. After the point of injection, Aβ40 inserted into the DMPG monolayer, increasing the trough area (the blue line) while surface pressure was held constant at 25 mN/m (red line). After 2.5 hours, the barriers had expanded completely, but Aβ40 was still inserting into the membrane. The trough was unable to expand further, so the trough was unable to maintain the surface pressure at 25 mN/m, and the surface pressure increased due to continued Aβ40 insertion. This was undesirable, because the data was impossible to interpret, as each percent insertion curve reached full expansion of the barriers at

different points (**Figure 29**). This occurred because the injection of Aβ40 occurred at different trough areas for each subphase condition.

As described in *Section 2.3.2*, the percent insertion was calculated by taking the change in trough area (ΔA) and dividing it by the trough area at the point of injection (A_0). This change in area is interpreted as the interaction of Aβ40 with the monolayer and is referred to as the percent insertion. There does appear to be a trend of larger trough area change and decreased lag time, but this data was impossible to interpret because none of the experiments reached an equilibrium change in trough area.

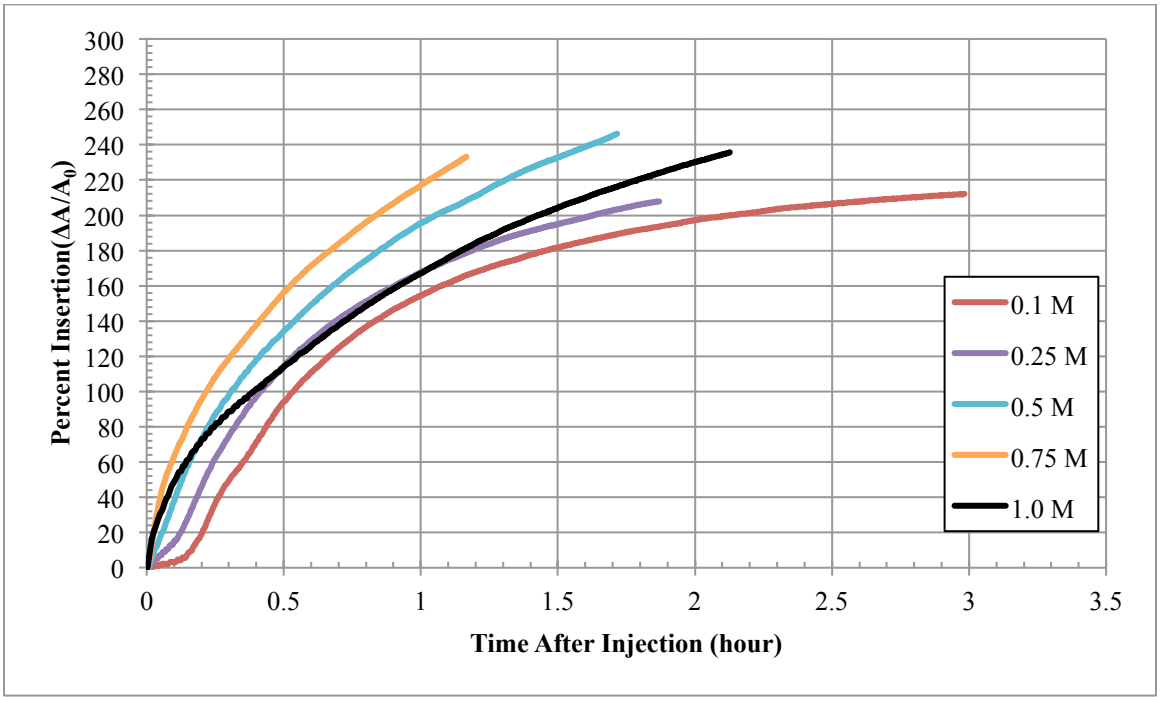

Figure 29: Aβ40 insertion into DMPG isotherms percent insertion vs. time after injection of Aβ40 into varying sucrose subphases. Final Aβ40 in trough is 250 nM, volume of subphase is 45 mL, all experiments conducted at a constant surface pressure of 25 mN/m and a trough temperature of 30±0.5 °C. As insertion occurs, the trough barriers expand to maintain 25 mN/m. Percent insertion is calculated as the change in trough area divided by the area at injection. All experiments fully expanded the trough barriers and surface pressure began to rise. A higher surface pressure (30 mN/m) was chosen in order to decrease the amount of insertion.

4.4.2. Aβ40 Insertion into DMPG at 30 mN/m

Because the interaction of Aβ40 with the DMPG monolayer was so large at 25 mN/m, the experiments were repeated at a higher surface pressure (30 mN/m) to increase

the quantity of lipid in the liquid condensed phase and reduce the overall amount of Aβ40 insertion. These experiments were repeated in triplicate at several sucrose subphase concentrations and interpreted as previously discussed (**Figure 30**). In short, DMPG was spread on the surface of a 45 mL subphase containing known concentrations of sucrose. The DMPG film was compressed to 30 mN/m after which the pressure was held constant. Aβ40 was injected to a final, bulk concentration of 250 nM. Insertion of Aβ40 resulted in an increase in surface area. **Figure 30** shows the relative change in trough area after Aβ40 injection.

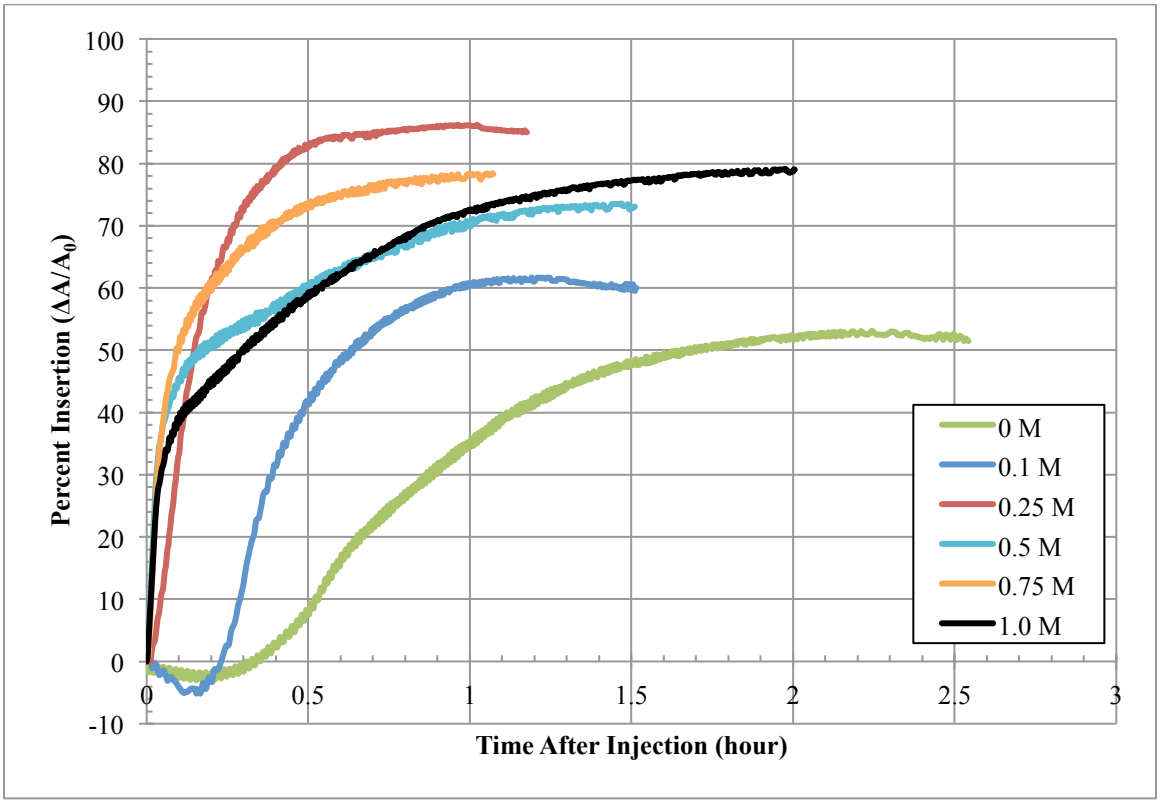

Figure 30: Aβ40 insertion into DMPG isotherms percent insertion vs. time after injection of Aβ40 into varying sucrose subphases at a constant surface pressure of 30 mN/m. Final Aβ in trough is 250 nM, volume of subphase is 45 mL, all experiments conducted at a constant trough temperature of 30±0.5 °C. As insertion occurs, the trough barriers expand to maintain 30 mN/m. Percent insertion is calculated as the change in trough area divided by the area at injection. Increasing sucrose concentration increases percent insertion of Aβ40, the rate of insertion, and decreases lag time before insertion occurs.

The trends that can be determined from **Figure 30** are that the final equilibrium percent insertion increases significantly as sucrose concentration increases, the rate of insertion increases and the lag time significantly decreases to the point where insertion begins as the injection occurred. This coincides with the adsorption isotherm data from *Section 4.2.1.* The data was analyzed as described in *Section 2.3.2* to determine the average final equilibrium percent insertion, lag time, and rate of insertion (See **Figures 31, 32,** and **33**, respectively). Insertion experiments for each concentration of Aβ40 were repeated in triplicate, unless otherwise noted

4.4.2. Final Equilibrium Insertion of Aβ40 into DMPG Monolayers

This data was analyzed to represent final equilibrium percent insertion into DMPG for three sets of isotherms (**Figure 31**). The error bars show one standard deviation. The final percent insertion ($\Delta A/A_0$) was calculated, as previously described, by taking the average of the last five minutes of the trough area change in the DMPG insertion isotherms (**Figure 30**), well after equilibrium had occurred. There was a steady increase of percent insertion from 0 M sucrose (49.46±8.68%), with a maximum insertion at 0.25 M sucrose (86.41±3.49%), and a slight decrease back down to 1 M sucrose (81.00±5.92%), indicating that the presence of sucrose increased the percent insertion of Aβ40 into DMPG.

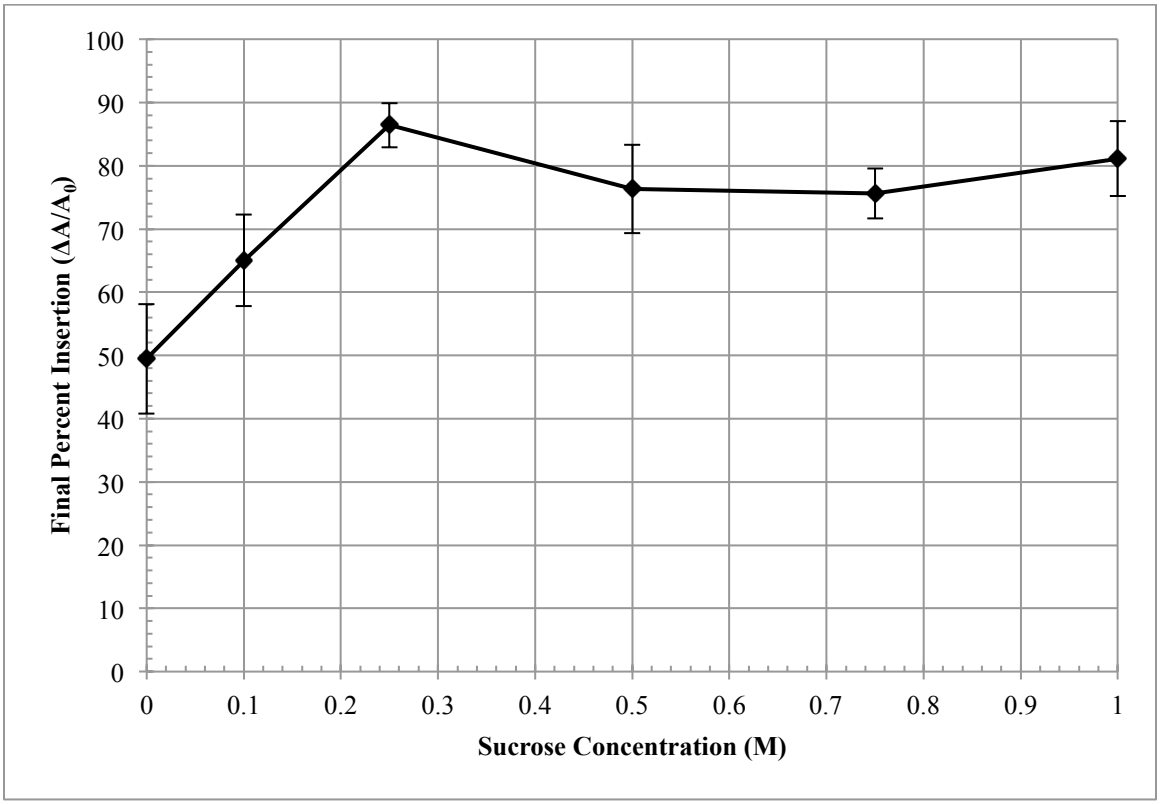

Figure 31: Final percent insertion vs. sucrose concentration of Aβ40 insertion into DMPG isotherms. Final pressure increases as sucrose concentration increases for Aβ40 adsorption to the air/subphase interface at 30±0.5 °C. Error bars indicated one standard deviation of triplicate repeats.

4.4.3. Lag Time of Aβ40 Insertion into DMPG Isotherms

The next property of the insertion into DMPG isotherms that was analyzed was the lag time between the injection of Aβ40 and the resulting increase in trough area (**Figure 32).** The lag time was calculated as previously described in *Section 2.3.2* by increasing the magnification in the adsorption isotherm around the area where surface pressure began to increase. This lag time indicates the time required for Aβ40 to reach and begin interacting with the DMPG monolayer. As sucrose concentration increased, the time before insertion began was significantly reduced. The lag time in a water subphase was 12.65±0.30 minutes. There was a significant drop even at 0.1 M sucrose (8.50±1.08 minutes) and higher concentrations reduced lag time down to an average of 0.225±0.09 minutes. The injection was carried out over 20-30 seconds so, at higher concentrations,

the trough area began expanding before the injection was even completed, meaning Aβ40 reached the surface before the injection was completed. This data correlates very well with the adsorption isotherm data from *Section 4.2.3*.

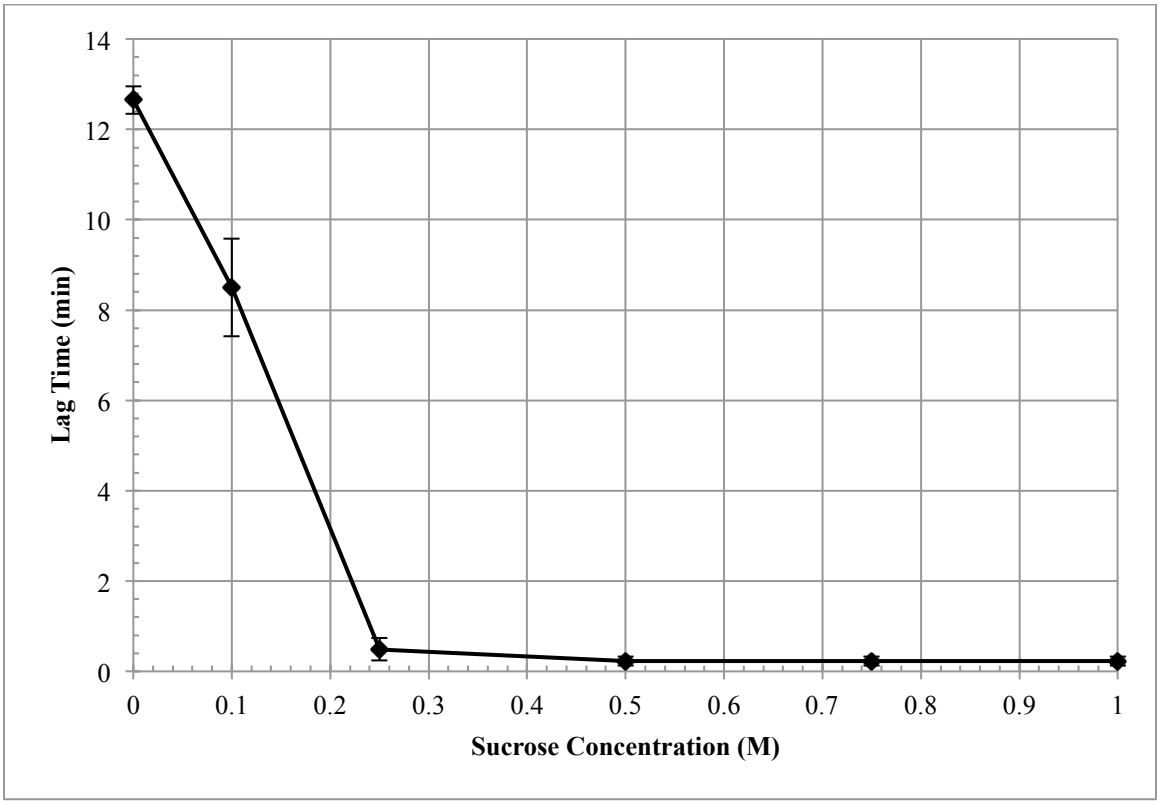

Figure 32: Lag time vs. sucrose concentration of Aβ40 insertion into DMPG isotherms. Lag time decreases as sucrose concentration increases for Aβ40 insertion into DMPG monolayers at 30±0.5 °C. Error bars indicated one standard deviation of triplicate repeats.

4.4.4 – Rate of Aβ40 Insertion in DMPG Isotherms

Figure 33 represents the rate of change of the percent insertion of Aβ40 into DMPG per minute with increases in sucrose concentration. The rate of change was calculated as previously described in *Section 2.3.2* by taking the slope of the line of the linear portion of each insertion isotherm. This indicates how quickly Aβ40 inserts into the DMPG film once adsorption begins. At low concentrations, Aβ40 inserts at much slower rates than at higher sucrose concentrations, which was expected from the previous

adsorption isotherms. The rate increases consistently as the sucrose concentration increases, until 1 M sucrose where it levels off within one standard deviation.

In water, the rate of adsorption of Aβ40 in the linear portion of the isotherm was an average rate of 0.93±0.25 percent area change/min, peaking at 0.75 M sucrose with an average rate of insertion at 15.85±1.11 percent area change/min, and decreasing at 1.0 M sucrose to 14.74±0.53 percent area change/min. The decrease in insertion rate in the DMPG insertion experiments when compared to the air/subphase adsorption isotherms from *Section 4.2.4* can be contributed to the difficulty of inserting into a lipid membrane, due to an increased energy barrier from electrostatic repulsion, over the ease of adsorbing to an air/subphase interface.

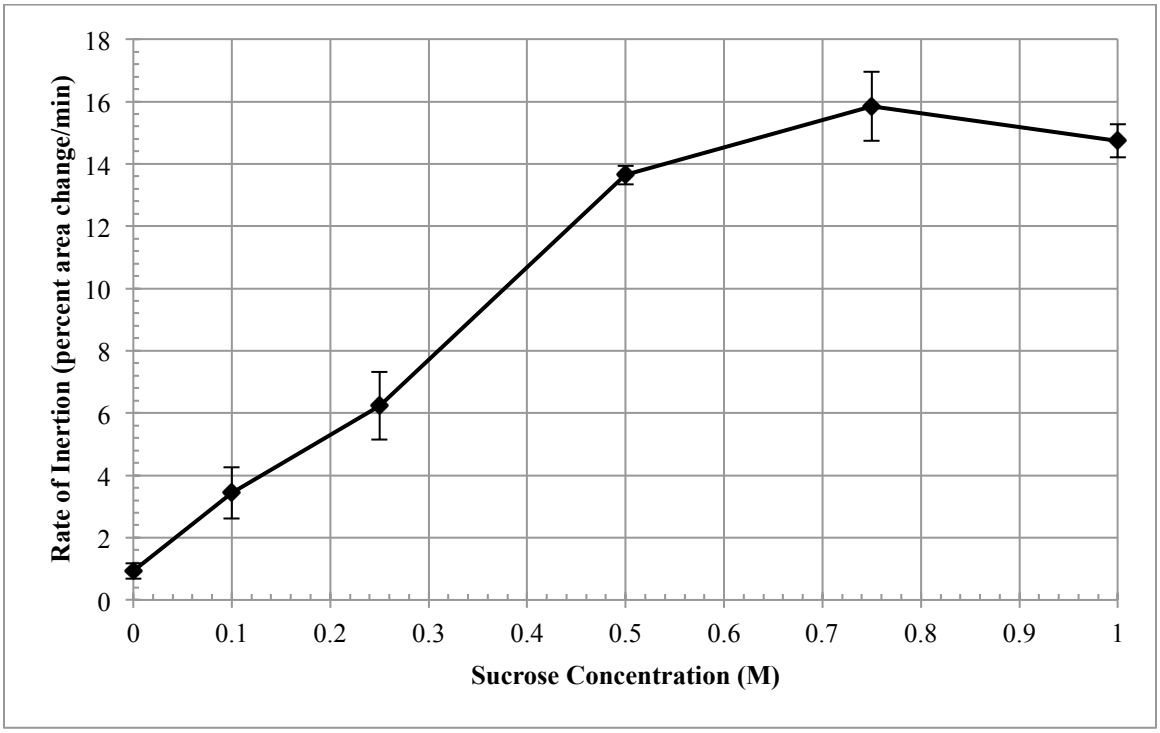

Figure 33: Aβ40 insertion rate vs. sucrose concentration of Aβ40 insertion into DMPG isotherms. Rate of insertion increases as sucrose concentration increases at 30±0.5 °C. Error bars indicated one standard deviation of triplicate repeats.

4.4.4. Aβ40 Insertion into DMPG Fluorescence Imaging

The graphs of the individual insertion experiments from a set (**Figures 34-39**) were prepared to show the morphological changes of the DMPG monolayer with fluorescence imaging as insertion of Aβ40 occurred. In short, images were taken of the DMPG monolayer before Aβ40 was injected into the subphase and at specific time intervals afterward as Aβ40 inserts into the lipid domains. Before injection, the condensed domains should be compact, with very distinct borders between the dark liquid condensed phase and the bright liquid expanded phase. As Aβ40 inserts into the monolayer, the amount of dark condensed domains decreases and the edges of the condensed domains become hazy, without a clear boundary to focus on. The condensed domains appear to be of inconsistent size in the higher sucrose concentrations sucrose concentration increases and there are many domains that are not uniform in size, which is unexpected. The size of the individual domains appears to increase with sucrose concentration as well. The amount of insertion and disruption of the membrane also appears to increase with sucrose concentration.

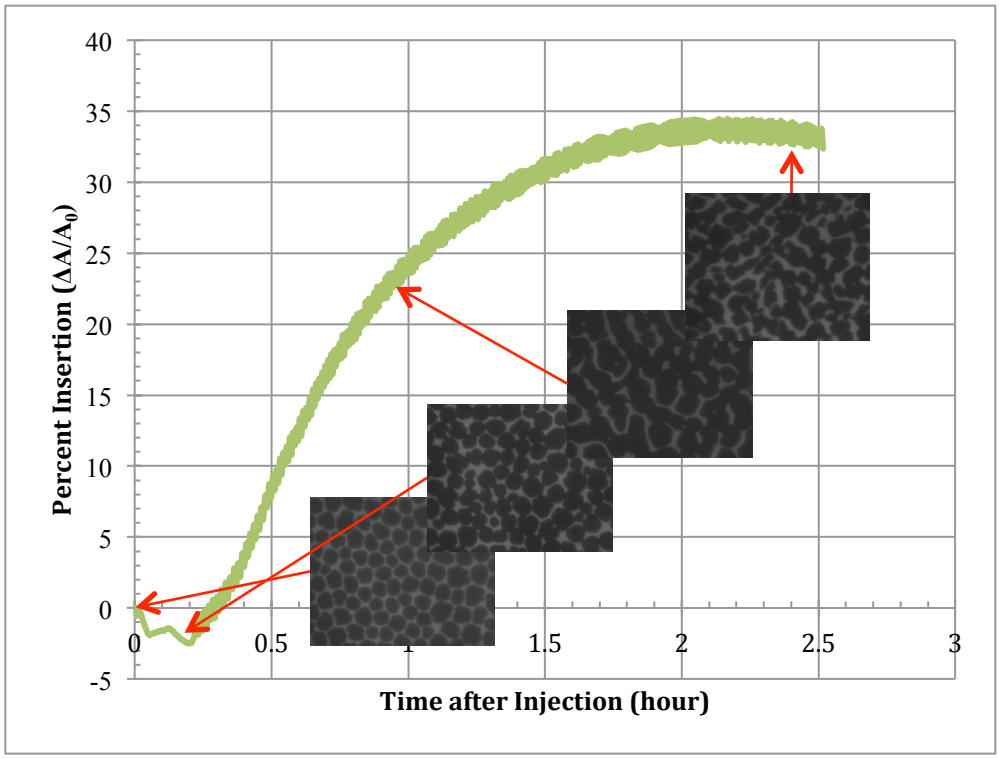

Figure 34: Aβ40 insertion into DMPG isotherm on water at 30±0.5 °C. 0.2 mg/mL DMPG with 0.5 mol% Texas Red-DHPE was spread on the clean subphase. Aβ40 induces disruption of the membrane. Fluorescence images were taken at several points to show the progression of insertion.

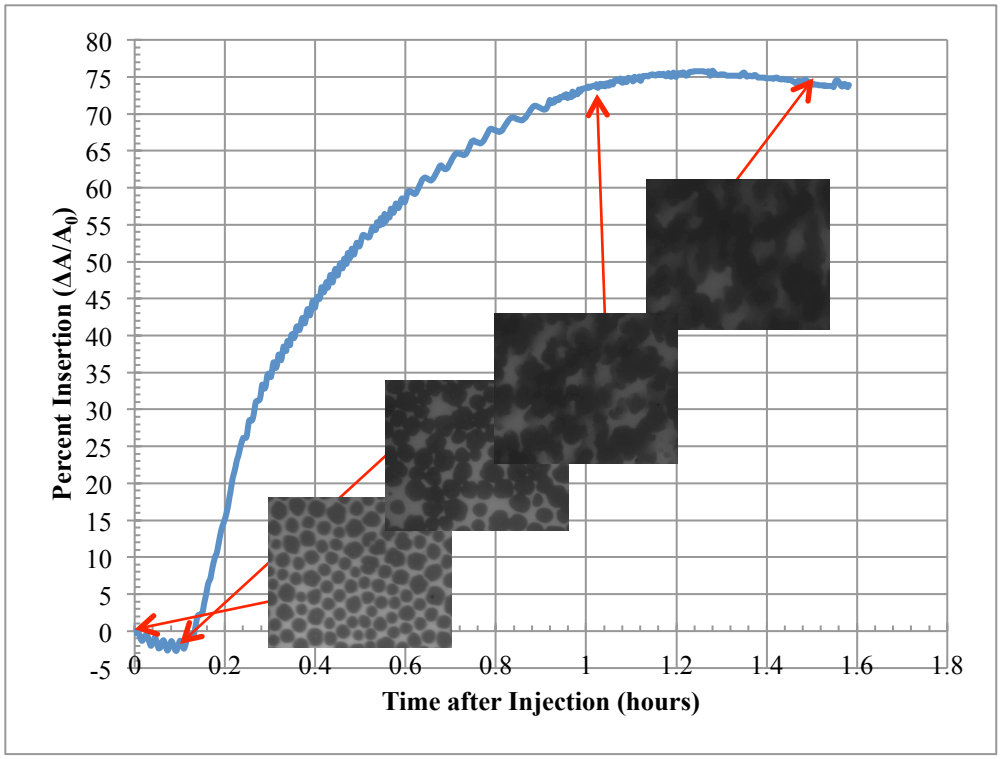

Figure 35: Aβ40 insertion into DMPG isotherm on 0.1 M sucrose at 30±0.5 °C. 0.2 mg/mL DMPG with 0.5 mol% Texas Red-DHPE was spread on the clean subphase. Aβ40 induces disruption of the membrane. Fluorescence images were taken at several points to show the progression of insertion.

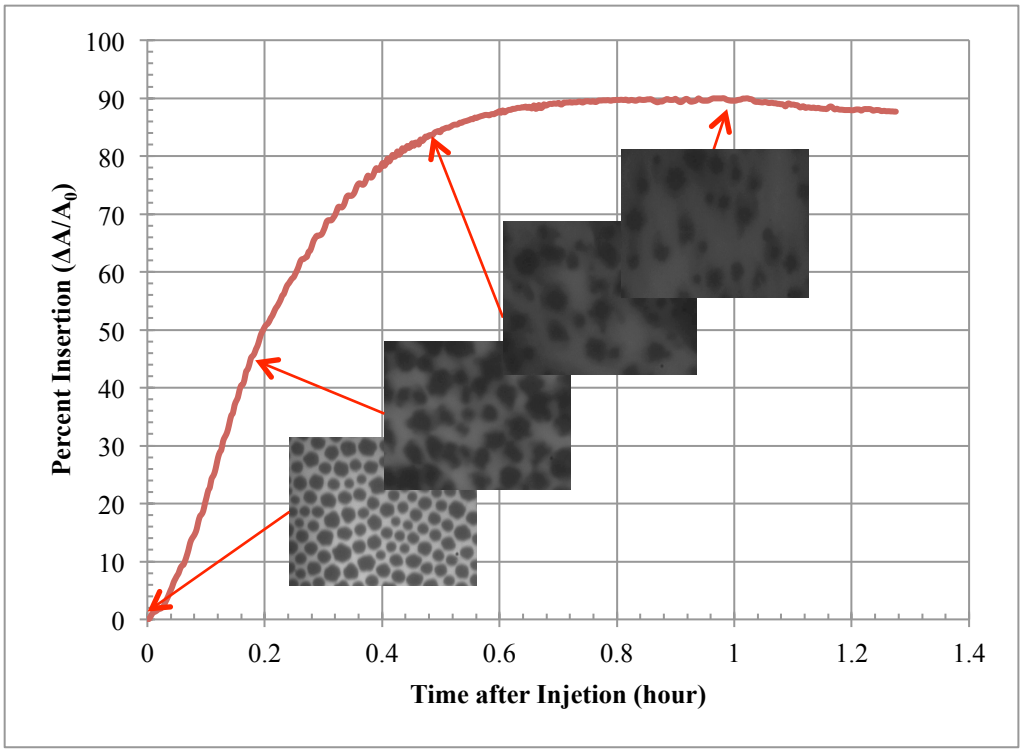

Figure 36: Aβ40 insertion into DMPG isotherm on 0.25 M sucrose at 30±0.5 °C. 0.2 mg/mL DMPG with 0.5 mol% Texas Red-DHPE was spread on the clean subphase. Aβ40 induces disruption of the membrane. Fluorescence images were taken at several points to show the progression of insertion.

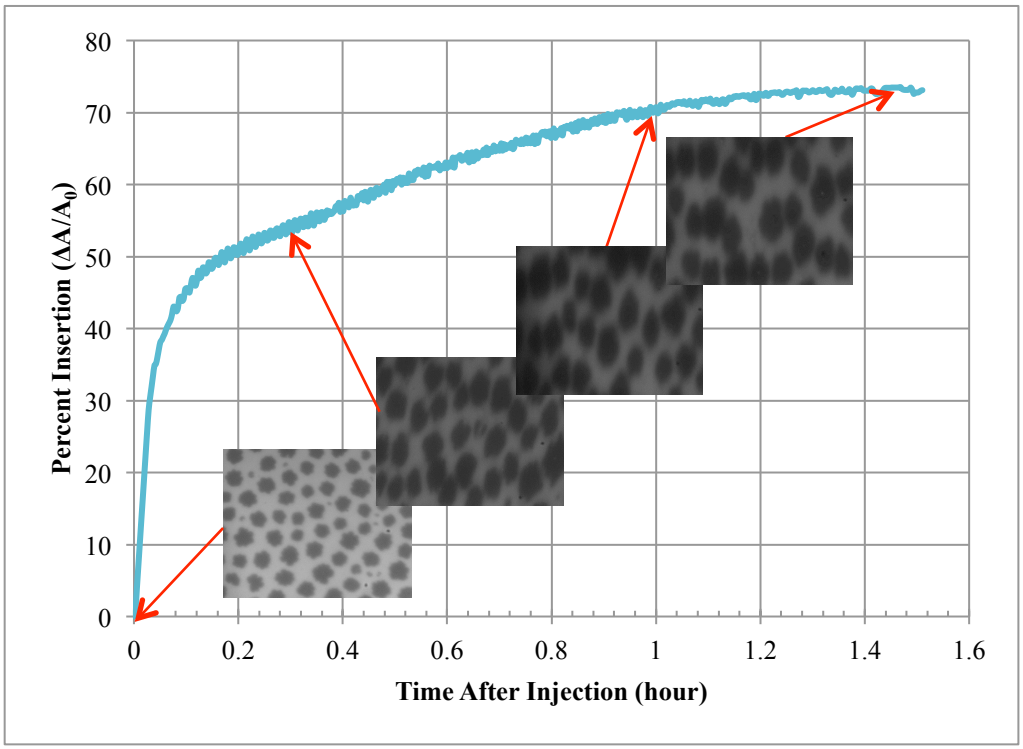

Figure 37: Aβ40 insertion into DMPG isotherm on 0.5 M sucrose at 30±0.5 °C. 0.2 mg/mL DMPG with 0.5 mol% Texas Red-DHPE was spread on the clean subphase. Aβ40 induces disruption of the membrane. Fluorescence images were taken at several points to show the progression of insertion.

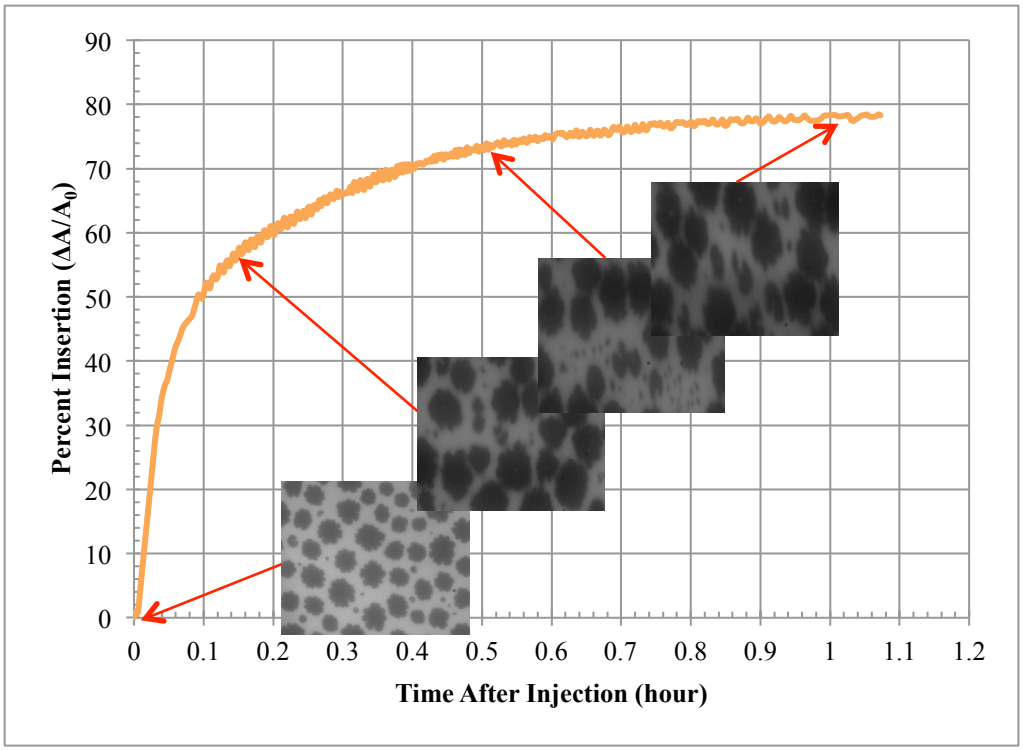

Figure 38: Aβ40 insertion into DMPG isotherm on 0.75 M sucrose at 30±0.5 °C. 0.2 mg/mL DMPG with 0.5 mol% Texas Red-DHPE was spread on the clean subphase. Aβ40 induces disruption of the membrane. Fluorescence images were taken at several points to show the progression of insertion.

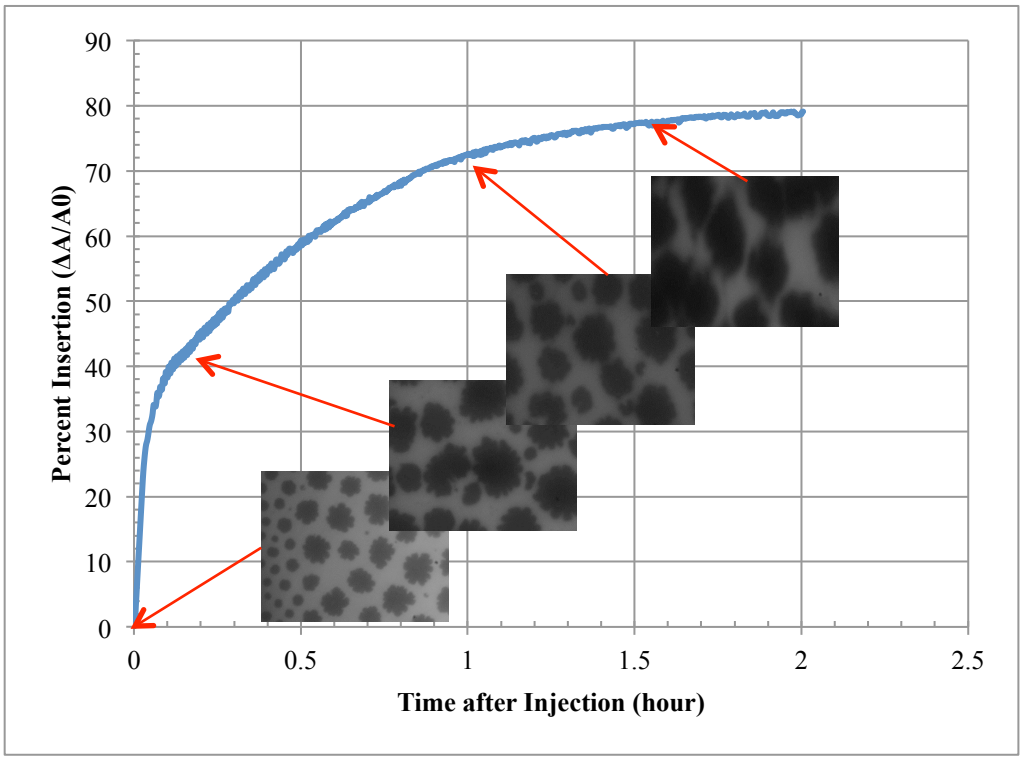

Figure 39: Aβ40 insertion into DMPG isotherm on 1.0 M sucrose at 30±0.5 °C. 0.2 mg/mL DMPG with 0.5 mol% Texas Red-DHPE was spread on the clean subphase. Aβ40 induces disruption of the membrane. Fluorescence images were taken at several points to show the progression of insertion.

4.5 Aβ40 Insertion into DPPC Lipid Monolayers

The effect of sucrose on the ability of Aβ40 to insert into a lipid that it does not readily insert into, zwitterionic DPPC, was investigated. Aβ40 does not readily insert into DPPC lipids on a water subphase at 25 mN/m, the surface pressure that represents the density of membrane packing in a cell.[28] The first set of experiments was to determine the maximum surface pressure that that Aβ40 will begin to insert into DPPC on various sucrose concentrations. The DPPC film was compressed to 30 mN/m (or higher) and held at a constant pressure of 30 mN/m and a constant temperature of 30±0.5 °C. Aβ40 was injected into the subphase and the trough area was recorded. If no insertion occurred after 30 minutes, the surface pressure was lowered at 1 mN/m intervals and the surface pressure was held constant at this new pressure. If after 10-15 minutes there was no increase in trough area, the surface pressure was dropped again. This was repeated until insertion occurred (**Figure 40**). The pressure at which Aβ40 insertion occurred was taken as the maximum insertion pressure.

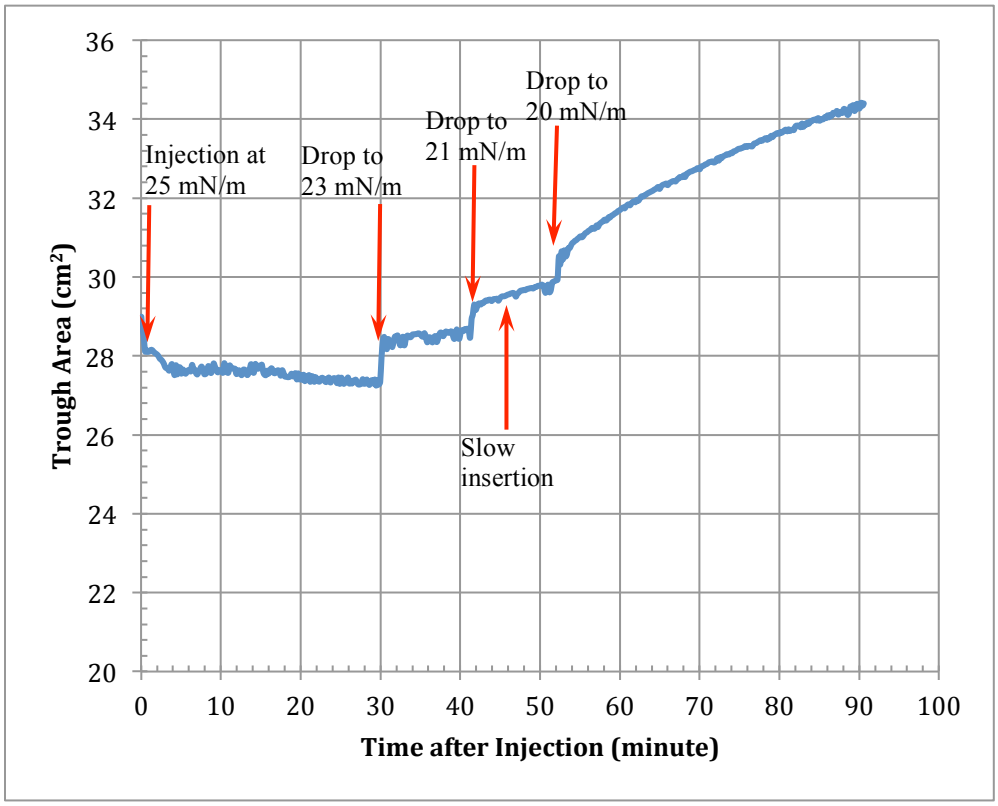

Figure 40: Maximum Aβ40 insertion pressure in DPPC on water. Aβ40 was injected into a water subphase below a DPPC isotherm held at a constant 25 mN/m and 30±0.5 °C. 0.2 mg/mL DPPC with 0.5 mol% Texas Red-DHPE was spread on the clean subphase. Aβ40 does not cause trough area change at 30 mN/m. The surface pressure was then lowered 2 mN/m every 10 minutes until insertion began. The maximum surface pressure where slow insertion began was 21 mN/m.

The maximum insertion surface pressure experiments with DPPC were repeated in triplicate for each sucrose concentration and compared against the final equilibrium Aβ40 adsorption pressure with varying sucrose concentrations, which was analyzed in *Section 4.2.2* (**Figure 41**). The DPPC maximum insertion pressure plot was repeated in triplicate, the error bars are 0 because each time this was repeated, insertion began at the same surface pressure. The maximum surface pressure for Aβ40 insertion into DPPC at 30±0.5°C was greater than the final equilibrium adsorption pressure reached by Aβ40 to a clean air/subphase interface.

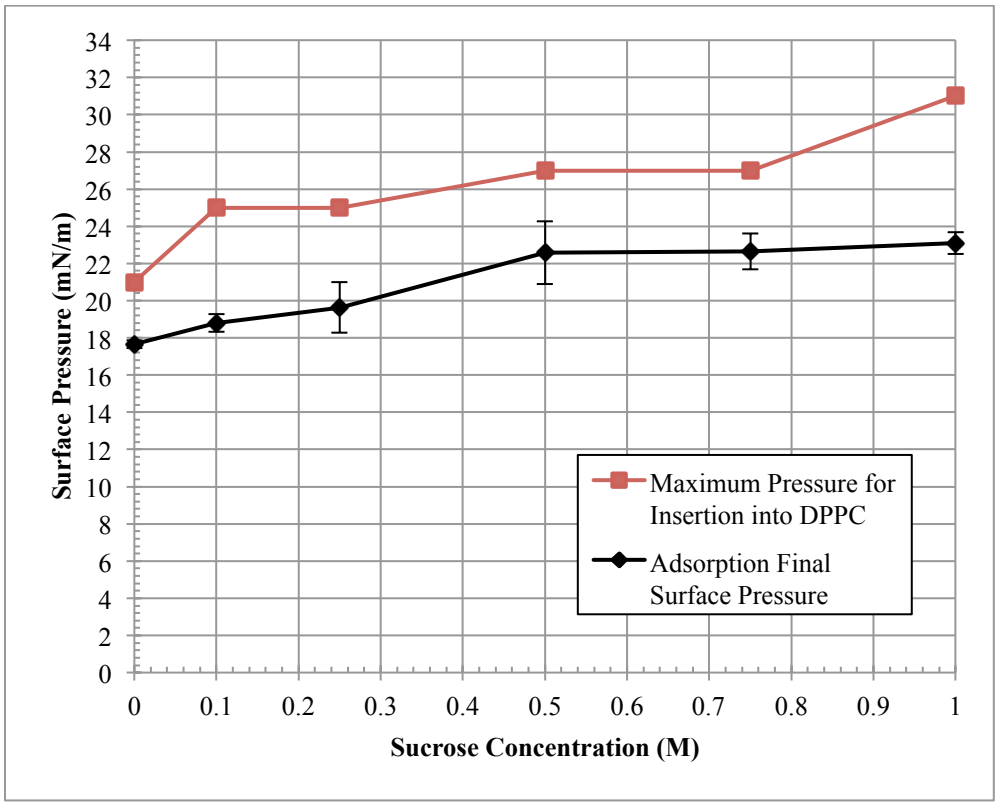

Figure 41: Surface pressure vs. sucrose concentration for maximum surface pressure for insertion of Aβ40 into DPPC compared with adsorption final surface pressure on a clean subphase at 30±0.5 °C. Maximum surface pressure for Aβ40 insertion into DPPC is higher than the final adsorption surface pressure on a clean subphase surface. Error bars are one standard deviation for triplicate repeats. There are no error bars in the DPPC plot because the maximum surface pressure was the same for each of three replicates.

4.5.1. Aβ40 Insertion into DPPC Monolayer with Varying Sucrose Concentration

Because Aβ40 was shown to insert into DPPC monolayers on sucrose containing subphases at 25 mN/m, constant pressure insertion assays were completed with varying sucrose concentrations. The experiments were repeated in triplicate and were repeated in the same manner as the DMPG insertion experiments in *Section 4.4.1,* described in detail in *Section 3.5*. The trends that can be gathered from the example set of experiments is that Aβ40 inserts more readily into DPPC as sucrose concentration increases and the lag phase is reduced significantly as sucrose concentration increase (**Figure 42**). There were no fluorescence images taken in the DPPC insertion experiments because DPPC does not form adequate condensed domains at 30±0.5 °C for imaging.

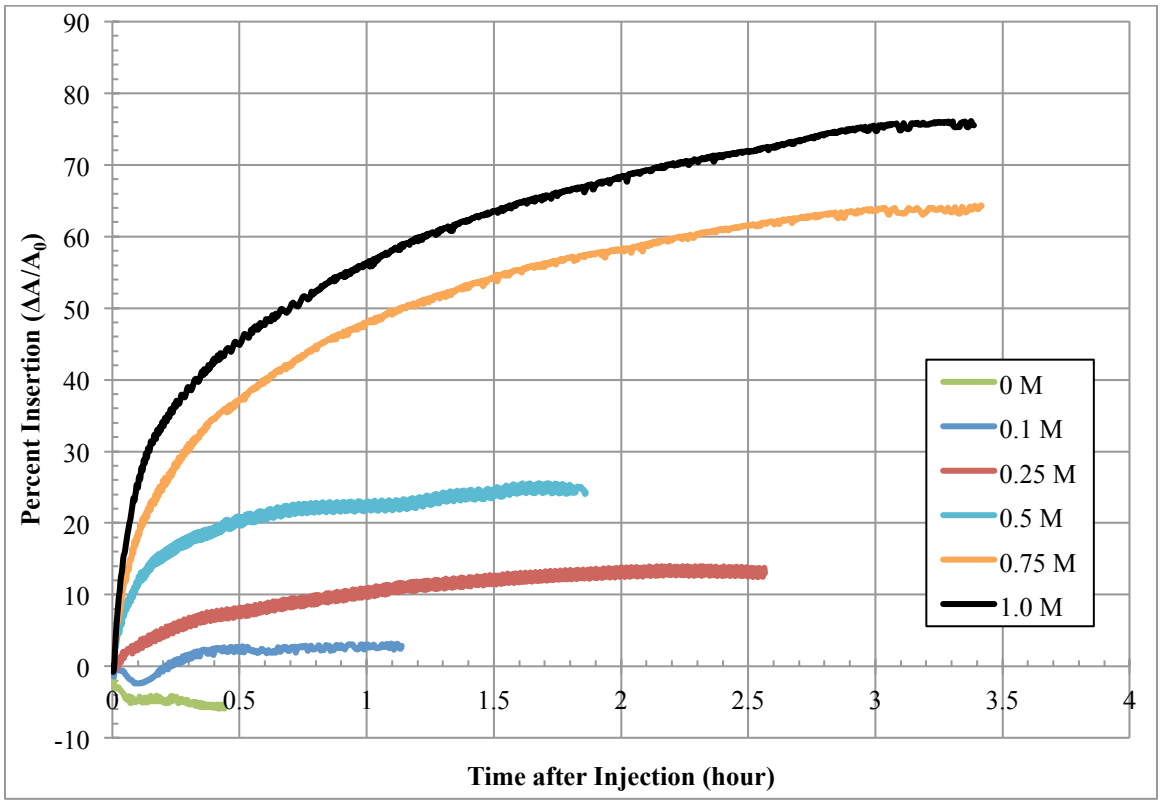

Figure 42: Aβ40 insertion into DPPC isotherms percent insertion vs. time after injection of Aβ40 into varying sucrose subphases at a constant surface pressure of 25 mN/m. Final Aβ in trough is 250 nM, volume of subphase is 45 mL, all experiments conducted at a constant trough temperature of 30±0.5 °C. As insertion occurs, the trough barriers expand to maintain 25 mN/m. Percent insertion is calculated as the change in trough area divided by the area at injection. Increasing sucrose concentration increases percent insertion of Aβ40, the rate of insertion, and decreases lag time before insertion occurs.

4.5.2. Final Equilibrium Insertion of Aβ40 into DPPC Monolayers

This data was analyzed to represent final equilibrium percent insertion into DPPC for three sets of isotherms (**Figure 43**). The error bars represent one standard deviation. The final percent insertion ($\Delta A/A_0$) was calculated by taking the average of the last five minutes of the trough area change in the DPPC insertion isotherms (**Figure 42**), well after insertion reached a plateau. There was a steady increase of percent insertion from 0 M sucrose (0±0%), increasing consistently up to 1.0 M sucrose (66.73±8.95%), which means that Aβ40 was able to readily insert into a lipid membrane that it did not normally interact with. Sucrose increases in the DPPC insertion isotherms continually as sucrose

concentration, whereas insertion into DMPG reached a maximum at 0.25 M sucrose in *Section 4.4.2.*

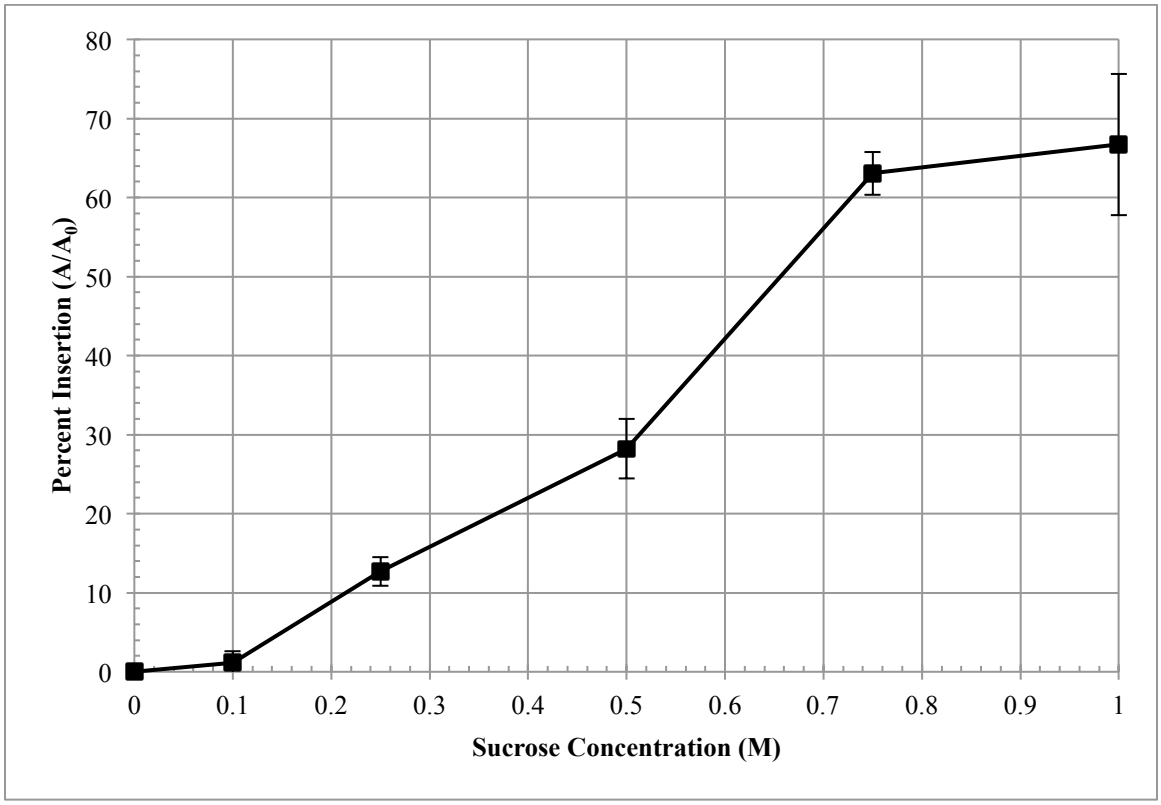

Figure 43: Final percent insertion vs. sucrose concentration of Aβ40 insertion into DPPC isotherms. Final pressure increases as sucrose concentration increases for Aβ40 adsorption to the air/subphase interface at 30±0.5 °C. Error bars indicated one standard deviation of triplicate repeats.

4.5.3. Lag Time of Aβ40 Insertion into DPPC Isotherms

The next property of the insertion into DPPC isotherms that was analyzed was the lag time between the injection of Aβ40 and the resulting increase in trough area (**Figure 44).** The lag time was calculated as previously described in *Section 2.3.2.* by increasing the magnification in the adsorption isotherm around the area where surface pressure began to increase. This lag time indicates the time required for Aβ40 to reach and begin interacting the DPPC film. As sucrose concentration increased, the time before insertion began was significantly reduced. Since there was no insertion into water, the lag time was longer than the length of the experiment, so the data point was not included. There was a

significant drop from 0.1 M sucrose (6.50±0.71 minutes) to higher concentrations, with a reduced lag time down to an average of 0.28±0.19 minutes at a 1.0 M sucrose subphase. Because the injection was carried out over 20-30 seconds, at higher concentrations, the trough area began expanding before the injection was even completed, meaning Aβ40 reached the surface before the injection was completed. This data correlates very well with the adsorption isotherm data from *Section 4.2.3* as well as the DMPG insertion isotherms from *Section 4.4.3*.

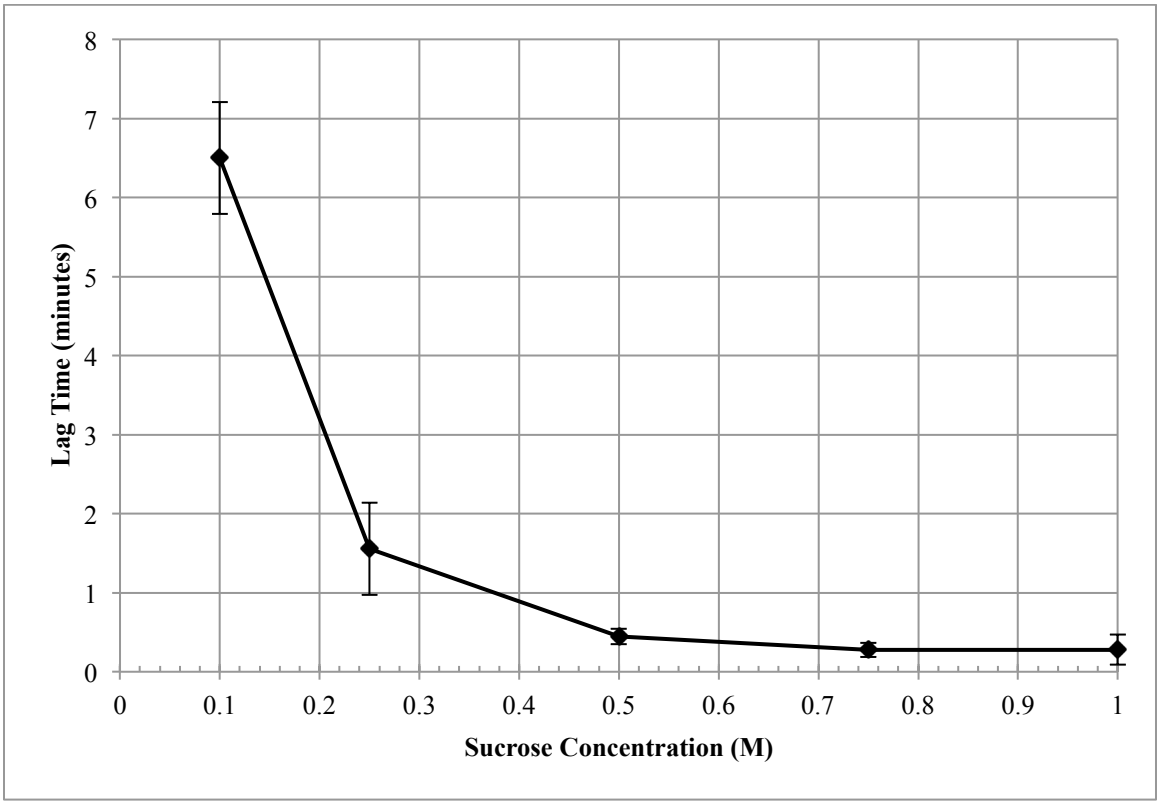

Figure 44: Lag time vs. sucrose concentration of Aβ40 insertion into DPPC isotherms. Lag time decreases as sucrose concentration increases for Aβ40 insertion into DPPC monolayers at 25 mN/m and 30±0.5 °C. Error bars indicated one standard deviation of triplicate repeats. Water was not included because Aβ40 did not insert into DPPC at 25 mN/m.

4.5.4. Rate of Aβ40 Insertion into DPPC Isotherms

Figure 45 represents the rate of change of the Aβ40 per minute as sucrose concentration increases. The rate of change was calculated as previously described in *Section 2.3.2* by taking the slope of the line of the linear portion of each insertion

isotherm. This indicates how quickly Aβ40 inserts into the DPPC film once adsorption begins. At low concentrations of sucrose, Aβ40 inserts at slower rates than at higher sucrose concentrations, which was expected from the previous adsorption isotherms. The higher concentrations had much lower rate of insertion than the adsorption isotherms, however. The rate increases consistently as the sucrose concentration increases, but at a slower rate than seen in the DMPG insertion isotherms from *Section 4.4.4*. The highest rate of insertion was at 1.0 M sucrose where the rate of insertion peaked at an average of 4.01±0.28 percent area change/min, which is still significantly slower than the insertion of 1.0 M sucrose (14.74±0.53 percent area change/minute) in the DMPG insertion assay (*Section 4.4.4*). This result is surprising and suggests that sucrose increases the ability of Aβ40 to interact with lipids that it would not interact with in water.

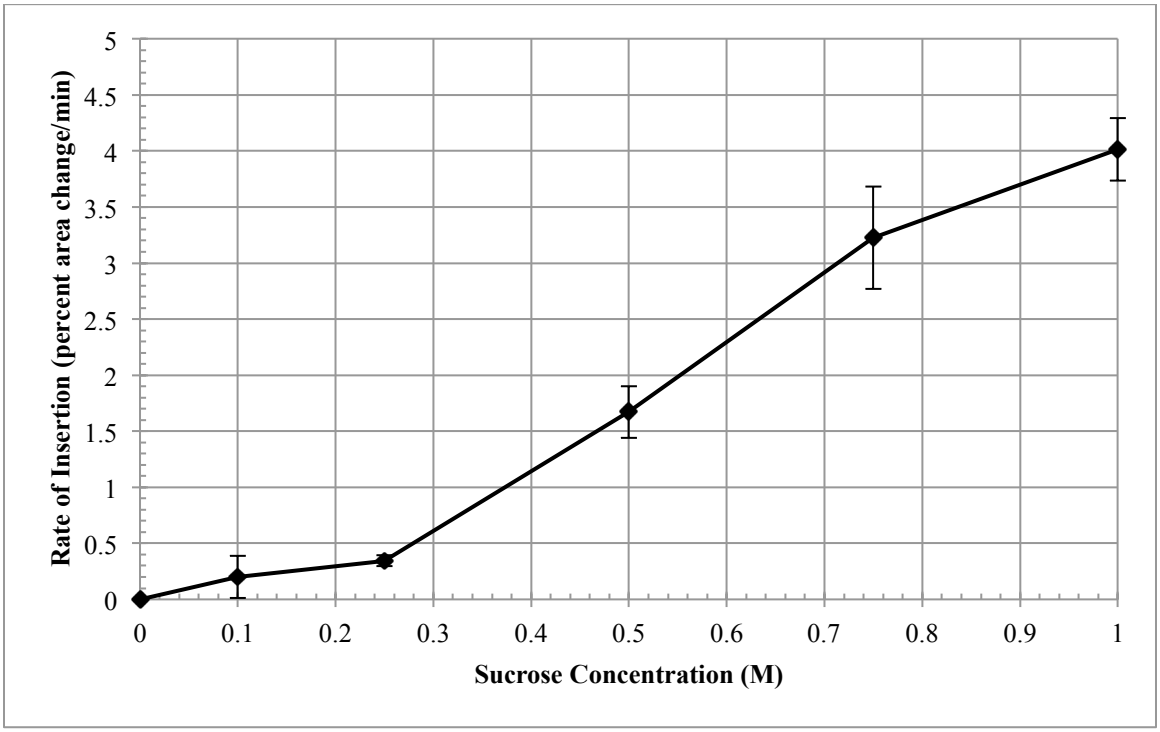

Figure 45: Aβ40 insertion rate vs. sucrose concentration of Aβ40 insertion into DPPC isotherms. Rate of insertion increases as sucrose concentration increases at 25 mN/m and 30±0.5 °C. Error bars indicated one standard deviation of triplicate repeats.

4.6 Ionic Strength and pH of Sucrose Solutions

Ionic strength and pH have previously been shown to affect the surface activity and membrane interaction of Aβ40 with the air/subphase interface and lipid monolayers, respectively.[28] Ka Yee Lee *et al.* have shown that increasing ionic strength and pH increases the surface activity of Aβ40 at the air/subphase interface, increasing the final adsorption surface pressure, reducing lag time, and increasing adsorption rate. Increasing pH also reduces the insertion of Aβ40 into anionic lipids due while slightly increasing the insertion into zwitterionic lipids. The reduction of insertion in anionic lipids was described by the repulsive forces between Aβ40 and the anionic head group as pH increased because above the isoelectric point (pI_t=5.43),[36] Aβ40 takes on a net negative charge.

Table 3 shows the pH and conductivity measurements of various sucrose solutions as well sucrose samples containing Aβ40 that were taken from the trough after completion of Aβ40 adsorption isotherms. While the pH of water was higher than expected at 6.59 (pure water has a pH of 5.5, but the solutions were un-buffered), the pH of the sucrose solutions did not vary with concentration, indicating that pH did not have an effect on the surface activity of Aβ40. In fact, the pH of sucrose solutions containing Aβ40 was very close to that of water. There is a difficulty in determining the pH of water at very low conductivity, so these pH values may not be completely accurate. The pH may be closer to 5.5, and in that situation, Aβ40 would still be slightly negative. Similarly, conductivity of sucrose solutions did not vary with concentration, indicating ionic strength did not change. The results suggest that pH and ionic strength did not play a role in the increased surface activity and insertion into DMPG and DPPC.

Table 3: Conductivity and pH of varying sucrose solutions

Sucrose (M)	Conductivity (μS/cm)	pH
0	5.4	6.59
0.1	3.0	6.98
0.25	2.8	7.09
0.5	5.0	7.11
0.75	2.4	7.12
1	2.4	6.85
0.5 w/ 250 nM Aβ40	3	6.74
0.75 w/ 250 nM Aβ40	2.8	6.54
1.0 w/ 250 nM Aβ40	1.8	6.48

5. Discussion

The mechanism of Aβ aggregation *in vivo* is unknown. It has been shown *in vitro* that the intrinsically disordered, monomeric Aβ can form highly ordered fibrils, which are present in the pathology of Alzheimer's disease.[29] Fibril formation of Aβ is a nucleation dependent event,[29] and Aβ insertion into lipid membranes acts as a nucleation point for fibrillogenesis.[21] In order to understand the mechanism of aggregation, the initial steps that lead to the nucleation event, which results in aggregation and fibril formation of Aβ, we investigated the effects of the osmolyte sucrose on the activity of Aβ40 at interfaces. We have examined the surface activity of Aβ40 at the air/subphase interface and the insertion of Aβ40 into two model membranes, anionic DMPG and zwitterionic DPPC monolayers, using a Langmuir trough. The air/subphase interface was an approximation of an idealized hydrophobic interface, and the membrane model was used as an approximation of the outer leaflet of the cell membrane. The interaction of Aβ40 with

both of these interfaces has been investigated previously on water,[20,28] showing surface activity of Aβ40 with both the air/subphase interface as well as with DMPG monolayers. This is, however, the first investigation of the effects of molecular crowding and preferential exclusion on the surface activity of Aβ40 in these two model systems.

The following description of adsorption of natively folded proteins to an interface will be used as a starting point to propose a mechanism for surface activity of the intrinsically disordered peptide (IDP) Aβ40. The mechanism will also propose a model for the effects of sucrose on folding and surface activity of IDPs. In natively folded proteins, the protein in the bulk solution diffuses to the surface, and a transition state that is partially unfolded occurs at the air/subphase interface. In this partially unfolded state, a minimal portion of the protein adsorbs to the interface so that adsorption could proceed spontaneously. The protein undergoes further conformational changes to unfold and spread to a conformation with several amino acids adsorbed to the interface (**Figure 46)**.[25]

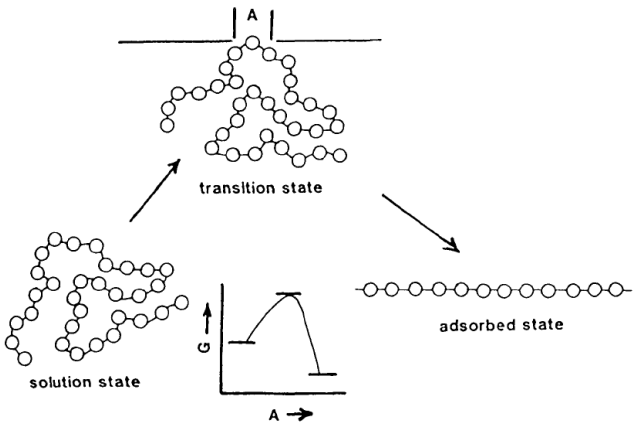

Figure 46: Schematic illustration of the adsorption of a natively folded protein to an air/liquid interface. The natively folded protein partially unfolds at the interface, where a small portion adsorbs to the interface. This adsorption and partial unfolding allow further unfolding and adsorption to occur spontaneously. The inserted graph shows how the free energy (G) of the system changes as the area of penetration of the molecule in the surface (A) increases. The maximum in G corresponds to the critical area for adsorption.[25]

5.1 Proposed Mechanism for Aβ40 Adsorption and the Effect of Sucrose

Since Aβ40 is an IDP, the mechanism for membrane interactions is different than that of a natively folded protein. The proposed mechanism of adsorption to an interface in **Figure 47** takes into account that it has been shown previously that when Aβ40 adsorbs to the an interface, the natively unfolded peptide folds into a β-sheet conformation at the interface.[20] The natively unfolded Aβ40 (N) diffuses to the air/subphase interface and undergoes an energy dependent ($\Delta G^{\ddagger}$) partial folding to a transition state (TS^{*}). In this partially folded state, a small portion of Aβ40 adsorbs to the interface. TS^{*} undergoes spontaneous folding at the interface to an even more compact conformation (AS). This adsorbed state of Aβ40 represents the β-sheet conformation that is seen in its aggregation competent conformations.[1,10,20]

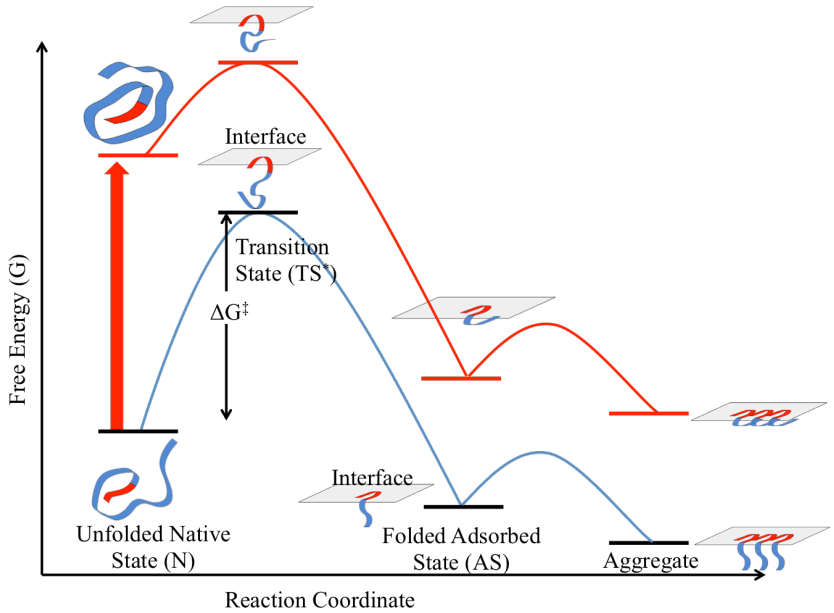

Figure 47: Schematic of proposed mechanism of Aβ40 interaction and adsorption to an interface. Aβ40 is natively in an unfolded state (N). Aβ40 partially folds at the interface to a transition state where a small portion adsorbs to the interface (TS^{*}). This folding requires energy ($\Delta G^{\ddagger}$). The partial folding and adsorption allow further folding to an adsorbed state to a more highly ordered conformation, containing a β-sheet at the interface. (red plot) Folding of the native state due to preferential exclusion increases the overall free energy of the system, making the solution state of Aβ40 highly energetically unfavorable. There is also a decrease in the energy barrier required for the transition state, increasing the rate of adsorption.

The proposed effect of sucrose (**Figure 47** red plot) on the folding and interaction of Aβ40 with an interface is to reduce the activation energy required for partial folding (a decrease in $\Delta G^{\ddagger}$ from N to TS^{*}) while stabilizing the adsorbed and aggregated state. Sucrose has been shown to stabilize proteins and prevent protein denaturation.[30] Sucrose is preferentially excluded over water from the protein surface, which increases the surface tension of the protein.[23] The effect of this preferential exclusion is a shift in the conformational equilibrium of Aβ40 towards a more compact conformational state (**Figure 4**). This leads to an increased overall energy of the system and is energetically unfavorable, so the adsorbed and aggregated states are more energetically favorable.

5.2 Sucrose Enhances the Adsorption of Aβ40 to the Air/Subphase Interface

Our adsorption isotherms show that the Aβ40 is highly surface active and spontaneously adsorbs to the air/subphase interface. In water, Aβ40 showed characteristic surface activity of a short lag time after injection followed by a rise in surface pressure to a final adsorption equilibrium pressure (**Figure 14**). This is consistent with previously obtained data by the Chi lab group, as well as others.[20,28] **Figure 14** also shows that sucrose drastically increases the rate of adsorption, increases the final equilibrium adsorption pressure (π) and drastically decreases the lag time that is seen before adsorption begins.

The difference in the total system energy of the solution state and the adsorbed, aggregated states are much greater in sucrose than in water. This is a driving force for the adsorption of Aβ40 to the interface and leads to an increase in adsorption in sucrose over water. The final adsorption surface pressure (**Figure 15)** increases from 17.65±0.21 mN/m in water to 23.09±0.59 mN/m in 1.0 M sucrose. Previous work by Chi *et al.* has

shown x-ray scattering data of Aβ40 adsorbed to the air/subphase interface to suggest that there is a slight packing density increase of the β-sheet structure of Aβ40 at the air/subphase interface with sucrose. This suggests that there is a slight conformational compaction in sucrose at the air/subphase interface,[20] which fits with the hypothesis of a shift in conformational equilibrium towards a more compact conformation in preferential exclusion. More interesting is the reflectivity data that showed a decrease in the thickness of the Aβ40 film just below the air/subphase interface in the presence of sucrose (**Figure 48**).[20] Again, this is consistent with our hypothesis that Aβ40 adopts a more compact conformation due to preferential exclusion. This slight increase in packing density and increased folding of Aβ40 just below the air/subphase interface that was found previously by Chi *et al.* means that there is slightly more Aβ40 at the surface, and that more of the protein is in a compact conformation slightly below the surface due to increased folding, which could lead to the increase in final adsorption pressure found in **Figure 15**.

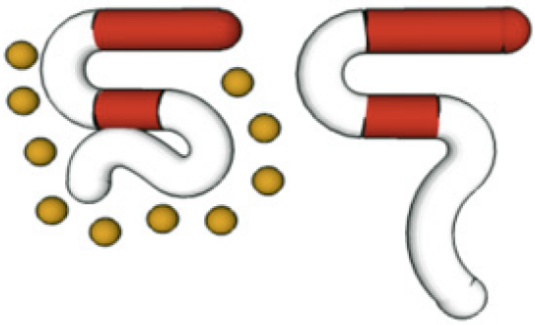

Figure 48: Effects of sucrose on the conformation of Aβ40 adsorbed to the air/subphase interface. The preferentially excluded sucrose causes a more compact conformation of the tail of Aβ40 that extends into the subphase when compared with water. This slight compaction right below the interface could partially explain the increase in final adsorption surface pressure attained with increasing sucrose concentrations in the subphase.

Our hypothesis of preferential exclusion can also explain the decrease in lag time (**Figure 16**) associated with adsorption of Aβ40 to the air/subphase interface. After incubation of Aβ40 in sucrose, due to preferential exclusion Aβ40 takes on a more

compact conformation (**Figure 4**). Since Aβ40 is already more compact and in a more energetically unfavorable state in the presence of sucrose than in water, according to our proposed model, the transition to the partially folded TS^* at the interface requires less energy ($\Delta G^{\ddagger}$) (**Figure 47**). This leads to a rapid decrease in the lag time associated with adsorption and folding to the final β-sheet containing adsorbed state. With the reduction in activation energy and increase in partial folding of Aβ40 in solution, there is more protein readily available to adsorb to the interface in a shorter time, increasing the rate of adsorption (**Figure 17**) as the concentration of sucrose increases.

There are at least three processes that can describe the adsorption of a protein to the air/subphase interface: (1) diffusion of the molecule from the bulk to an interface and attachment to this surface; (2) penetration of the new molecules into the adsorbed layer; (3) molecular rearrangement of the adsorbed molecules.[25] The last two processes have energy barriers (**Figure 46** and **47)**. Diffusion was ruled out as a limiting process with adsorption experiments using a water-soluble surfactant, Triton X-100. Triton X-100 is an amphiphilic molecule that does not require any conformational changes to become surface active. This means that there is no energy barrier for adsorption, so diffusion to the interface is the limiting factor. During injection, Triton X-100 adsorbed to the air/water interface within the time it took to complete the injection (data not shown). This is similar to the lag time associated with adsorption observed in the Aβ40 adsorption experiments at concentrations of 0.5 M sucrose and above. This suggests that the process involved in the lag time observed is energy dependent. The slow increase in surface pressure in water followed by a rapid rise implies that adsorption is dependent on the penetration of a small portion of the partially folded Aβ40 to the air/subphase interface,

followed by further folding to the final β-sheet containing adsorbed state (as described earlier). This indicates that at 30°C, the partial folding of Aβ40 when incubated in sucrose solution decreases the energy of activation of the transition of Aβ40 in solution to the partially folded adsorbed state, increasing the surface activity of Aβ40 (**Figure 48**).

5.3 Sucrose Increases the Rigidity of Lipid Membranes

While this idealized air/subphase interface has shown increased Aβ40 surface activity in the presence of sucrose, in order to understand how Aβ40 interacts with interfaces in a cellular environment, it is important to investigate Aβ40 interactions with membranes. The effect of sucrose on the ability of Aβ40 to insert into lipid was explored using the Langmuir trough to complete Aβ40 insertion into a model membrane, a lipid monolayer. Before that was done, however, a series of compression isotherms on the DMPG was completed in order to understand the effects of bulk sucrose on the lipid film.

There have been conflicting reports of what the effect stabilizing carbohydrates like sucrose and trehalose have on lipids.[38] Molecular dynamics models have indicated water is displaced by a layer of carbohydrates at the head group of lipids exposed to sucrose and other carbohydrate enriched solutions.[33-35] An experimental study has shown the opposite, however.[31] This study uses differential vapor pressure measurements of lipids to quantify the free energy of interaction of the osmolytes glucose, sucrose and trehalose with lipid bilayers to suggest that sucrose is preferentially excluded from the surface of the lipid head groups, hydrating them. There was also a study by Westh *et al.* discovered that at low concentrations of the sugars sucrose, glucose, and trehalose there is a buildup of sugar near the head groups of the lipids at high lipid densities. At high concentrations of sugar and high lipid densities, however, there was shown to be a

preferential exclusion of the sugar from the head groups.[38]

These different effects of sucrose show that there may be different explanations for liftoff and domain formation. The increase in liftoff area for DMPG at very low lipid densities may be attributed to the solvation shell of the lipid becoming larger as sucrose is enriched at the head group when in the gas phase, which leads to liftoff occurring at lower lipid densities than in water (**Figure 20**).[32,38] At liftoff areas of such low densities, the largest contribution to the lipid-lipid interaction comes from the subphase-embedded head groups, which include the hydrophilic part of the lipid molecule and any associated solvation shell.[32] As compression continues, however, there may be a shift towards preferential exclusion of sucrose from the head group of the lipid.[38]

The preferential exclusion of sucrose from the lipid promotes lipid conformations with smaller solvent exposed areas. This would stabilize the condensed phase over the fluid phase because there is less solvent exposed area of each lipid molecule in condensed domains. This explains why the onset of domain formation occurs at much lower surface pressures as sucrose concentration increases (**Figure 19**). ImageJ analysis of fluorescence imaging data at high surface pressures, 25 mN/m and 30 mN/m (**Figure 27)**, show an increase in condensed domain coverage as sucrose increases at 25 mN/m, but not a significant change in condensed domain coverage with increasing sucrose concentration at 30 mN/m. At the lipid packing densities and pressures that will be relevant for insertion experiments (25 and 30 mN/m), DMPG does appear to be less compressible in sucrose than in water (**Figure 26**). This was be determined by calculating the compressibility of each isotherm at the specified surface pressure (**Figure 26**). The compressibility at 25 mN/m ranges from 0.0222±0.000527 m/mN in water to

0.0115±0.000237 m/mN in 0.5 M sucrose at 25 mN/m, meaning the monolayer was more compressible in water than in sucrose. In water, the DMPG is in the liquid expanded-liquid condensed coexistence phase (plateau) so the slope of the compression isotherm is smaller, meaning the monolayer is more compressible. In sucrose, the lipid is past the coexistence phase and well within the liquid condensed phase so the slope is larger, meaning the lipid is less compressible. These changes in the fluidity and compressibility of the DMPG monolayer in the presence of sucrose suggest that the increase in insertion of Aβ40 may be due to these morphological changes in addition to the effects of preferential exclusion and molecular crowding.

5.4 Sucrose Greatly Enhances the Insertion of Aβ40 into Anionic and Zwitterionic Membranes

The insertion of Aβ40 into the anionic DMPG monolayer and the zwitterionic DPPC monolayer was affected by the presence sucrose. Insertion into both DMPG and DPPC was enhanced dramatically in the presence of sucrose. The final percent insertion was greatly increased, the lag time was reduced to the limit of detection of the instrument, and the rate of adsorption was significantly increased over water. On water, the interaction of Aβ40 with the anionic DMPG is related to the ion-dipole interaction between the lipid and Aβ40, and the absence of interaction between Aβ40 and the zwitterionic DPPC monolayer arises from the much weaker dipole-dipole interactions.[28]

The increase in insertion is more drastic in DPPC (0% on water to 66.73% on 1 M sucrose) than in DMPG (49.46% on water to 86.41% on 0.25 M sucrose) even if the overall percent insertion is lower in DPPC. The insertion experiments were completed at different surface pressures so the actual values of insertion in the two lipids cannot be

directly compared. However, the trends are similar, indicating sucrose does have an effect on the ability of Aβ40 to insert into both membranes. The effects of sucrose on Aβ40 insertion into DMPG and DPPC coincide with the previously observed trends in the adsorption of Aβ40 to the air/subphase interface. The increase in insertion in DMPG and DPPC (**Figures 31 and 43 Results**) can be attributed to multiple effects of sucrose. Ionic strength and pH can greatly affect the electrostatic interactions between the lipid head group and Aβ40 as well as the interactions between head group molecules.[28] The effect of sucrose on the ionic strength and pH of the solution was shown to be minimal with changes in sucrose concentration (**Table 3**). This suggests that the increase in insertion is due to the previously described preferential exclusion sucrose, which partially folds Aβ40, reducing the energy required for penetration into the monolayer.

The limiting factor of Aβ40 insertion into the DMPG monolayer appears to also be an energy barrier.[7] As described previously, penetration of Aβ40 into the adsorbed layer and molecular rearrangement of the adsorbed Aβ40 are the two processes involved in activity at an interface. The pH of Aβ40 was above the Penetration of Aβ40 into the DMPG may be the limiting factor in insertion because of the electrostatic repulsion of the negatively charged Aβ40 (net charge ranging from -2.3 to -2.7) with the negatively charged DMPG head group. Insertion is favored, however, because it reduces the electrostatic repulsion of the negatively charged head groups of DMPG that are in close proximity to one another. So, Aβ40 being physically located between the head groups is favored, but insertion itself has an energy barrier. This energy barrier is reduced by compaction of Aβ40 due to preferential exclusion. This compaction allows insertion to follow the mechanism described in **Figure 47**, where only a small portion of the partially

folded protein inserts and then more folding occurs, resulting in insertion of the peptide into the membrane. While Aβ40 carries an overall negative charge at the pH we were investigating, there are still individual residues that are still positively charged and can interact with the negatively charged head group of DMPG, initiating insertion. The difference between the energy of the system in solution and in the aggregated state in the presence of sucrose leads to a strong driving force towards insertion. The solution state of Aβ40 is very energetically unfavorable due to the compaction of the protein, and the aggregated state is much more favorable because the aggregated, inserted state contains the least solvent exposed surface area. This means that, in the presence of sucrose, insertion is more energetically favored so insertion occurs to a greater extent.

Our theory of preferential exclusion can be used to explain the decrease in lag time linked to the insertion of Aβ40 into the DMPG and DPPC monolayers with increasing sucrose concentrations (**Figures 32 and 44**). After incubation of Aβ40 in sucrose, due to preferential exclusion, Aβ40 takes on a more compact conformation (**Figure 4**). This more compact conformation is energetically unfavorable, so, in the presence of sucrose, the transition to the partially folded transition state (TS^*) at the interface requires less energy ($\Delta G^{\ddagger}$) (**Figure 47**). This leads to a rapid decrease in the lag time associated with interaction with the membranes. With the reduction in activation energy the rate of insertion also increases(**Figures 33** and **45**).

5.5 Sucrose Increases the Disruption of Membranes by Aβ40

Fluorescence imaging of the insertion of Aβ40 into DMPG monolayers is shown in **Figures 34-39**. As insertion occurs, the ordered phase of DMPG is disrupted. During insertion, the boundary between the ordered phase (black) and the disordered regions

(light) becomes fuzzy, without a clear boundary to focus on. This suggests that Aβ40 may insert into the easily accessible disordered phase and decreases the interfacial energy at the interface between the ordered and disordered phases. This disruption effect was qualitatively increased with sucrose concentration. In preliminary experiments, insertion into DPPG showed disruption of the internal portion of condensed domains 3-4 hours after injection of Aβ40 (data not shown).

6. Conclusion

Since the association of Aβ in membranes has been associated with nucleation of fibril formation that leads to the neurodegenerative pathology of Alzheimer's disease, it is important to understand the interaction of monomeric Aβ with membranes. Previous studies have investigated association of Aβ with membranes in the presence of water. This does not accurately represent a model for the *in vivo* investigation of Aβ interactions with interfaces, such as a leaflet of the cell membrane. The cellular environment is very crowded, containing macromolecules and osmotically active solutes that affect the interfacial activity of Aβ. Our results indicate that the osmolyte sucrose greatly enhances the interfacial activity of Aβ at an ideal air/subphase interface and in a model membrane system, regardless of head group charge. The effects of preferential exclusion and molecular crowding associated with sucrose on the interfacial dynamics of Aβ thus play an important role in formation of fibrils. The cellular environment is even more crowded and osmotically active than the dilute solutions investigated here. This suggests that the interactions of Aβ with membrane interfaces may be even more significant in the cellular environment and may serve as a nucleation site for the aggregation of Aβ *in vivo*.

7. References

1. Butterfield, S. M. and H. A. Lashuel (2010). "Amyloidogenic protein-membrane interactions: mechanistic insight from model systems." Angew Chem Int Ed Engl **49**(33): 5628-5654.

2. LaFerla, F. M., K. N. Green, et al. (2007). "Intracellular amyloid-beta in Alzheimer's disease." Nat Rev Neurosci **8**(7): 499-509.

3. Alzheimer's, A., W. Thies, et al. (2011). "2011 Alzheimer's disease facts and figures." Alzheimers Dement **7**(2): 208-244.

4. Kim, J. R., T. J. Gibson, et al. (2003). "Targeted control of kinetics of beta-amyloid self-association by surface tension-modifying peptides." J Biol Chem **278**(42): 40730-40735.

5. Kayed, R., Y. Sokolov, et al. (2004). "Permeabilization of lipid bilayers is a common conformation-dependent activity of soluble amyloid oligomers in protein misfolding diseases." J Biol Chem **279**(45): 46363-46366.

6. Lin, H., R. Bhatia, et al. (2001). "Amyloid beta protein forms ion channels: implications for Alzheimer's disease pathophysiology." FASEB J **15**(13): 2433-2444.

7. Relini, A., O. Cavalleri, et al. (2009). "The two-fold aspect of the interplay of amyloidogenic proteins with lipid membranes." Chem Phys Lipids **158**(1): 1-9.

8. Chi, E. Y., C. Ege, et al. (2008). "Lipid membrane templates the ordering and induces the fibrillogenesis of Alzheimer's disease amyloid-beta peptide." Proteins **72**(1): 1-24.

9. Chi, E. Y., S. Krishnan, et al. (2003). "Physical stability of proteins in aqueous solution: mechanism and driving forces in nonnative protein aggregation." Pharm Res **20**(9): 1325-1336.

10. Soto, C. (2003). "Unfolding the role of protein misfolding in neurodegenerative diseases." Nat Rev Neurosci **4**(1): 49-60.

11. Bowirrat Abdalla, Mustafa Yassin, Menachem Abir, Bishara Bisharat and Zaher Armaly (2012). Traditional and Modern Medicine Harmonizing the Two Approaches in the Treatment of Neurodegeneration (Alzheimer's Disease – AD), Complementary Therapies for the Contemporary Healthcare, Prof. Marcelo Saad (Ed.), ISBN: 978-953-51-0801-6, InTech, DOI: 10.5772/48558.

12. Turner, P. R., K. O'Connor, et al. (2003). "Roles of amyloid precursor protein and its fragments in regulating neural activity, plasticity and memory." Prog Neurobiol **70**(1): 1-32.

13. Duce, J. A., A. Tsatsanis, et al. (2010). "Iron-export ferroxidase activity of beta-amyloid precursor protein is inhibited by zinc in Alzheimer's disease." Cell **142**(6): 857-867.

14. Priller, C., T. Bauer, et al. (2006). "Synapse formation and function is modulated by the amyloid precursor protein." J Neurosci **26**(27): 7212-7221.

15. Tabaton, M., X. Zhu, et al. (2010). "Signaling effect of amyloid-beta(42) on the processing of AbetaPP." Exp Neurol **221**(1): 18-25.

16. Soscia, S. J., J. E. Kirby, et al. (2010). "The Alzheimer's disease-associated amyloid beta-protein is an antimicrobial peptide." PLoS One **5**(3): e9505.

17. Dunker, A. K., I. Silman, et al. (2008). "Function and structure of inherently disordered proteins." Curr Opin Struct Biol **18**(6): 756-764.

18. Hou, L., H. Shao, et al. (2004). "Solution NMR studies of the A beta(1-40) and A beta(1-42) peptides establish that the Met35 oxidation state affects the mechanism of amyloid formation." J Am Chem Soc **126**(7): 1992-2005.

19. Crescenzi, O., S. Tomaselli, et al. (2002). "Solution structure of the Alzheimer amyloid beta-peptide (1-42) in an apolar microenvironment. Similarity with a virus fusion domain." Eur J Biochem **269**(22): 5642-5648.

20. Chi, E. Y., S. L. Frey, et al. (2010). "Amyloid-beta fibrillogenesis seeded by interface-induced peptide misfolding and self-assembly." Biophys J **98**(10): 2299-2308.

21. Chi, E. Y., C. Ege, et al. (2008). "Lipid membrane templates the ordering and induces the fibrillogenesis of Alzheimer's disease amyloid-beta peptide." Proteins **72**(1): 1-24.

22. Uversky, V. N. (2009). "Intrinsically disordered proteins and their environment: effects of strong denaturants, temperature, pH, counter ions, membranes, binding partners, osmolytes, and macromolecular crowding." Protein J **28**(7-8): 305-325.

23. Cino, E. A., M. Karttunen, et al. (2012). "Effects of molecular crowding on the dynamics of intrinsically disordered proteins." PLoS One **7**(11): e49876.

24. Yancey, P. H., M. E. Clark, et al. (1982). "Living with water stress: evolution of osmolyte systems." Science **217**(4566): 1214-1222.

25. Magdassi, Shlomo. (1996) "Surface Activity of Proteins: Chemical and Physicochemical Modifications". New York, NY. Dekker. Print.

26. KSV Brochure. " KSV NIMA Langmuir and Langmuir-Blodgett Deposition Troughs". Print.

27. KSV. "Software Manual". Print.

28. Ege, C., Lee, K. Y. C. (2004). "Insertion of Alzheimer's Aβ40 Peptide into Lipid Monolayers". Biophys J. **87**: 1732-1740.

29. Paravastu, A. K., I. (2009). "Seeded growth of b-amyloid fibrils from Alzheimer's brain-derived fibrils produces a distinct fibril structure". Proc Natl Acad Sci. **106**: 7443–7448.

30. Lee, J.C; Timasheff, S. N. (1981). "The stabilization of proteins by sucrose". J Biol Chem. **256**: 7193-7201.

31. Westh, P. (2008). "Glucose, sucrose and trehalose are partially excluded from the interface of hydrated DMPC bilayers". Phys Chem Chem Phys. **10**: 4110-4112.

32. Pocivavsek, L., Gavrilov, K., et al. (2011). "Glycerol-induced membrane stiffening: the role of viscous fluid adlayers". Biophys. J. **101**:118-127.

33. Luzardo, M. C. (2000). "Trehalose and sucrose on the hydration and dipole potential of lipid bilayers". Biophys J. **78**: 2452-2458.

34. Skibinsky, A., Venable, R. M., et al. (2005) "Molecular dynamics study of the response of lipid bilayers and monolayers to trehalose". Biophys J. **89**: 4111-4121.

35. Villarreal, M. A., Diaz, S. B., et al. (2004). "Molecular dynamics simulation study of the interaction of trehalose with lipid membranes". Langmuir. **20**: 7844-7851.

36. Hortchansky, P., Schroeckh, V. (2005) "Aggregation kinetics of Alzheimer's β-amyloid peptide is controlled by stochastic nucleation". Protein Sci. **14**: 1753-1759.

37. Kaganer, V. M. (1999). "Structure and Phase Transitions in Langmuir Monolayers". Rev Mod Phys. (**71**): 779-819.

38. Andersen, H. D., Westh, P. (2011). "Reconciliation of Opposing Views on Membrane-Sugar Interactions". PNAS. (**108)**: 1874-1878.